UNIVERSITY OF KWAZULU-NATAL

USE OF FREQUENCY RESPONSE MASKING TECHNIQUE IN DESIGNING A/D CONVERTER FOR SDR

SIBONGISENI ELLIOT PHAKATHI

Use of Frequency Response Masking Technique in Designing A/D Converter for SDR

By Sibongiseni Elliot Phakathi

University of KwaZulu-Natal

2005

Submitted in fulfillment of the academic requirements for the degree of Masters of Science in Engineering in the School of Electrical, Electronic and Computer Engineering, University of KwaZulu-Natal, 2005.

ABSTRACT

Analog-to-digital converters (ADCs) are required in almost all signal processing and communication systems. They are often the most critical components, since they tend to determine the overall system performance. Hence, it is important to determine their performance limitations and develop improved realizations. One of the most challenging tasks for realizing software defined radio (SDR) is to move A/D conversion as close to the antenna as possible, this implies that the ADC has to sample the incoming signal with a very high sample rate (over 100 MSample/s) and with a very high resolution (14 -to -16 bits). To design and implement A/D converters with such high performance, it is necessary to investigate new designing techniques.

The focus in this work is on a particular type of potentially high-performance (high-resolution and high-speed) analog-to-digital conversion technique, utilizing filter banks, where two or more ADCs are used in the converter array in parallel together with asymmetric filter banks. The hybrid filter bank analog-to-digital converter (HFB ADC) utilizes analog filters (analysis filters) to allocate a frequency band to each ADC in a converter array and digital synthesis filters to reconstruct the digitized signal. The HFB improves the speed and resolution of the conversion, in comparison to the standard time-interleaving technique by attenuating the effect of gain and phase mismatches between the ADCs.

Many of the designs available in the literature are compromising between some metrics: design complexity, order of the filter bank (computation time) and the sharpness of the frequency response roll-off (the transition from the pass band to the stop band).

In this dissertation, five different classes of near perfect magnitude reconstruction (NPMR) continuous-time hybrid filter banks (CT HFBs) are proposed. In each of the five cases, two filter banks are designed; analysis filter bank and synthesis filter bank. Since the systems are hybrid, continuous time IIR filter are used to implement the analysis filter bank and digital filters are used for the synthesis filter bank. To optimize the system, we used a new technique, known in the literature as frequency response masking (FRM), to design the synthesis filter bank. In this technique, the sharp roll-off characteristics can be achieved while keeping the complexity of the filter within practical range, this is done by splitting the filter into two filters in cascade; model filter with relaxed roll-off characteristics followed by a masking filter.

One of the main factors controlling the overall complexity of the filter is the way of designing the model filter and that of designing the masking filter.

The dissertation proposes three combinations: use of IIR model filter and IIR masking filter, IIR model filter/FIR masking filter and FIR model filter/FIR masking filter. To show the advantages of our designs, we considered the cases of designing the synthesis filter as one filter, either FIR or IIR. These two filters are used as base for comparison with our proposed designs (the use of masking response filter).

The results showed the following:

1. Asymmetric hybrid filter banks alone are not sufficient for filters with sharp frequency response roll-off especially for IIR/FIR class.
2. All classes that utilize FRM in their synthesis filter banks gave a good performance in general in comparison to conventional classes, such as the reduction of the order of filters
3. IIR/IIR FRM gave better performance than IIR/FIR FRM.
4. Comparing IIR/IIR FRM using FIR masking filters and IIR/IIR FRM using IIR masking filters, the latter gave better performance (the performance is generally measured in terms of reduced filter order).
5. All classes that use the FRM approach have a very low complexity, in terms of reduced filter order. Our target was to design a system with the following overall characteristics: pass band ripple of -0.01 dB, stop band minimum attenuation of – 40 dB and of response roll-off of 0.002. Our calculations showed that the order of the conventional IIR/FIR filter that achieves such characteristics is about $N = 2000$. Using the FRM technique, the order N reduced to about $N = 244$, $N = 179$ for IIR/FIR and IIR/IIR classes, respectively. This shows that the technique is very effective in reducing the filter complexity.
6. The magnitude distortion and the aliasing noise are calculated for each design proposal and compared with the theoretical values. The comparisons show that all our proposals result in approximately perfect magnitude reconstruction (NPMR).

In conclusion, our proposal of using frequency-response masking technique to design the synthesis filter bank can, to large extent, reduce the complexity of the system. The design of the system as a whole is simplified by designing the synthesis filter bank separately from the design of the analysis filter bank. In this case each bank is optimized separately. This implies that for SDR applications we are proposing the use of the continuous-time HFB ADC (CT HFB ADC) structure utilizing FRM for digital filters.

PREFACE

The research work presented in this dissertation was performed by Mr. Sibongiseni Elliot Phakathi, under the supervision of Prof. David Dawoud, at the centre for Radio Access Technologies University of KwaZulu-Natal in the School of Electrical, Electronic and Computer Engineering. This work was partially supported by Alcatel SA, THRIP and Telkom South Africa as part of the Centers of Excellence programme at the University of KwaZulu-Natal.

The whole dissertation, unless specifically indicated to the contrary in the text, is the student's own work, and has not been submitted in part, or in whole to any other University for degree purpose.

The dissertation is submitted with the approval of its supervisor.

Professor David Dawoud
University of KwaZulu-Natal

ACKNOWLEDGEMENTS

I would like to offer my sincere thanks to Professor Dawoud for his guidance, dedication, invaluable help, encouragement, motivation and constructive criticism as my supervisor for the last two years. His patience and support have been greatly appreciated.

Secondly, a great thanks is owed to my savior, redeemer, deliverer, LORD Jesus. For his enduring love, patience, encouragement and support, he showed me not only over the past two years, but throughout my tertiary education.

Thirdly, a great thanks is also owed to my family (Siyabonga, Lindiwe, Hlengiwe, Thando and Mzwandile), my brothers and sisters in the LORD for their patience, prayers and support. In particular, I would like to thank my mother for supporting and understanding me, since day one, when she gave birth to me and throughout my education. My mother, this dissertation is dedicated to you, I know you cannot understand even a single sentence in this work, but I know it will be a reminder to you that I love you very much; you have been through a lot carrying us as a single mother.

Thanks is also owed to Telkom SA Ltd, THRIP and Alcatel Telecomms for their valued financial support over the last two years, and for providing the equipment necessary for the completion of this Masters degree.

Finally, thanks go to my other postgraduate colleagues who provided hours of criticism (constructive and destructive) and support during the times when work was so hard, challenging and the last thing on my mind.

TABLE OF CONTENTS

LIST OF FIGURES/TABLES

CHAPTER 1

CHAPTER 2

CHAPTER 3

CHAPTER 4

CHAPTER 5

LIST OF ACRONYMS

ADC	analog to digital converter
DAC	digital to analog converter
IF	intermediate frequency
RF	radio frequency
SDR	software defined radio
SNR	signal-to-noise ratio
BER	bit error rate
SQNR	signal-to-quantization-noise ratio
SFDR	spurious-free dynamic range
SINAD	signal-to-noise-and-distortion ratio
SINR	signal-to-interference-noise ratio
THD	total harmonic distortion
ENOB	effective number of bits
FB	filter Bank
FIR	finite-length impulse response
IIR	infinite-length impulse response
LP	linear programming
MPR algorithm	McClellan-Parks-Rabiner's algorithm
NLP	nonlinear programming
NPMR	near perfect magnitude reconstruction
NPR	near perfect reconstruction
PR	perfect reconstruction
FRM	frequency-response masking
LWDFs	lattice wave digital filters

CHAPTER 1

INTRODUCTION AND OVERVIEWS

1.1 Motivation

Today's wireless telecommunications services are characterized by competing and often incompatible standards, modes and frequencies. Software radio or simply software-defined radio (SDR) is a rapidly emerging and evolving technology that provides an efficient and comparatively inexpensive mechanism for the production of multimode, multiband, multifunctional wireless systems that can be enhanced using software upgrades. One of the most challenging tasks for realizing SDR's is to move A/D conversion as close to the antenna as possible. This implies that the ADC has to sample the incoming signal with a very high sample rate, corresponding also to a very high resolution. For future wideband communications systems, the required sample rates are in the range of 100 to 500 MHz with a resolution range corresponding to 12-to-14 bits, whereas for SDR the required sample rate is over 100 MSa/s with the resolution in the range of 14-to-16 bits. Such high requirements on A/D might not be feasible with current technologies and are not expected to be feasible if current ADC techniques are used. Thus, the requirements for higher sample rates, and high resolution in ADCs and the need for faster ADCs in modern communication technology are ever increasing. To increase the bandwidth of the A/D conversion, several A/D converters can be used in parallel. The focus in this work is on a particular type of potentially high-performance (high-resolution and high-speed) analog-to-digital conversion technique, utilizing filter banks, where two or more ADCs are used in the converter array in parallel together with asymmetric filter banks. Using a filter bank for analog-to-digital (A/D) or digital-to analog (D/A) conversion is an unconventional application of the filter bank architecture that improves the speed and resolution of the conversion over the standard time-interleaved array conversion technique [9, 10]. Applications of high-speed, high-resolution A/D and D/A conversion include direct digital receivers for wireless communications applications; radar receivers; test equipment such as oscilloscopes, spectrum analyzers, network analyzers, signal and pattern generators, modems, and medical imaging systems.

One approach that has been proposed in literature for Hybrid Filter Bank (HFB) is to design the analog filter bank from a digital prototype. However, to only consider the magnitude response is not sufficient to control aliasing, and hence, the use of the bilinear transformation and impulse invariance method are not sufficient. Then, higher-order transformations were also proposed, similar to Padé approximation, which yielded better matching. However, the main drawback of mapping a digital prototype filter bank to an analog filter bank is that the order of the analog filters tends to become unacceptably high. For instance, when using higher order transformations, the resulting filter order of the analog filters becomes the product of the digital prototype and the order of the transformation. To alleviate or to reduce the complexity of the analog filters from using higher-order transformations, the concept of asymmetric filter banks was recently

introduced in literature [10], which is also used in this work. The concept of asymmetric filter banks showed a significant reduction in the complexity of analog filters. Its main drawback however is noticeable when considering the condition given in [9]. Thereby stating that for HFB based ADCs, the filters should have a sharp frequency response roll-off so that the transition regions are as narrow as possible and maximum stopband attenuation and, hence minimum spurious free dynamic range (SFDR) is achieved across as much of the band as possible. If this condition is left out, asymmetric HFB will achieve reasonable results. If it's embraced however, the synthesis filter bank complexity becomes too high and sometimes unacceptably high. This implies that there is a need of good design procedures that will reduce the complexity of synthesis filter bank, at the same time retaining low order for analysis filter bank. In this dissertation the objective is to find good design procedures that will offer reasonable results, even in the case of filters having a sharp frequency response roll-off. The work presented in this dissertation is only limited to continuous-time hybrid analog/digital filter bank (CT-HFB).

1.2 Terminology and Building Blocks

1.2.1 Types of Filters

In the most general sense, a filter is a system or a device that alters in a prescribed way the input that passes through it [1-10]. In essence, a filter converts inputs into outputs in such a fashion that certain desirable features of the inputs are preserved or retained in the outputs while undesirable features are suppressed. There are many types of filters, though only a few will be addressed here, i.e. electrical filters, and on the small scale, filters are basic electronic components in many communication systems. An electrical filter is designed to separate and pass a wanted signal from a mixture of wanted and unwanted signals.

Electrical filters may be categorized in a number of ways, i.e. analog filters and/or digital filters. Analog filters are utilized to process continuous-time signals, whereas digital filters are used to process digital signals (discrete-time signals). In more abstract terms, a filter is a system characterized by a set of input-output pairs as illustrated in Fig. 1-1, where

$$y(t) = \int_0^{\infty} h(t-\tau)x(\tau)d\tau \tag{1.1}$$

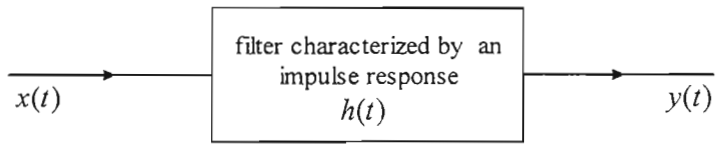

Figure 1.1: A filter is a system with a set of prescribed input-output properties [1]

where $h(t)$ is the impulse response of the filter, in addition to this, it is assumed that the single-input single-output (SISO) analog filter under consideration is casual, linear, lumped, and time-invariant. The Laplace transform of (1.1) gives

$$Y(s) = H(s)X(s) \tag{1.2}$$

where $Y(s)$, $H(s)$ and $X(s)$ are the Laplace transforms of $y(t)$, $h(t)$ and $x(t)$, respectively. This implies that the filter is characterized by $H(s)$, the transfer function. In this work, we only consider lowpass filter, bandpass filter, highpass filter and allpass filter as shown in Fig. 1.2 below.

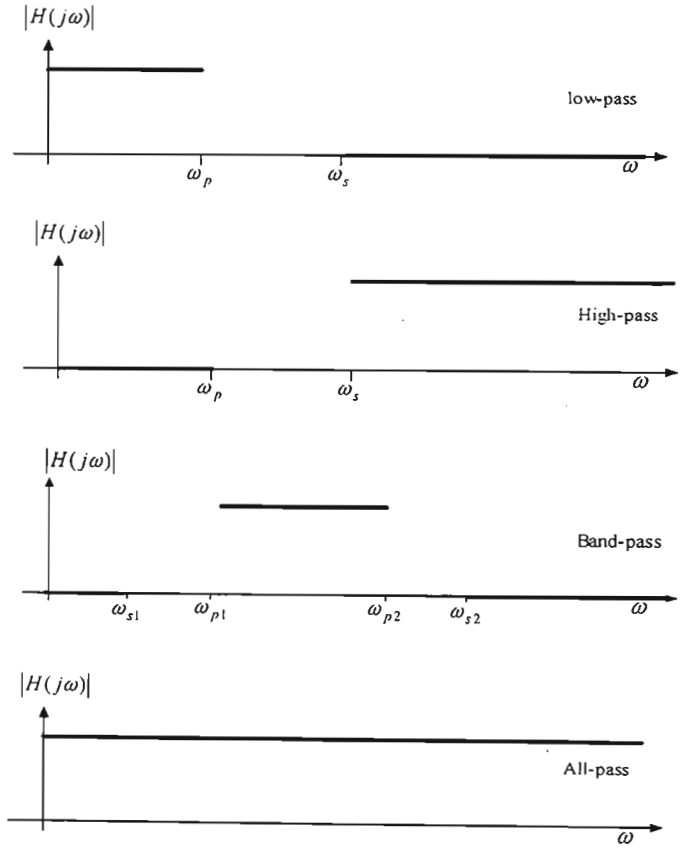

Figure 1.2: Types of some of frequency-selective filters

We can then define the frequency selective filters shown in Fig. 1.2 as follows:

- *Low-pass filter (LP)* : A filter whose passband is from zero to some frequency ω_p and whose stopband extends from some frequency ω_s to infinity , where $\omega_p < \omega_s$
- *High-pass filter* (HP): A filter whose passband is from some frequency ω_p to infinity and whose stopband is from zero to ω_s , where $\omega_s < \omega_p$
- *Band-pass filter* (BP): A filter whose passbands is from some frequency ω_{p1} to some other frequency ω_{p2} and whose stopbands are from zero to ω_{s1} and from ω_{s2} to infinity , where $\omega_{s1} < \omega_{p1} < \omega_{p2} < \omega_{s2}$
- *All-pass filter (AP):* A filter whose magnitude is one for all frequencies, for instance whose passband is from zero to infinity. This type of filter is utilized mainly for phase compensation and phase shifting purposes.

Fourier transform of the impulse responses are known as frequency responses and will be frequently utilized to describe and analyze the frequency behavior of the filters in subsequent chapters. The Laplace transform of $h(t)$, as well as the z-transform of $h(n)$, are called transfer functions. The transfer function $H(s)$ of an analog continuous-time filter is given as

$$H(j\omega) = \int_0^\infty h(t)e^{-j\omega t}dt \tag{1.3}$$

and the transfer function of a discrete-time filter $H(z)$ can be written as

$$H(e^{j\omega T}) = \sum_{n=-\infty}^{\infty} h(n)e^{-j\omega Tn} \tag{1.4}$$

respectively.

1.2.2 Filter Banks

Filter bank is defined as a system of several filters with a common input or a common output. In other words, it is a set of several frequency-selective filters in parallel that partitions the frequency range of the input signal spectrum into number of adjacent frequency bands. The partitioning can be done uniformly or in octaves [2, 5-10]. The partitioning of the available frequency band can, in many cases, be very useful, i.e. HFB ADC, where a reduced signal bandwidth allows for a reduced sampling rate and where some errors, which occur during quantization and sampling are attenuated by filters. Filter banks are mainly used whenever a signal needs to be split up into different frequency bands. An asymmetric filter bank is a filter bank where the analysis or the synthesis filter bank has lower arithmetic complexity compared to the other [10]. This is the result of optimizing each side separately. An example of an asymmetric filter bank application is a base station and a mobile unit, where it is important to minimize the complexity in the mobile unit as much as possible. Present design methods are not suitable for this kind of applications, since they only consider the total complexity. Traditionally, filter banks have been designed such that the analysis and synthesis filters have about same complexity. If the object function is to minimize complexity in either the analysis filter bank or the synthesis filter bank, new filter bank classes are needed. These new filter bank classes are designed differently [11]. Since filter banks that are designed in a traditional manner are not suitable for mobile unit. This implies that even for software-defined radio applications the present design is not suitable. Asymmetric filter banks therefore become a possible solution because asymmetric filter bank offers a low arithmetic complexity, which is very important when designing a mobile unit and other communication systems.

The filter banks considered in this work is a uniform filter bank, which consists of an analysis filter bank and synthesis filter bank. Uniform filter banks consist of low-pass, band-pass and high-pass filters partitioning signal spectra into directly adjacent bands of equal width, and later recombining these frequency bands again. All filters have the same bandwidth, and the centre frequencies are uniformly spaced in frequency. The configuration illustrated in Fig. 1.3 shows an M – channel analog filter bank. Analysis filter bank decomposes the spectrum of the input signal into a set of adjacent subspectra. Each has a bandwidth of π / M, where M is the number of channels. Fig 1-3 basically partitions the input signal into M frequency bands where different filters pass signals belonging to different frequency regions.

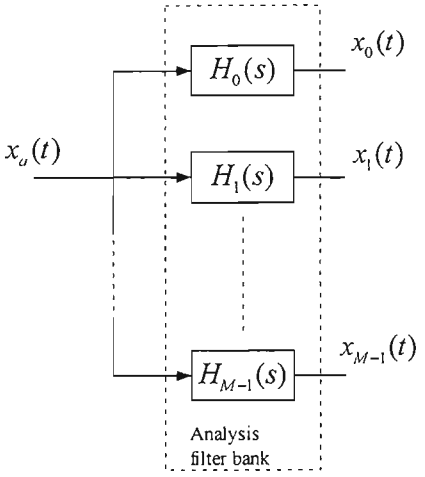

Figure 1.3: M – channel analog analysis filter bank

Filter bank can also be used to combine the signal into a single signal, which can be easily illustrated as in Fig. 1.4(a), but in order to recombine the signal; it has to be filtered by the same equivalent filter as in analysis filter bank, i.e. the signal or subband signal from lowpass filter, will be also filter by a lowpass filter in the later stage before recombination of the subband signals as shown in Fig. 1.4(a).

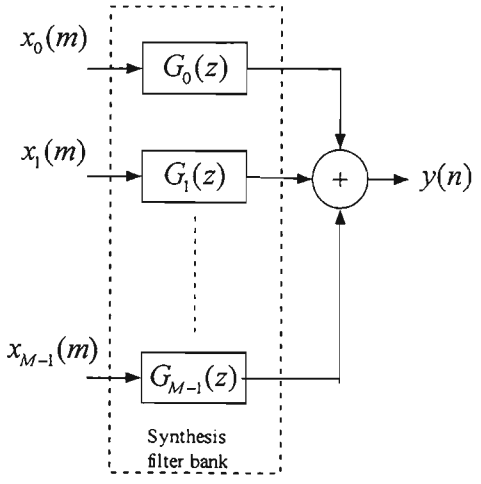

Figure 1.4 (a): M – channel digital synthesis filter bank

Halfband filters play a dominant role in the design of filter banks. In this work, halfband filters are employed in the synthesis filter bank. Two types of halfband filters are used, finite-length impulse response (FIR) filters and infinite-length impulse response (IIR) filters [5]. Halfband filters are filters that divide the frequency range of a discrete-time system into two equal parts. FIR filters are most often employed as half-

band filters due to their linear phase response. If the phase response however is not an important requirement IIR half-band filters are used. This is due to the fact that halfband IIR can have fewer multipliers than FIR filter for the same sharp cut-off specifications. Elliptic IIR filters are rated as the most efficient. However, they have non-linear phase response. To overcome phase non-linearity, one can either utilize optimization to design IIR filter with approximately linear phase response or apply the double filtering technique with Powell and Chau modification for real-time processing (Powell and Chau, 1991 and Lutovac *et al, 2000)*, details in [12].

An ideal half-band filter has a frequency response as depicted by Fig. 1.4(b). Its impulse response can be given as

$$h(n) = \frac{\sin\left(\frac{\pi}{2}n\right)}{\pi n} \tag{1.4b}$$

which implies that $h(n) = 0$ for all even n, except for $n = 0$. In the non-ideal cases the passband and stopband edges are not equal, i.e. $\omega_s = \omega_p$ but $\omega = \pi/2$ must belong to the transition band, and the corresponding value of the magnitude response for this value is 0.5. Halfband filters generally have considerably lower complexity compared to other filters. This is due to the fact that every second filter coefficients are set to zero.

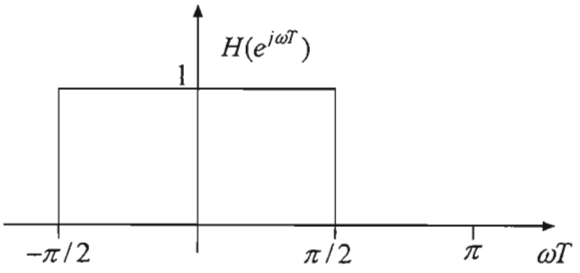

Figure 1.4(b): Magnitude response of an ideal Halfband filter

Other important operations include sampling, decimation and interpolation, which form the basic concepts behind the changing of the sampling rate, these operations are discussed in subsequent subsections.

1.2.3 Sampling and Sampling Rate Conversion

The term sampling was initially employed when continuous signals were converted into discrete-time signals. Systems that utilize multiple sampling rates in the processing of digital signals are called multirate

digital signal processing systems. Sampling rate conversion is one of the main operations in a multirate system [5, 12].

1.2.3.1 Sampling

Basic to digital filtering are problems associated with the sampling of continuous signals to form digital signals and the construction of continuous signals from their digital counterparts. In this subsection, we deal with these problems using the Fourier representation, in particular to show how sampling operation is done and how continuous signal is related to digital signal; details are given in [1-5]. Fig. 1.5 shows a uniform sampling.

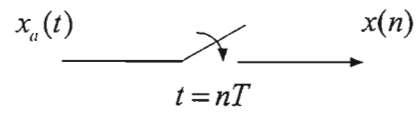

Figure 1.5: An illustration of uniform sampling

Let $x_a(t)$ be a continuous-time signal that has a Fourier representation

$$x_a(t) = \frac{1}{2\pi} \int_{-\infty}^{\infty} X_a(j\omega) e^{j\omega t} d\omega \tag{1.5}$$

where

$$X_a(j\omega) = \int_{-\infty}^{\infty} x_a(t) e^{-j\omega t} dt \tag{1.6}$$

$X_a(j\omega)$ is known as the Fourier transform of $x_a(t)$, let $x(n)$ be the sequence defined as follows

$$x(n) = x_a(nT) \tag{1.7}$$

where T is the sampling period, and $f_s \triangleq 1/T$ is called the sampling frequency. The Fourier transform of the sequence $x(n)$ is given as

$$X(e^{j\theta}) = \sum_{n=-\infty}^{\infty} x(n) e^{-jn\theta} dt \tag{1.8}$$

$X(e^{j\theta})$ is a periodic function of θ with period of 2π. Equation (1.8) represents the Fourier series expansion of $X(e^{j\theta})$ with Fourier co-efficients being $x(n)$. It is possible to relate $X_a(j\omega)$ and $X(e^{j\theta})$ by substituting (1.5) into (1.7) and also with $t = nT$, therefore we obtain

$$\begin{aligned} x(n) = x_a(nT) &= \frac{1}{2\pi}\int_{-\infty}^{\infty} X_a(j\omega)e^{j\omega nT}\,d\omega \\ &= \frac{1}{2\pi}\sum_{p=-\infty}^{\infty}\int_{[(2p-1)\pi]/T}^{[(2p+1)\pi]/T} X_a(j\omega)e^{j\omega nT}\,d\omega \end{aligned} \tag{1.9}$$

let $j\omega = j\omega' + j\dfrac{2\pi p}{T}$ and note that

$$\begin{aligned} e^{j\omega nT} &= e^{j[\omega'+(2\pi p/T)]nT} \\ &= e^{j\omega' nT}e^{j2\pi pn} \\ &= e^{j\omega' nT} \end{aligned} \tag{1.10}$$

equation (1.9) can be written as

$$\begin{aligned} x(n) &= \frac{1}{2\pi}\sum_{p=-\infty}^{\infty}\int_{-\pi/T}^{\pi/T} X_a\left(j\omega' + j\frac{2\pi p}{T}\right)e^{j\omega' nT}\,d\omega' \\ &= \frac{1}{2\pi}\int_{-\pi/T}^{\pi/T}\sum_{p=-\infty}^{\infty} X_a\left(j\omega + j\frac{2\pi p}{T}\right)e^{j\omega nT}\,d\omega \end{aligned} \tag{1.11}$$

where the dummy variable ω' is replaced with another dummy integration variable ω. With another change of variable $\theta = \omega T$, we can write (1.11) as

$$x(n) = \frac{1}{2\pi}\int_{-\pi}^{\pi}\frac{1}{T}\sum_{p=-\infty}^{\infty} X_a\left(j\frac{\theta}{T} + j\frac{2\pi p}{T}\right)e^{jn\theta}\,d\theta \tag{1.12}$$

By comparing (1.9) and (1.12), we obtain

$$X(e^{j\omega T}) = \frac{1}{T}\sum_{p=-\infty}^{\infty} X_a\left(j\omega + j\frac{2\pi p}{T}\right) \tag{1.13}$$

equation (1.13) means that the frequency characteristic of the sampled sequence $x(n)$ is a scaled sum of an infinite number of frequency-shifted replicas of the frequency characteristic of the corresponding continuous-time signal $x_a(t)$. Equations (1.13) will be used in the subsequent chapter.

1.2. 3.2 Decimation

The reduction of a sampling rate is known as decimation, this operation consists of filtering and downsampling. Only down sampling will be considered in this work. Fig. 1.6 shows decimation process.

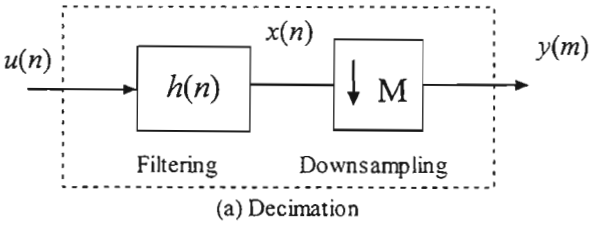

(a) Decimation

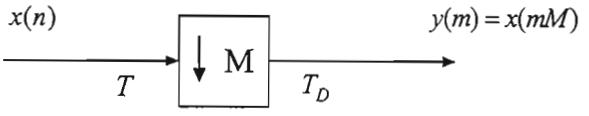

(b) Downsampling

Figure 1.6: An illustration of the Decimation operation

where $T_D = MT$. Downsampling reduces the input sampling rate by an integer factor M, known as the downsampling factor. The output signal $y(n)$ is called a downsampled signal and is found by taking only every M-th sample of the input signal and discarding all others, hence $y(m) = x(nM)$. The details of down sampling is given in [1-6, 12]. Downsampling operation is not an invertible operation, since it requires setting some of the samples to zero. In other words, $x(n)$ cannot be recovered from $y(m)$ exactly. We can, however only compute an approximate value. The downsampling in general can be envisioned mathematically as follows

$$Y(e^{j\omega T_D}) = \frac{1}{M}\sum_{m=0}^{M-1} X\left(e^{j(\omega T_D - 2\pi m)/M}\right)$$
$$= \frac{1}{M}\sum_{m=0}^{M-1} X\left(e^{j(\omega T - 2\pi m/M)}\right) \tag{1.14}$$

The downsampling is a linear and time-varying operation; the proof is given in [12].

1.2.3.3 Interpolation

The process of increasing the sampling rate is called interpolation and it also consists of upsampling and filtering. Fig. 1.7 shows an interpolation procedure. Again, only the upsampling operation will be discussed here. Upsampling increases the sampling rate by an integer factor M, by inserting $M-1$ equally spaced zeros between each pair of samples,

$$y(n) = \begin{cases} x(n/M), & for\ n = mM \\ 0 & otherwise \end{cases} \tag{1.15}$$

where M is an interpolation factor.

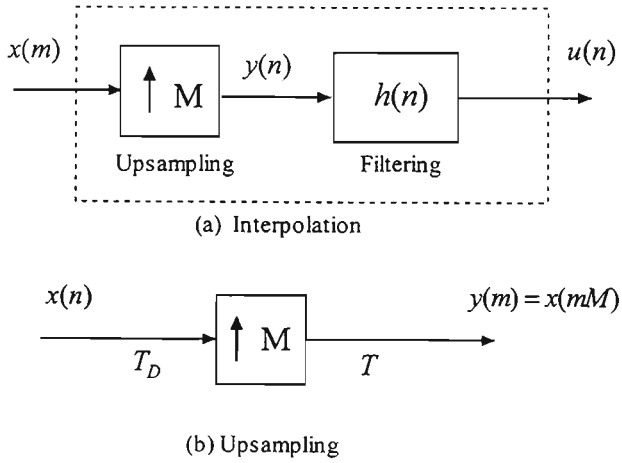

Figure 1.7: An illustration of the upsampling operation

The process of upsampling does not change the content of the input signal, and it only introduces the scaling of the time axis by a factor M. In frequency domain, the frequency scale is multiplied by M. The

operation of upsampling, unlike downsampling, is invertible. The Fourier transform of (1.15) can be written as:

$$\begin{aligned} Y(e^{j\omega T}) &= \sum_{n=-\infty}^{\infty} y(n)e^{-j\omega Tn} = \sum_{n=-\infty}^{\infty} x(n/M)e^{-j\omega nTM/M} \\ &= \sum_{n=-\infty}^{\infty} x(n/M)e^{-j(\omega TM)(n/M)} = X(e^{j\omega TM}) \end{aligned} \tag{1.16}$$

hence, $Y(e^{j\omega T}) = X(e^{j\omega T_D}) = X(e^{j\omega MT})$. Upsampling operation is linear and time-varying, see details in [12].

1.3 Analog-to-Digital Conversion

Analog-to-digital converter (ADC) is a physical device that converts a voltage or current amplitude at its input into a binary code, representing a quantized amplitude value closest to the input. Analog-to-digital conversion consists of two processes or stages, (1) sampling and (2) quantization as shown in Fig 1.8. Fig. 1.9 depicts an analog-to-digital conversion of a signal, where sampled signal $x(n)$ is found by sampling an analog signal $x_a(t)$ equidistantly at $t = nT$ followed by quantization.

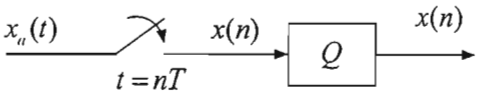

Figure 1.8: An illustration of analog-to-digital conversion

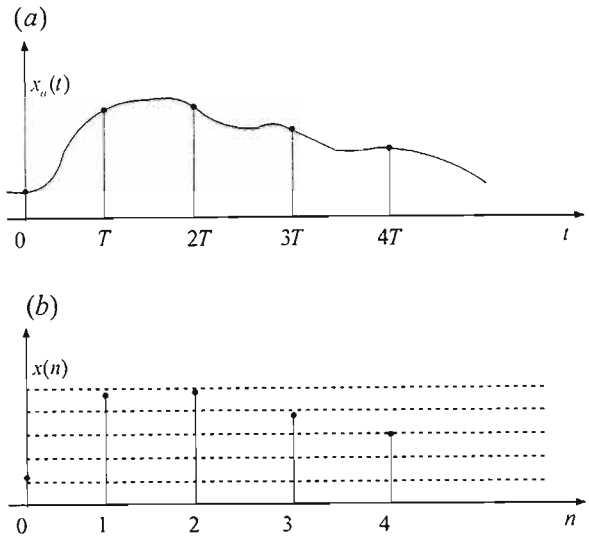

Figure 1.9: (a) Sampling of an analog signal $x_a(t)$. (b) Uniform quantization of the sampled signal $x(n)$

1.4 Introduction to Software Radio

A software radio is a wireless communications device that uses software, instead of hardware, to perform all of its signal processing and implement radio applications. By simply downloading a new program, a software radio is able to interoperate with different wireless protocols, incorporate new services and upgrade to new standards. In other words, SDR can be taken or defined as future proof radio that can be configured by software to operate in several radio systems simultaneously. A single communications device can operate within many different wireless systems by simply running different software. For example, a device can be reprogrammed to be an analog cellular phone, a digital personal communications system (PCS) phone, a cordless home phone or even a garage door opener, baby monitor or TV. In addition to incorporating multiple communication devices into one, a software radio can be easily upgraded to enable new standards and services, which is crucial in today's uncertain market. New waveforms can be implemented by software download without hardware changes. All functions of the radio are defined by software. Fig.1.10 illustrates the model of software defined radio. Fig. 1.10 however, is not an ideal software radio, since it includes intermediate frequency (IF) stage. Fig. 1.11 shows the evolution from traditional radios to software radio over time, further details are given in [16, 17].

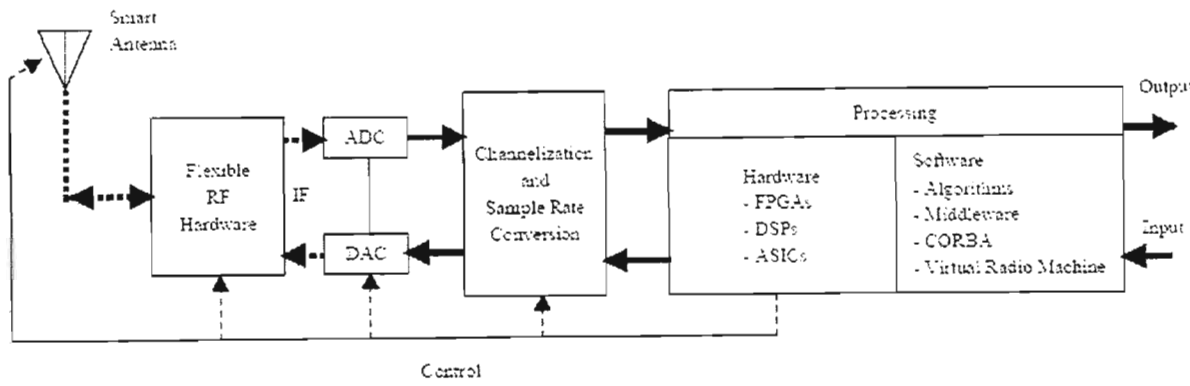

Figure 1.10 Software defined radio [1]

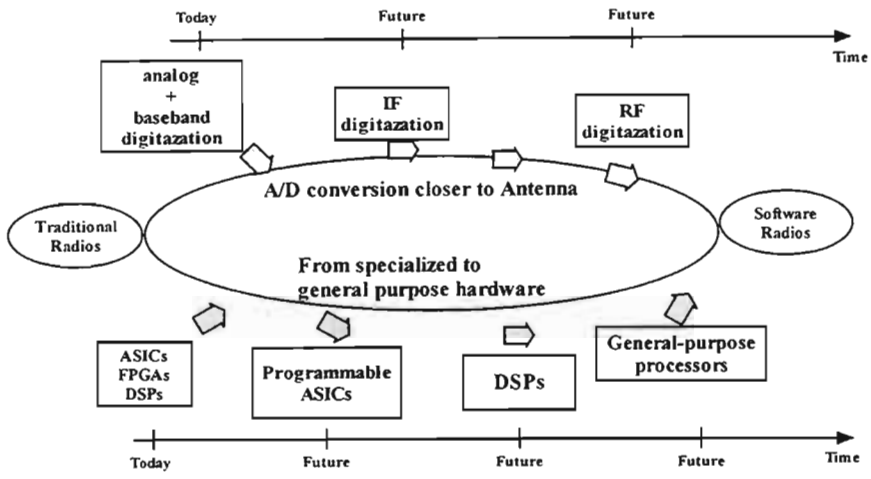

Figure 1.11: Possible model for evolution over time [16]

There are many problems in the realization of the SDR systems. Much higher demands are placed on implementation of handheld terminals than on the base stations. This is because the handheld terminals architecture requires low power dissipation, complexity, weight and small dimensions. It is very difficult to produce RF stage and antenna which are frequency independent. There is an antenna array solution for SDR base stations, but for handheld terminals other solutions are required. One of the weakest links in SDR architectures are ADCs, and our focus in this dissertation, is to propose and simulate an A/D conversion technique that will at least meet the minimum SDR requirements. The ADC is the most difficult component to select and is also the component that places the most constraints on the system design. Its limitation is likely to be the one to drive the overall architecture design. A trade-off must thus be made between the real limitations such as sampling rate, dynamic range, ADC resolution and lastly power consumption. Normally an ADC must sample a real signal under Shannon sampling theorem [13], in other words, sampling at a rate

that is at least twice the bandwidth of the signal, and in the case of multimode receivers, the highest bandwidth signal dictates the sampling rate. Another important issue to consider is that different signaling standards require different amount of dynamic range. The dynamic range is usually set by the amount of adjacent channel interference the system may encounter. Since proper selection of data converter is the most challenging steps in designing the software radio, the data converter will definitely be the determining factor for the performance of the overall radio design. It will also impact on the radio's power consumption, dynamic range, bandwidth and total cost. Many authors use the proximity of the data conversion process to the antenna as a way of judging how close a radio comes to being an ideal software radio [13-15]. This proximity will give an indication of the degree of the programmability that a radio can accommodate, because the closer the ADC is to the antenna, the higher the degree of programmability a radio can offer. In an ideal software radio, data conversion process occurs immediately after the antenna in the receiver chain. This implies that the ADC samples the RF signal and then completes the downconversion process entirely in the digital domain, thus alleviating the need for troublesome analog components. Data conversion at RF, places some rather extreme device constraints on the data converter; this implies that the data converter in general would need the following:

- a very high sampling rate to support wide signal bandwidths,
- a high number of effective quantization bits to support a high dynamic range,
- an operating bandwidth of several GHz to allow the conversion of a signal over a greatly varying (and theoretically arbitrary) range of frequencies,
- a large spurious-free dynamic range to allow for the recovery of small-scale signals in the presence of strong interferers while producing very little distortion,
- an ability to meet these above mentioned criteria without consuming an excessive amount of power and at a reasonable price.

These above mentioned demands exceed the capabilities of currently available technology. That is the reason why there is a need of RF conversion receivers that use analog preselection before the ADC (see Fig. 1.10). Moreover, that is the reason why receivers that perform data conversion at IF are far more prevalent due to fabrication and performance limitations of data converters. Because of the limitations of fabrication technology, priorities must be set and trade-offs must be made between the following parameters, bandwidth, dynamic range, power consumption and cost to find an acceptable design solution for both the data converter, and the entire radio system.

In the basic implementation of SDR, analog to digital conversion is required in the early stages of the receiver chain (as mentioned before). This means that the ADC has to sample signal on RF or IF, which requires high sampling rates (over 100 Msamples/S). High dynamic range of received signals orders high number of resolution bits. Today's technology offers converters with sampling rates of 1 Gsamples/s and resolution of 6-to-8-bits. With the resolution increasement, the sampling rate is decreasing exponentially. For 10-bits resolution commercially available sampling rate is 100 Msamples/s, and for 16-bits 150

Ksamples/s [17]. Therefore, high-speed, high-resolution A/D converters are required in future wideband communications systems, including software radios. The required sample rates for SDR is over 100 Msamples/S with a dynamic range corresponding to 14-to-16-bits. Furthermore, for mobile terminals the power consumption is a critical issue. Such high performance A/D converters might not be feasible with current technologies and are not expected to be feasible if current A/D converter techniques are used. New, innovative solutions are therefore required. For SDR a high-performance analog-to-digital conversion technique is needed. One of the schemes that could be used is a hybrid filter bank (HFB) based analog-to-digital converter (ADC) where two or more ADCs are operated in parallel. This technique gives rise to two classes, discrete-time hybrid filter banks ADC (DT HFB ADC), and CT HFB ADC. The latter class is the one that is proposed for SDR application in this work. Since, CT-HFB ADC is potentially more suitable for high-speed analog-to-digital conversion, we are recommending using it to meet minimum requirement for SDR application. This is due to the fact that analog filters are more suitable for high bandwidth signals than discrete-time filters [6] and this scheme is using the filter banks as a means of attaining high-resolution while at the same time having high-speed. This scheme is known in literature as hybrid filter bank analog/digital converter (HFB ADC) [9, 10, 19]. The preliminary work of HFB ADC is done in [9]. Generally, however, every technique, has its pros and cons. The problem with this technique is coming up with an efficient transformation for the analog analysis filter banks.

If one tries to design the HFB analytically, one needs to use some transformation(s), to convert from the continuous domain (the domain of the analysis filter bank) to digital domain (the domain of the synthesis filter bank), for instance *Z to S* domain. The problem with this technique(s), is that the transformation of order one is a bilinear transformation, which, in general, does preserve the magnitude response, but fail dismally to preserve the phase response. Since a good HFB requires a well matched frequency response, the bilinear transformation will not do the work. That is the reason why the author of [10] proposes the use of higher order transformations, by which the analog filters can be designed from digital prototypes. The problem with this is that the analog filter order becomes unacceptably high and the resulting distortion[1] and aliasing[2] are not satisfactory. These two problems are handled in [10]. One possible solution to deal with these difficulties is by using asymmetric filter banks as a way to attenuate the aliasing, resulting from mismatch errors (details in [9-11, 18-24]). It remains however, a challenge to every researcher in this field to come up with efficient design procedures for hybrid analog/digital filter. In [10] it is stated that at the moment no efficient design procedures for hybrid analog/digital filter banks with more than two channels exist. One of the reasons is that the design problem is quite difficult from an optimization point of view, so good initial solutions are necessary for successful design. This is the main objective of a design procedure, for instance to yield high-quality initial solutions to further optimization [9]

[1] The distortion function describes how the unshifted version of the input signal is distorted as it propagates through the system.

[2] On the other hand, aliasing function determines how much of the undesired, aliased versions of the input signal frequency response will appear in the output frequency response.

1. 5 Review of A/D Conversion Techniques

The microelectronic (r)evolution that took place over the last four decades has affected many domains of our daily life. It has absolutely left its footprints in the field of analog-to-digital conversion (ADC). Data converters like ADCs form the interface between the analog world and the digital world and hence have to cope with many adverse effects and limitations of the real world, such as component noise, clock jitter, non-linear device characteristics, etc. This implies that no matter how complicated a system one devices, the performance of ADCs will always be limited by a physical deficiency of an element or device, which is assessed in terms of resolution and conversion rate [12,13]. To date, there are several existing analog-to-digital conversion techniques, which can be categorized as flash converters (parallel structures), subranging and successive converters (iterative structures), oversampling sigma-delta converters, time-interleaving and the recent one which belongs to parallel ADC with filter banks known as hybrid quadrature mirror filter bank(HQMF ADC) as well as hybrid filter bank (HFB ADC, the most recent one) .

1.5.1 Parallel Structures (Flash ADC)

A flash ADC is made up of two basic components, comparators and encoder. Flash ADC is the fastest architecture available. Block diagram of this structure is shown in Fig. 1.12. The analog input signal produced by sample and hold circuit is applied simultaneously across the entire bank of comparators. Fast 8-bit flash ADCs exist with sampling rates as high as 1.5GS/s, but it is much harder to find a 10-bit flash, because the number of comparators goes up by a factor of 2 for every extra bit of resolution, at the same time the comparator has to be twice as accurate [12,13, 25-27].

The key objective of a comparator is to make a decision whether or not an input voltage is larger than a reference voltage. The comparator output is logic 1 or 0, depending upon the result of the comparison. In order for a comparator output to be logic 1 or 0, the input must be sufficiently large to push it to one direction or the other, towards a decision. The fact is there will be always a non-zero probability where the input will be such that a comparator is unable to make a decision. When this happens, a metastable output has occurred. This metastable occurs when a digital output of a comparator is ambiguous (neither a one nor a zero), therefore defining output as metastable. This problem can be reduced by allowing more time for regeneration. Gray-code encoding can also greatly improve this problem. Gray-code encoding allows only one bit in the output to change at a time. The comparator outputs are first converted to gray-code encoding and then later decoded to binary if desired. This problem which results in a metastable output is known as metastability (here another problem occurs when a metastable output drives two distinct circuits. It is

possible for one circuit to declare the input a "1" while the other circuit thinks it's a "0". This can create major errors. To avoid this, only one circuit should sense a potentially metastable output). Since the decoder only takes 1 or 0, in the case of metastable condition, the result can be catastrophic. Because the decoder may decide that the input is closest to a reference that is far from the correct one. Consider the case where an input is near the bottom-most reference voltage and a metastable condition occurs in the comparator associated with that reference. The metastable output level from this comparator into a decoder may result in the decoder decision that the input is nearest the top-most reference. Such output codes that are far away and seemingly unrelated to the actual output code, are called sparkle codes. Normally, the comparator outputs will be a thermometer code, such as 00011111. Errors may cause an output like 00010111 (i.e., there is a spurious zero in the result). This out of sequence "0" is called a sparkle. This may be caused by imperfect input settling or comparator timing mismatch. The magnitude of the error can be quite large. Modern converters employ an input track-and-hold in front of the ADC along with an encoding technique that suppresses sparkle codes.

Flash ADCs are very prone to sporadic and erratic outputs which have two major sources. The first one is the metastability and the second, thermometer-code bubbles. Mismatched comparator delays can turn a logical 1 into 0 or vice versa, causing the appearance of bubbles in an otherwise normal thermometer code (thermometer code is the code coming out of the comparators as shown in Fig. 1.12). The encoder unit cannot detect this error; it will just generate an out-of-sequence code (output spark). These problems however, can be greatly reduced or avoided. The main disadvantage of this approach is that it requires a large number of comparators that are carefully matched and properly biased to ensure that the results are linear. Since the number of comparators needed for an n-bit resolution ADC is equal to 2^{n-1}, this limits the physical integration and input loading, keeping the maximum resolution fairly low. For example, a 4-bit ADC requires 15 comparators, an 8-bit ADC requires 255 comparators, and a 16-bit ADC would require 65,535 comparators.

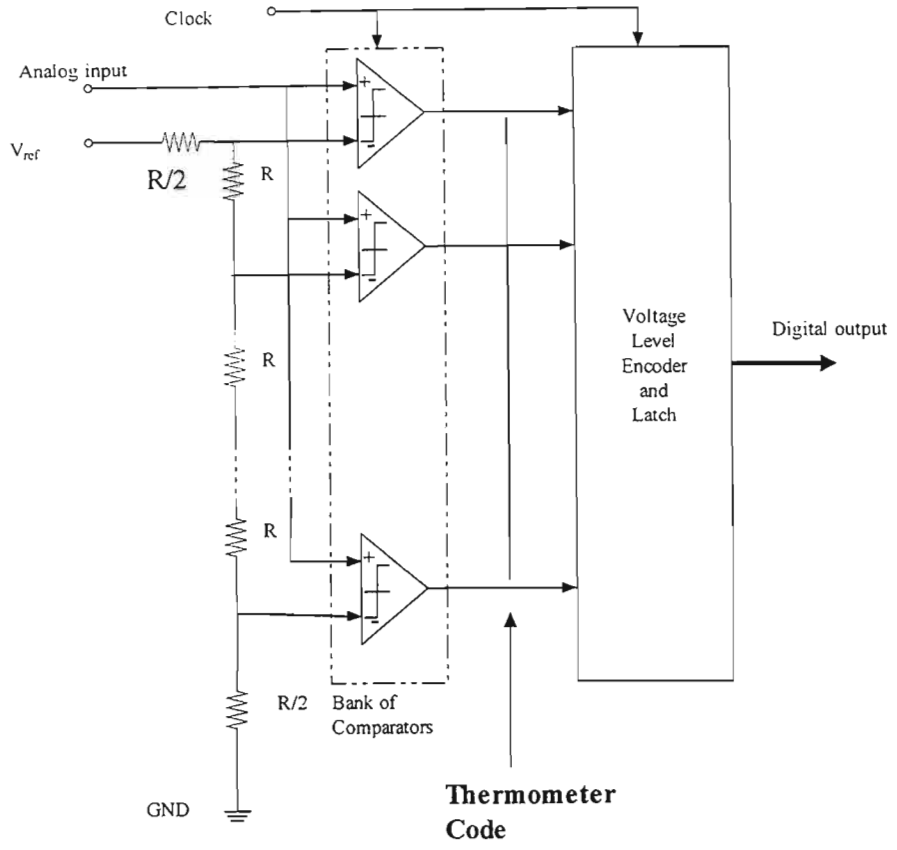

Figure 1.12: n-bit Flash ADC

1.5.2 Iterative Structures (SAR ADC and Subranging ADC)

The aim of the iterative structures is to reduce the complexity of a parallel structure by converting at first the signal using a data converter with a resolution of less than B bits, which is the final desired resolution. The result of the first stage of converting the signal forms a number of the most significant bits (MSBs) of the digitized signal and regenerates an analog signal that is subtracted from the input of this stage. This residual signal is then quantized again and the entire process is repeated until the desired signal level of precision is achieved [12, 13, 25, 26]. In iterative structure the process is carried out in serial rather than in parallel, but it achieves the reduction in complexity by splitting the signal into MSB and least significant bit (LSB) components.

1.5.2.1 Successive Approximation ADC

The successive approximation ADC, pictured in Fig. 1.14, attempts to generate an analog signal that closely approximates the analog input by iteratively refining the signal generated by the successive approximation register (SAR) and DAC. SAR ADC is the choice for medium-to-high-resolution applications with sample rate fewer than 5 Msps; they commonly range in resolution from 8-16 bits and provide low power [27]. Fig. 1.13 shows the feasible resolution, and maximum sample rate of SAR ADCs. A successive approximation ADC has a DAC, Track/Hold and SAR register with N-bit register in a single circuit; it works by using a DAC and a comparator to perform a binary search to find the input voltage. A sample and hold circuit (S&H) is employed to sample the analog input voltage and hold the sampled value whilst the binary search is performed. The binary search starts with the MSB and works toward the LSB for N-bit output resolution, this implies N comparisons are needed in the binary search, taking at least N clock cycles. If the sampled analog voltage is greater than the output of the DAC, the logic one is the output, or otherwise zero. In the SAR ADC there are two critical components, the comparator and the DAC, which contributes in limiting the speed of an ADC. Thereafter DAC is required and must settle to within the resolution of the overall converter, otherwise settling time contribute in limiting the speed of SAR ADCs, also the comparator must resolve small differences in analog input voltage (V_{IN}) and the V_{DAC} within the specified time (this implies that the comparator needs to be as accurate as the overall system). So the requirements of a comparator are speed and accuracy. Moreover, the serial nature of SAR ADC limits the speed to no more than a few Msps.

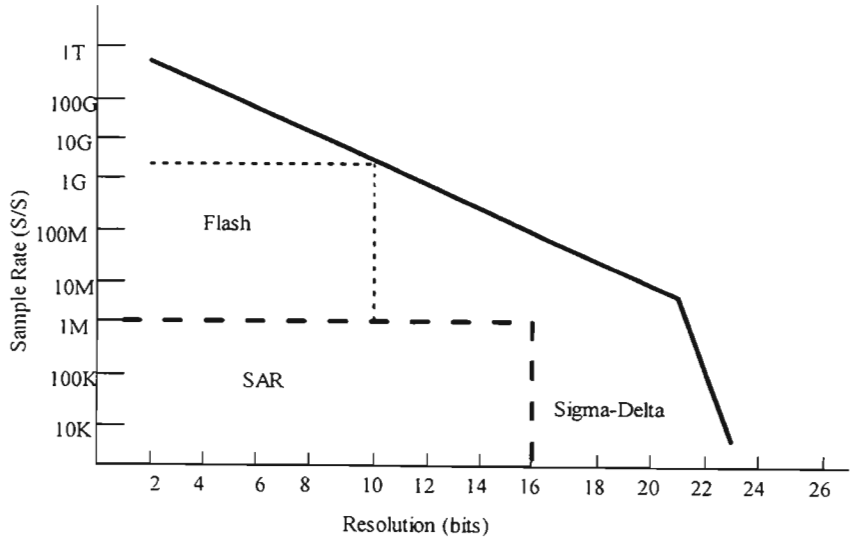

Figure 1.13: the graph showing the range of the SAR [1]

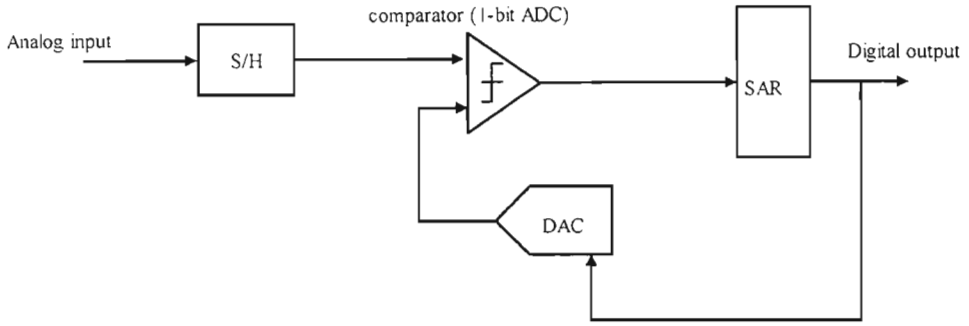

Figure 1.14: Successive approximation

1.5.2.2 Subranging ADC

Subranging ADC combines the ideas of the Flash ADCs and Successive approximation, and sometimes they are known as multi-step or half-flash converters. Sub-ranging ADCs reduce the number of bits to be converted into smaller groups, which are then run through a lower resolution flash converter. This approach reduces the number of comparators and reduces the logic complexity, compared to a flash converter. The tradeoff results in slower conversion speed compared to flash [4]. Subranging ADCs also implements the iterative structure, but using two distinct Flash ADCs, each with $B/2$ bits of resolution (half Flash converters). The description of operation can be simplified as follows: the analog signal is converted to the digital domain using B/2-bit Flash ADC; the output of this Flash converter forms the B/2 MSBs of the output signal. After the digital output of this converter is converted back to the analog domain using a B/2-bit DAC, a difference is found by subtracting the output of the DAC from the original input. This difference signal is scaled by a factor $2^{B/2}$ and converted by a different ADC with B/2-bits of resolution. This second ADC is used to form the LSBs at the output of the subranging structure. Again, like the SAR ADCs, the settling time limits the speed of the Subranging converters for the first stage of ADC and the subsequent DAC. In general, reducing the settling time degrades a data converter's performance [13, 25, 26, 27]. Subranging ADC uses fewer comparators than parallel structures, this implies that subranging draw less power, and it can attain higher resolution. Subranging ADCs can digitize at a speed of about 100 Msamples /s at 8-bit resolution. Subranging ADCs are in the same range as SAR ADCs. Block diagram of Subranging ADC is shown in Fig. 1.15.

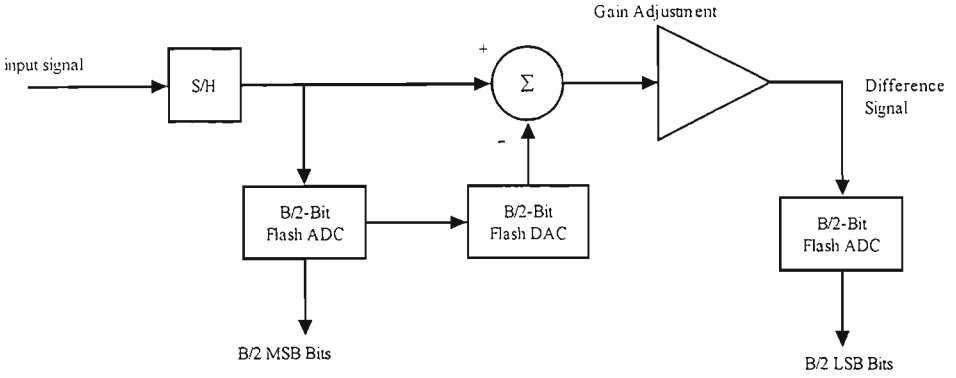

Figure 1.15: Subranging ADC

1.5.3 Pipelined ADC

Pipeline ADCs consist of numerous consecutive stages, each containing a track/hold (T/H), a low-resolution ADC and DAC, and a summing circuit that includes an interstage amplifier to provide gain. The generic Pipelined architecture, shown below builds upon the Subranging architecture by linking together multiple Subranging stages. For an N-stage Pipeline, each stage of the Pipeline will produce B/N bits where B is the total number of quantization bits produced by the Pipeline architecture. Each stage has a B/N bit ADC and DAC except for the last stage, which has only an ADC. One of the well known problems of Flash ADCs is that the number of comparators grows exponentially with the number of bits. The Flash ADC for N-bits will need $2^N - 1$. This problem of Flash ADC is alleviated by pipelined ADCs, which will need less number of comparators as compared to Flash ADC (i.e. pipelined ADCs will need the following number of comparators $N(2^{\frac{B}{N}}) + (N-1)\frac{B}{N})$, which less than $2^N - 1$. Fig. 1.16 illustrates the structure of a pipeline ADC.

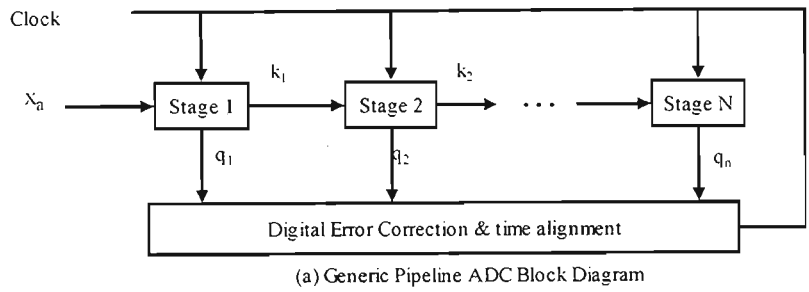

(a) Generic Pipeline ADC Block Diagram

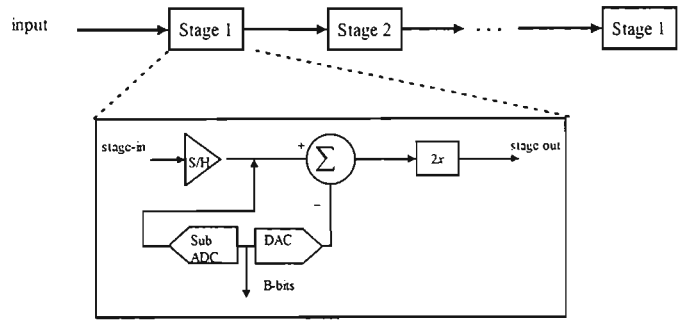

(b) Blocking diagram of components in each stage

Figure 1.16: Pipelined ADC

It is clear that the use of multiple stages can alleviate the exponential growth present in Flash topologies. Pipeline enables potentially faster conversion while avoiding the exponential growth of comparators. In pipeline architectures, the analog input is applied to the first stage in the chain, and ql bits are detected. The analog residue is also generated and applied to the next stage. This procedure repeats up to the end of the chain. The pipelined architecture offers a number of merits. First, the throughput rate is determined by the speed of only one stage in the pipeline. Second, interstage residue amplification relaxes the precision required of subsequent stages.

The main drawback of the conventional pipelined topology is the need for high precision in the interstage SHAs, DACs, and substrators especially at the front-end.

1.5.4 Sigma-Delta Structure (Sigma-Delta ADC)

The basic component of Sigma-Delta is a modulator, which consists of the following: a loop filter, a 1-bit quantizer, a summing node and a 1-bit DAC. The rest are for altering the data rate to appropriate rate. The difference between Sigma-Delta ADC and DAC is that the DAC implements its loop filter in the digital domain.

Sigma-Delta ADC uses oversampling; (as will be explained later). Considering the fact that every doubling of the sampling rate above the Nyquist rate a 3dB processing gain can be achieved, this can be shown by looking at equation below [3,13].

$$SQNR = 3\left(\frac{2^{2B}}{\eta}\right)\left(\frac{F_{So}}{2B_o}\right) \qquad (1.17)$$
$$= 6.02B + 4.77 - 10\log\eta + 10\log OSR\ dB$$

where B represents the quantization bits (number of bits), η is the ratio of the signal's peak power to its average power and OSR is the oversampling rate given as

$$OSR = \frac{F_{so}}{2B_o} \qquad (1.18)$$

with F_{S0} and B_0 being sampling frequency and bandwidth of input signal, respectively. Thus every doubling of oversampling rate, which implies doubling of F_{so}, the SQNR will improve by 3dB. For example, taking equation (1.17) and doubling OSR, we get

$$SQNR = 6.02B + 4.77 - 10\log\eta + 10\log(2*OSR)\ dB$$
$$= 6.02B + 7.78 - 10\log\eta + 10\log OSR\ dB \qquad (1.19)$$

Correlating (1.17) and (1.19), where in (1.19) the OSR is doubled (7.78-4.77 = 3.01 dB). This proves the point that every doubling of OSR results in 3dB improvement.

The problem will arise when higher effective number of bits (ENOB) values has to be achieved for instance 12-bits or greater than 12-bits from a 1-bit quantizer. This implies that the input signal has to be oversampled by a factor of over 4 million. For instance take WCDMA using bandwidths of 5MHz, a 1-bit data converter would have to sample at a rate of over 40 THz. This situation clearly shows that oversampling, though it's useful, but cannot provide adequate resolution. This provides two options that a data converter can have either a high resolution or a high conversion rate. Sigma-Delta solves this problem by using noise shaping technique.

Sigma-Delta conversion technology is based on noise shaping, decimation filtering, and oversampling. Sigma-Delta is predominantly based on digital signal processing, hence the cost of implementation will be

low and will continue to decrease. For Sigma-Delta conversion, since oversampling alone cannot provide enough resolution, Sigma-Delta technique uses oversampling coupled with noise shaping which assist in achieving high resolution [13]. The noise shaping properties of the Sigma-Delta converter is provided by the transfer function of the modulator. Oversampling basically spreads the quantization noise power over a bandwidth equal to the sampling frequency, which is much greater than the signal bandwidth. The modulator behaves as the lowpass filter on the signal and as a highpass filter on the noise, hence shaping the quantization noise in such a way that most of the energy will be above the signal bandwidth. The digital filtering stage then attenuates the out-of-band quantization noise and the downsampling brings the sampled signal to the Nyquist rate. The limitation of Sigma-delta converters is the complexity of the digital circuitry, which comes from the fact that the hardware has to operate at the oversampled rate, much larger than the maximum signal bandwidth. This limitation relegates or confines the converter to high-resolution, but at the expense of very low frequency applications operating at the range of about $1M$ (see Figure 1.13). The block diagram of first order Sigma-Delta ADC is shown in Fig 1.17. Moreover, the digital filtering stage in Sigma-Delta converters results in long latency between the start of the sampling cycle and the first valid digital output.

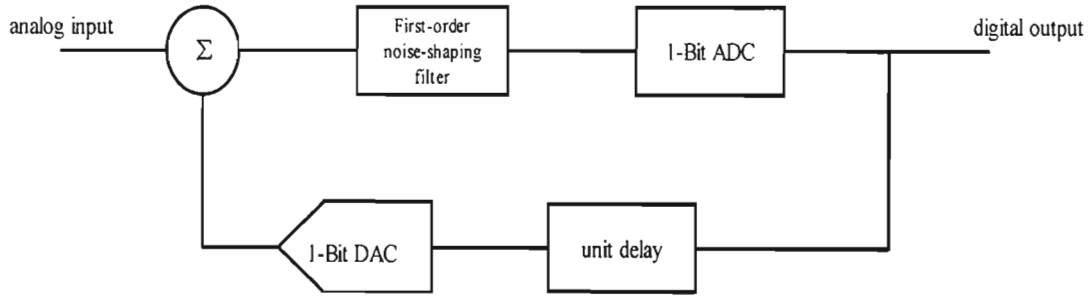

Figure 1.17: Sigma-Delta ADC (first order)

To show how the modulator shapes the quantization noise, consider the z-plane model of the first order Sigma-Delta modulator shown in Fig. 1.18

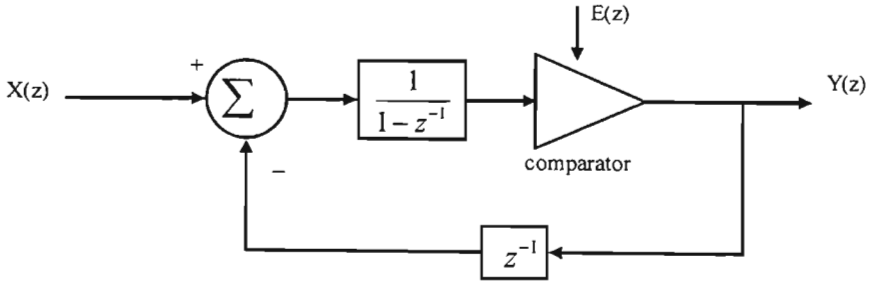

Figure 1.18: The Z-plane model Sigma-Delta ADC

It is assumed that the noise samples are uncorrelated. From the Fig.1.18, the Z-transform of the output is given by

$$\begin{aligned} Y(z) &= X(z)\left(\frac{1}{1-z^{-1}}\right) - Y(z)\left(\frac{1}{1-z^{-1}}\right) + E(Z) \\ &= X(z) + E(z)\left(1-z^{-1}\right) \end{aligned} \tag{1.19}$$

where $X(z)$ is the z-transform of the input signal, $Y(z)$ is the z-transform of the bit stream output, $E(z)$ is the z-transform of the quantization noise and $(1-z^{-1})$ is the noise transfer function. The equation (1.19) above shows that the output transform is the same as the input transform plus the quantization noise, modified by the noise transfer function. The noise transfer function is essentially the highpass filter with zero at d.c. Its effect is to push the quantization noise energy into the higher frequency spectrum. For the first-order SDM (Sigma-Delta Modulator), doubling the sampling rate increases the SNR (or SQNR) by 9dB, of which 6dB is attributable to the noise shaping and the other 3dB to the oversampling (this was proved before for oversampling). The author of [13] showed that the improvement, which can be achieved by oversampling in case of first order SDM is given by equation (1.20)

$$SNR_{improvement\,LP} = (6N+3)OSR\ dB. \tag{1.20}$$

The proof equation (1.20) can be shown by considering the following equation for SNR. It's given in [13] as follows

$$SNR = 10\log(\sigma_x^2) - 10\log(\sigma_e^2) - 10\log\left(\frac{\pi^{2N}}{2N+1}\right) + (20N+10)\log\left(OSR\right) \tag{1.21}$$

where σ_x^2 is the input signal power, N represent the order and σ_e^2 is the quantization noise power. Taking the last term $(20N+10)\log\left(OSR\right)$, then doubling the oversampling rate will result in the following

$$\begin{aligned} SNR_{improvement_{LP}} &= (20N+10)\log(2OSR) \\ &= (6.02N+3.01)dB. \end{aligned} \tag{1.22}$$

Therefore, doubling the sampling rate will improve SNR by ($6.02N+3.01$) dB (i.e. for first-order SDM, where N=1, then the gain will be, 9dB).This relationship shows that for 2nd order, there will be a gain of 15dB (where N represent the order of an SDM). Further reduction in quantization noise can be achieved by

increasing the order of the noise transfer function (i.e. the integrator). This can be shown that for an Nth order SDM the output transform is given by

$$Y(z) = X(z) + E(Z)\left(1 - z^{-1}\right)^{N}$$

In literature however, it is stated, that for N>3 the stability of the modulator cannot be guaranteed due to large phase shifts. For such SDMs with order higher than two, special configurations are used to avoid instability. One such arrangement is known as the MASH (which will not be discussed here). The graphs below show the effect of oversampling and noise shaping techniques over a nyquist converter.

Nyquist converter quantization noise spectrum is shown in below

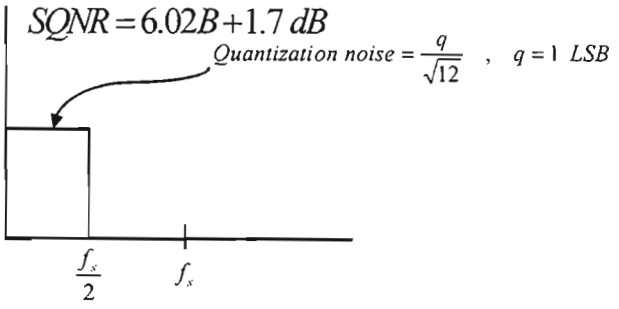

Figure 1.19: The block diagram showing Nyquist converter quantization noise

Oversampled converter quantization noise spectrum and noise shaping effect is shown in Fig. 1.20 (C is the oversampling ratio)

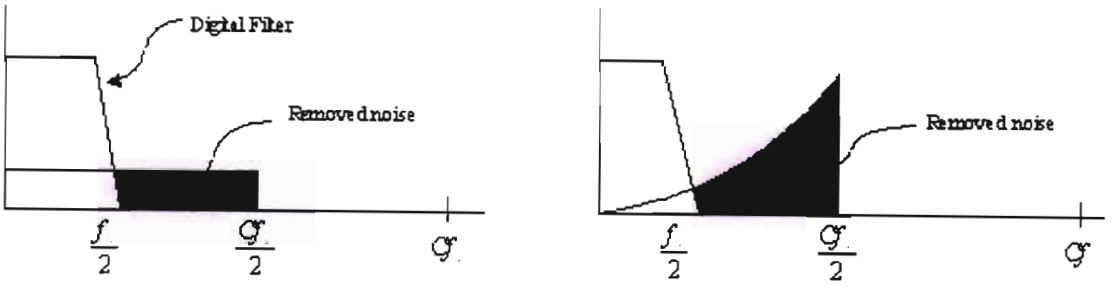

Figure 1.20: The block diagram showing oversampled converter quantization noise spectrum and the noise shaping effect

Table 1.1: The Comparison of Various Structures

	Flash (Parallel)	SAR (Iterative)	Pipeline (Iterative)	Sigma-Delta
Factors to be considered when	Ultra-high speed when power	Medium to high resolution (8 to	High speeds, few Msps to 100+	High resolution, low to medium

picking the ADC for certain application	consumption is not primary concern.	16bit), 5Msps and under, low power, small size.	Msps, 8-bits to 16-bits, lower power consumption than flash.	speed, no precision external components, simultaneous 50/60Hz rejection, digital filter reduces anti-aliasing requirements.
Conversion method	N bits - 2^N -1 Comparators caps increase by a factor of 2 for each bit.	Binary search algorithm, internal circuitry runs higher speed.	Small parallel structure, each stage works on one to a few bits.	Oversampling ADC, 5-Hz - 60Hz rejection programmable data output.
Conversion time	Conversion Time does not change with increased resolution.	Increases linearly with increased resolution.	Increases linearly with increased resolution	Tradeoff between data output rate and noise free resolution.
Resolution	Component matching typically limits resolution to 8-bits.	Component matching requirements double with every bit increase in resolution.	Component matching requirements double with every bit increase in resolution.	Component matching requirements double with every bit increase in resolution.
Disadvantages	Sparkle codes / metastability, high power consumption, large size, expensive.	Speed limited to ~5Msps. May require anti-aliasing filter.	Parallelism increases throughput at the expense of power and latency.	Higher order (4th order or higher) - multibit ADC and multibit feedback DAC.
Encoding method	Thermometer Code Encoding	Successive Approximation	Digital correction logic	Over-sampling modulator, digital decimation filter.
Size	2N-1 comparators, Die size and power increases exponentially with resolution.	Die increases linearly with increase in resolution.	Die increases linearly with increase in resolution.	Core die size will not materially change with increase in resolution.

1.6 Time-Interleave ADC

To increase the bandwidth of the A/D conversion, several A/D converters can be used in parallel. One ADC scheme that achieves such high sampling rate is time-interleaved ADCs (TI ADCs) [34-37], for which a number of converters, belonging to the categories above, work in parallel at a lower sampling rate. This enables an overall high sampling rate. The principle of TI ADC is depicted diagrammatically in Fig. 1.21

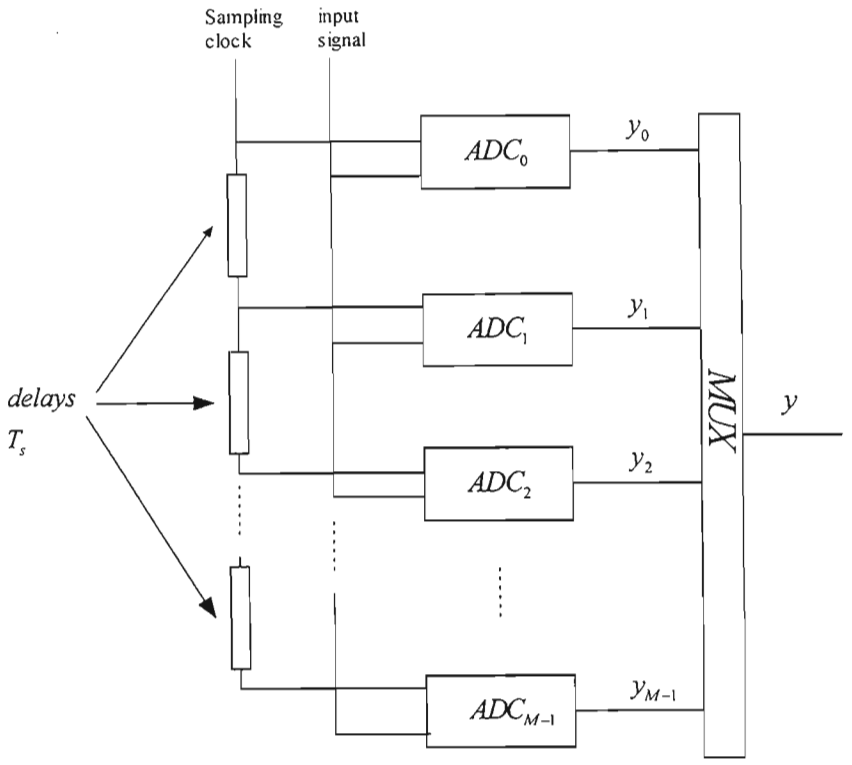

Figure 1.21: General structure of TI-ADC system

In this scheme the ADCs are interleaved in time so that the effective sampling frequency is M times higher if M ADCs are utilized. This kind of maneuvering, by exploiting the concept of parallelism, reduces the demands of conversion speed compared to a single ADC. However, the sample-and hold circuit must still be fast enough to track the signal that should be converted. In a TI A/D conversion each ADC works at $1/M$ of the desired sampling frequency f_s. The ADC is generally interleaved in time so that the k^{th} ADC takes samples at time instant $(k+nM)T_s$ where T_s is the sampling interval, which is defined as the inverse of the sampling frequency. This is fulfilled by a delay line from the clock to each ADC, with many ADCs in parallel the sampling rate can be increased a lot. In other words, the TI ADC works as follows: the input signal is connected to all ADCs and each ADC works with a sampling interval of MT_s,

where M is the number of ADCs in the converter array. The clock to k^{th} ADC is delayed with kT_s, this gives an overall sampling interval of T_s. There is however, a serious problem that arises because of having many ADCs. This problem is due to the sample-and hold circuit. To have a good signal quality the requirement on TI ADC scheme is that the sample-and hold circuit must be fast enough to track the high frequency parts of the input signal. Even if the sample-and hold is fast and good enough, the signal quality will impair or deteriorate in TI ADC architecture. This is due to different offsets in the different ADCs, for instance, the zero level is not the same for all converters. This problem causes the spurious harmonics in the output. Another reason is errors in the delay lines to different ADCs; the signals will be non-uniformly sampled.

The main drawback, however, is the limited dynamic range. This is due to channel mismatch errors, i.e. time errors known as static jitter (delay times of the clock between different ADCs are not equal, this means that the signal will be periodic but non-uniformly sampled), amplitude offset errors (the ground level differs between the different ADCs, this implies that there is a constant amplitude offset in each ADC), and gain errors (the gain from analog input to digital output, differs between the different ADCs). The effect of gain and offset errors in TI ADCs are analyzed in [38]. The timing errors are also studied in great details in [39]. The design of integrated analog circuitry, for example conventional data converters, has come to a stage where the performance of the implemented circuit is mostly limited by the errors introduced in fabrication (if a good design has been made) and the design effort is merely concentrated on minimizing the effect of such fabrication-induced errors. However, the minimization of the actual fabrication errors is sometimes not enough to meet the increasing requirements. The invention of new schemes and structures for data conversion is therefore necessary. Two such schemes for high-speed and high-resolution ADCs are the HFB ADC and TI ADCs with mismatch error correction [9]. The work that has been performed in this dissertation is designated to continuous-time hybrid filter bank CT HFB ADC.

1.7 Hybrid Filter Bank ADCs

High-speed, high-resolution analog-to-digital and digital-to-analog conversion is a critical technology in many modern electronic systems, such as radar systems and digital receivers for wireless communications. In general, high-speed, high-resolution converters enable wide bands of analog data to be converted to digital form to be processed more accurately and efficiently than is possible in analog form. Systems can be updated as requirements change and new standards arise by simply updating software to change the digital signal processing. A high-performance converter would significantly reduce the cost, size and power consumption of systems by eliminating much of the analog circuitry, while improving versatility and performance [6, 13, 19, 18, 24, 25, 28, 30-32, 40].

Using filter banks for analog-to-digital or digital-to-analog conversion is an unconventional application of the filter bank architecture that improves the speed and the resolution of the conversion over the standard time-interleaved array conversion technique [19]. In filter bank based converters, a discrete-time or analog analysis filter bank is used together with a digital synthesis filter bank. Such filter banks are known as hybrid filter banks (HFBs). The term hybrid is used because discrete-time or analog filters are used together with the digital filters, forming a hybrid filter bank system. Filter bank-based ADC scheme give rise to two classes known as hybrid discrete-time/digital filter banks (DT-HFB) and hybrid analog/digital filter banks (CT-HFB). The latter will be the one considered over the DT-HFB. Since CT-HFB ADC is potentially more suitable for high-speed analog-to-digital conversion. This is due to the fact that analog filters are more suitable for high bandwidth signals than discrete-time filters [18].

1.7.1 Hybrid Discrete-Time/Digital Filter Bank ADCs (DT HFB ADCs)

The basic principle of an M-channel DT HFB ADC is shown diagrammatically in Fig. 1.22

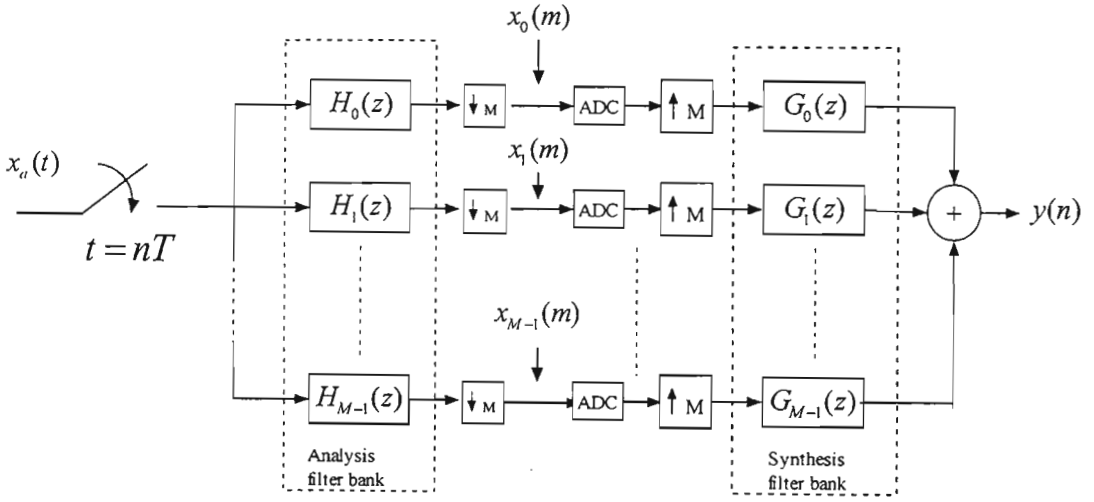

Figure 1.22: Block diagram of an M-channel DT HFB ADC

The DT HFB ADC was first proposed by Petraglia and Mitra (1992) and was incorporated in [11] (1993). The idea was further investigated by Velazquez in 1996, under a thesis title Hybrid Quadrature Mirror Filter Bank Approach to A/D conversion in [2]. Then in 1997, a further investigation on hybrid filter banks for analog/digital conversion was done in [19]. Recently, in 2002, further studies were performed and a detail survey of filter bank A/D converter was given in [18, 24, 30-32]. In the DT HFB ADC, the analog input signal $x_a(t)$ is sampled at the input of a discrete-time analysis filter bank with filters $H_k(z)$. The filter banks considered here are uniform-band that partitions the input signal frequency band into M

equally wide bands. Then the signal in each channel can be downsampled by a factor corresponding to the signal bandwidth without any loss of information. The subband signals are then quantized before they are upsampled by a factor of M and filtered through a digital synthesis filter bank with filters $G_k(z)$. Thereafter the output signal $y(n)$ is obtained by adding the corresponding subband output signals. DT HFB ADC has its advantages and disadvantages depending on the specification at hand.

DT HFB ADC has an obvious advantage that involves its realization. For instance, it is very easy and very simple to realize a DT HFB ADC, since the design behind it, is exactly the same as for maximally decimated filter banks, and the techniques for realizing the required discrete-time filter can be implemented with higher accuracy than what usually can be achieved by integrated continuous-time filters. Another advantage of DT HFB ADC is that the channel mismatch errors in terms of timing errors will not occur, since one sampling operation is performed-as illustrated in Fig. 1.22. The other error caused by static gain errors like aliasing will further be attenuated by filter banks.

The main drawback with the DT HFB ADC is that the sampling of the analog input signal, which is intrinsic in discrete-time filter banks, need to be performed with a sampling rate corresponding to the full bandwidth. This implies that any errors that are introduced during sampling operation will not be attenuated by the filter banks since the effect of the combined filter banks corresponds to a delay or an allpass function. Moreover, the maximum sampling rate of discrete-time filters is low and thus the DT HFB ADC class is not suitable for very high sampling frequency A/D conversion. It can be useful however, to use this scheme for lower sampling rates, but with higher requirements on the dynamic range. The disadvantages of DT HFB ADC are vitally important to consider, if the specification of the required systems are known. For instance, for our system SDR, the DT HFB ADC is not suitable for it, this is the reason why the major part of this work is focused on CT HFB ADC. CT HFB ADC is described below.

1.7.2 Hybrid Analog/Digital Filter Bank ADCs (CT HFB ADCs)

In the design of a CT HFB ADC, it is always assumed that the input signal is strictly bandlimited to $|\omega| < \pi / T$, this implies that the Nyquist criterion for sampling with effective sampling frequency of $1/T$ without aliasing is met. Therefore, it is very possible to, in principle completely eliminate aliasing by properly designing the filter banks (analysis and synthesis). The actual aliasing in the overall ADC will thus be determined by the anti-aliasing filter that must precede the filter bank. The aliasing will then be exactly equal to that of a single conventional ADC that uses the same anti-aliasing filter.

The principle of a CT HFB ADC is illustrated diagrammatically in Fig. 1.23.

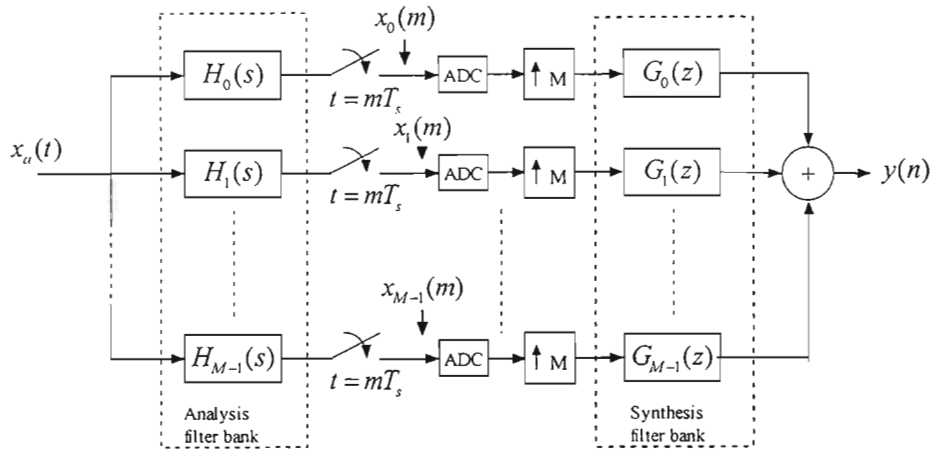

Figure 1.23: Block diagram of an M-channel CT HFB ADC

The main difference between the CT HFB ADC and DT HFB ADC is where the sampling operation takes place. In the CT HFB ADC, the analog input signal is directly fed into an analog analysis filter bank with filters $H_k(s)$. These are designed to be uniform-band and hence, each channel can be sampled at one M^{th} of the sampling frequency of the overall ADC. One important part to notice in this architecture is that the sampling operation takes place at the output of the analysis filters. Thus, static gain and timing errors that occur in the sampling process are attenuated by a combination of the filters of the analysis and synthesis filter banks. Another aspect to note is that the sampling of the signal in the lowpass channel is a lowpass sampling process. The sampling frequency in that channel is larger than, or equal to, twice the highest component of the signal, therefore, the Nyquist criteria for lowpass sampling

$$2\pi f_{sample} = 2\pi/(MT) \geq \Delta\omega = \pi/(MT) \tag{1.23}$$

is met, this condition is showed in [2]. In the remaining channels, bandpass signals are sampled. This is due to the fact that the highest frequency components in each band,

$$2\pi k/(MT),\ k = 1,\ldots,M \tag{1.24}$$

are integer multiples of the signal bandwidth $\Delta\omega = \pi/(MT)$ and the sampling frequency in each channel is larger than or equal to twice the signal bandwidth. Therefore the Nyquist condition for bandpass sampling is also met. It is well known however, that with practical filters, a certain amount of aliasing will inevitably occur during sampling in all channels. This aliasing is controlled in the filter design. After sampling and quantization each subband signal is upsampled before filtered through a digital synthesis filter bank. The important factor to note is that each converter works with a reduced sampling rate. One of the reasons why CT HFB ADC was proposed over DT HFB ADC, is that analog filters are more suitable

for high bandwidth signals than discrete-time filters. Hence, the CT HFB is potentially more suitable for high-speed A/D conversion. Even though mismatch errors (gain and time-skew errors) will occur, the introduced aliasing will be attenuated by filters.

There are other vitally important elements to consider when analyzing and designing the HFB ADC. In order to properly design and understand HFB ADCs, a thorough analysis must be made. Important issues to be investigated are frequency response, including distortion and aliasing, quantization noise, requirements on the filters given certain requirements on the effective resolution, sensitivity analysis and reduction of channel mismatch-induced aliasing by using filter banks. Another issue to consider when designing the filter banks is a distortion function and several aliasing terms have to be optimized to meet some prescribed characteristics. For instance in the case of, the DT HFBs, the design problem is in fact the same as for purely digital maximally decimated filter banks. Whereas, it is possible for digital filter banks (and therefore also DT HFBs) to achieve perfect reconstruction (PR), but it appears to be impossible for CT HFBs if the analog filter bank is assumed to be realized using only lumped elements. If transmission lines are used as components, it would be possible to find CT HFBs with PR. The design of the analog/digital type is a more challenging task. The frequency responses of the analog filters, which are rational functions in $j\omega$, need to be matched with the frequency responses of the digital filters, which are rational functions of $e^{j\omega T}$,in order to simultaneously minimize both distortion and aliasing

Again, in order to minimize the hardware cost of the analog parts, we propose to use the same concept of asymmetric filter design procedures that was used in [10] and frequency response masking in the synthesis filter banks, where the analog part is designed independently of the digital filters. By first designing the analog filters, the complexity of these can be minimized, given that the frequency selective requirements due to the dynamic performance requirements of the HFB ADC, are met. Then, with a fixed analysis filter bank, the digital filters can be designed in order to meet the requirements on distortion and aliasing. Due to the possibility to minimize the complexity of the analog or discrete-time filters and the reduction of the number of design parameters, all of the HFB structures proposed in this work are asymmetric in the sense that the analysis and synthesis filter banks have different complexities.

1.8 Dissertation Outline

There are six chapters in this dissertation. In chapter 1, we introduced different available techniques for designing A/D converters. We presented basic building blocks with terminology used in subsequent chapters and gave a very brief introductory to software radio, stating the reason why we use the requirements on ADC imposed by software radio applications.

Chapter 2 is a literature survey on HFB. Firstly, we discussed an analysis of HFB ADCs that is essential for understanding and designing hybrid filter banks; this analysis gave the correct frequency response expression for CT HFBs. We also presented the frequency response of uniform DT HFB and CT HFB, respectively. Lastly, we discussed the properties of the distortion and aliasing occurring in HFB.

In chapter 3, we reviewed the design of Hybrid filter banks, but only considering the CT HFB ADC, this included the investigation on one of the fundamental aspect to the ADC performance, which is the noise (quantization) in the filter bank based ADCs. The analysis of the ADC performance is done by comparing the case of the conventional case with the multirate filter bank ADC, only concentrating on the numerical values for typical design for CT HFB. In this chapter we also investigated the spurious free dynamic range in the presence of static gain and time-skew errors.

In chapters 4 and 5, we focused on designing two channels of CT HFB ADC, one with the FIR synthesis filter bank and the other with the IIR synthesis filters. The dissertation proposed three combinations: use of IIR model filter and IIR masking filter, IIR model filter/FIR masking filter and FIR model filter/FIR masking filter (presented in chapter 5). To show the advantages of our designs, we considered the cases of designing the synthesis filter as one filter, either FIR or IIR. These two filters are used as base for comparison with our proposed designs (the use of masking response filter).

Finally, chapter 6 concludes the dissertation, highlighting its findings and suggesting areas where the work may be expanded upon. Main contributions of this dissertation include:

- ❖ The use of frequency-response masking with asymmetric hybrid filter bank is proposed, to mitigate or reduce the complexity of digital filters
- ❖ A thorough analysis of HFB ADC and a suitable structures and reliable design procedures for CT HFB ADC utilizing FRM technique

The following publications have resulted from this work:

- Phakathi S. E. and Dawoud D. S., *"Advanced Asymmetric Filter Bank Based ADC for Software Defined Radio Applications Utilizing Frequency-Response Masking (FRM) Approach"*, SATNAC 2004 [Southern African Telecommunication Networks and Applications Conference] 6 pages CD-ROM. [Conference Proceedings]
- Dawoud D S and Phakathi S E, *"Time-Interleaved Filter Bank A/D Converters"*, MICSA 2003 [The Military Information and Communication Symposium of South Africa] 8 pages on CD-ROM [Conference Proceedings].
- Dawoud D S and Phakathi S E, *" Advanced Filter Bank based ADC for Software Defined Radio Applications "*, IEEE AFRICON 2004, Gaberone, Botswana, September 2004.

CHAPTER 2

HYBRID FILTER BANKS

2.1 Hybrid Filter Bank Transfer Functions

One important aspect and also a very useful one when designing and analyzing filter banks in particular hybrid filter banks (HFBs), is its frequency response. The Fourier transform of the output signal $y(n)$ of the HFB can, in general, be formulated as the number of differently shifted replicas of the Fourier transform of the input signal $x_a(t)$, in frequency, these are also multiplied by different frequency dependent functions, which characterize the filter bank, these functions are known as distortion function and aliasing functions.

When designing the filter banks, a distortion function and a number of aliasing terms are very important. For instance, when using a discrete-time analysis filter bank, the design problem is in fact the same as for purely digital maximally decimated filter banks. In this instance, it is therefore possible to directly use expressions for the frequency response of the distortion function and aliasing terms of digital filter banks. For the hybrid analogue/digital filter bank, it is not possible to do so because the Fourier transform of the analogue filter is not periodic, and this fact was re-examined in [5, 6, 9, 10] and the corresponding equation for this case was derived. The corresponding formulas for the discrete-time/digital case are given in this chapter in order to give the clarity and point out the differences and similarities between DT HFB and CT HFB.

2.1 Hybrid Uniform-Band Analog/Digital Filter Banks

The continuous-time hybrid filter bank ADC (CT HFB ADC) employs continuous-time analogue analysis filters. $H_k(s)$ and a discrete-time digital Synthesis filters $G_k(z)$. In this type, an M-channel uniform-band CT HFB ADC takes an input signal, which is an analog signal. The important part to notice is that for CT HFB ADC the sampling occurs at the output of the analysis filters with a sampling frequency of $\frac{1}{T_s} = f_{sample} / M$, where T_s is defined as $T_s = MT$. In this type of ADC, both the sampling and quantizations are performed at the low rate f_{sample} / M. An M-channel uniform-band CT HFB ADC is shown in Fig. 1.23. Again ignoring the quantizations, the Fourier transform of the output signal $y(n)$ of the filter bank in Fig 2.1 can be obtained as follows:

$$Y(e^{j\omega T}) = \sum_{k=0}^{M-1} G_k(e^{j\omega T}) X_k(e^{jM\omega T}) \tag{2.1}$$

where

$$\begin{aligned} X_k(e^{jM\omega T}) &= X_k(e^{j\omega T_s}) \\ &= \frac{1}{MT} \sum_{l=-\infty}^{\infty} X_a\left(j\omega - j\frac{2\pi l}{MT}\right) H_k\left(j\omega - j\frac{2\pi l}{MT}\right) \end{aligned} \tag{2.2}$$

therefore equation (2.1) can be rewritten as

$$Y(e^{j\omega T}) = \frac{1}{T} \sum_{l=-\infty}^{\infty} V_l(j\omega) X_a\left(j\omega - j\frac{2\pi l}{MT}\right) \tag{2.3}$$

where

$$V_l(j\omega) = \frac{1}{M} \sum_{k=0}^{M-1} G_k(e^{j\omega T}) H_k\left(j\omega - j\frac{2\pi l}{MT}\right) \tag{2.4}$$

When designing hybrid CT HFB it is convenient to assume that the input signal is strictly bandlimited to $|\omega| < \pi / T$. Since the bandlimitation assumption is important, it is a necessary condition to show how the frequency responses are affected by this assumption.

2.1.1 Bandlimitation [3, 4]

The Bandlimitation assumption affects the input signal as well as the analysis filters. This assumption assumes that if the input signal is bandlimited to $|\omega| < \pi / T$, then the bandlimited signal is defined as follows:

$$X_B(j\omega) = \begin{cases} X_B(j\omega), & |\omega| < \pi/T \\ 0, & |\omega| \geq \pi/T \end{cases} \tag{2.5}$$

where X_B is the bandlimited signal, the analysis filters will then be defined as

$$H_{Bk}(j\omega) = \begin{cases} H_k(j\omega), & |\omega| < \pi/T \\ 0, & |\omega| \geq \pi/T \end{cases} \tag{2.6}$$

hence, the output of the system is now given as

$$Y(e^{j\omega T}) = \frac{1}{T}\sum_{l=-\infty}^{\infty} V_{Bl}(j\omega) X_B\left(j\omega - j\frac{2\pi l}{MT}\right) \tag{2.7}$$

where

$$V_{Bl}(j\omega) = \frac{1}{M}\sum_{k=0}^{M-1} G_k(e^{j\omega T}) H_{Bk}\left(j\omega - j\frac{2\pi l}{MT}\right) \tag{2.8}$$

Then for CT HFB, it suffices to consider $Y(e^{j\omega T})$ in $-\pi \leq \omega T \leq \pi$. The benefit here is that in this region, only a finite number of terms in the summation of (2.7) needs to be considered since $X_B(j\omega)$ and $H_{Bk}(j\omega)$ are bandlimited as in (2.5) and (2.6).

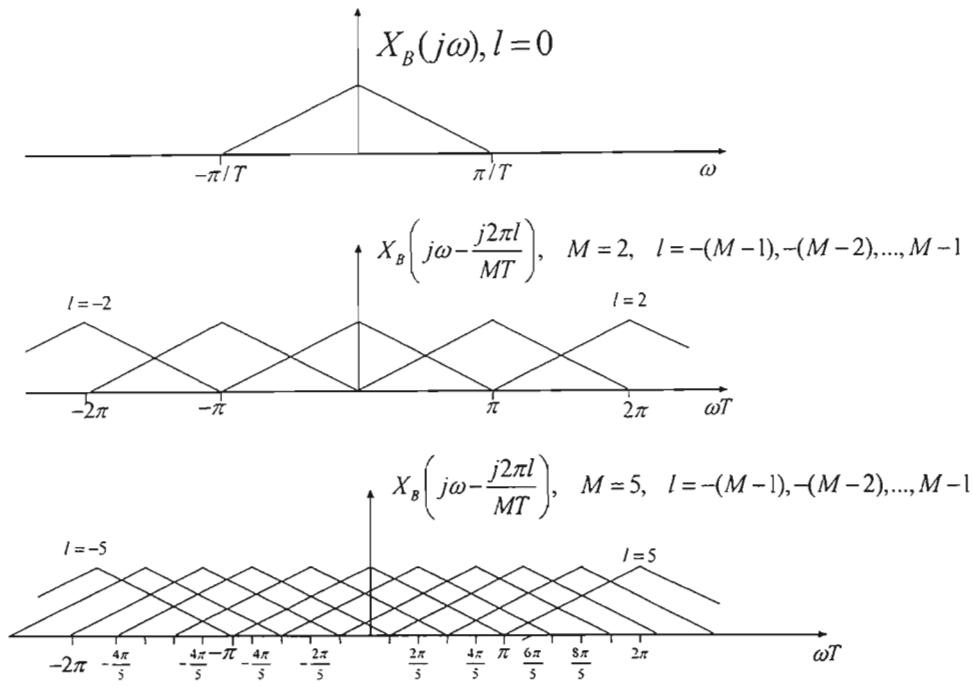

Figure 2.1: Illustration of aliasing

For the sake of simplicity it is assumed that all $H_k(j\omega)$ and $G_k(e^{j\omega T})$ are equal to one, then considering (2.7), only $X_{Bl}(j\omega)$ is left in the summation over l which basically gives Fig. 2.1. We catered only for $M=2$ and $M=5$ as illustrated in Fig.2.2 (From Fig. 2.1 we only need to include $l=-(M-1),...,M-1$ terms, this holds true for arbitrary values of M, thus, in the interval $-\pi \le \omega T \le \pi$, the terms that are beyond the lower and the upper bound are discarded, given as follows $2\pi l/M+\pi \le -\pi$ and $2\pi l/M-\pi \le \pi$, which are lower and upper bound, respectively). Bandlimiting the signal changes equation (2.7), takes the form

$$Y(e^{j\omega T})=\frac{1}{T}\sum_{l=-(M-1)}^{M-1} V_{Bl}(j\omega)X_B\left(j\omega-j\frac{2\pi l}{MT}\right), \quad -\pi \le \omega T \le \pi \tag{2.9}$$

The component $V_{B0}(j\omega)$ from (2.9) is the frequency response of the distortion, term whereas the other remaining terms $V_{Bl}(j\omega)$ are the frequency responses of the aliasing components. Then for the sake of simplicity we can just drop the subscript B from (2.9), then the frequency response expression becomes

$$Y(e^{j\omega T}) = \frac{1}{T}\sum_{l=-(M-1)}^{M-1} V_l(j\omega)X_a\left(j\omega - j\frac{2\pi l}{MT}\right), \quad -\pi \le \omega T \le \pi \tag{2.10}$$

with V_l expressed as follows,

$$V_l(j\omega) = \frac{1}{M}\sum_{k=0}^{M-1} G_k(e^{j\omega T})H_k\left(j\omega - j\frac{2\pi l}{MT}\right) \tag{2.11}$$

The bandlimitation assumption has some effect on the following conditions of perfect reconstruction (PR), near perfect reconstruction (NPR), perfect magnitude reconstruction (PMR), and near perfect magnitude reconstruction (NPMR). This can be clarified more easily using equations (2.12) to (2.15). A system is said to be a PR system if for an integer c and non-zero constant k, the output signal is a scaled and delayed version of the input signal, i.e. $y(n) = kx(n-c)$. Then a PR CT HFB is only obtained only if:

$$V_l(j\omega) = ke^{-j\omega Tc} \quad l = 0$$
$$V_l(j\omega) = 0, \quad l \neq 0 \tag{2.12}$$

A PMR case is obtained if the magnitude response of the distortion function is constant and the aliasing function is zero, therefore the condition is written as:

$$|V_l(j\omega)| = k, \quad |\omega T| \le \pi \text{ and } l = 0$$
$$V_l(j\omega) = 0, \quad l \neq 0 \tag{2.13}$$

This implies that, as in this case, there is no magnitude distortion, though there is phase distortion. The filter banks can also be designed in such a way that the PR and PMR are approximated. In the case of approximated PR, we termed such filter banks as NPR filter bank and is obtained by considering the following conditions.

$$\begin{aligned} &|V_l(j\omega)| \approx k, \quad |\omega T| \le \pi \; and \; l = 0 \\ &\arg[V_l(j\omega)] \approx \omega Tc, \quad l = 0 \\ &|V_l(j\omega)| \approx 0, \quad l \neq 0, \quad |\omega T| \le \pi \end{aligned} \tag{2.14}$$

If the requirement on the approximately linear phase response of the distortion term is relaxed, a NPMR is obtained, which can be written as

$$\begin{aligned} &|V_l(j\omega)| \approx k, \quad |\omega T| \le \pi \; and \; l = 0 \\ &|V_l(j\omega)| \approx 0, \quad l \neq 0, \quad |\omega T| \le \pi \end{aligned} \tag{2.15}$$

For CT HFB, there is one important comment to be made: it includes $-(M-1),...,M-1$ terms of aliasing, which is basically $2(M-1)$ aliasing terms. The reason is that the Fourier transform of analog signals is not periodic, thus, we need to consider more terms. For comparison reasons hybrid uniform-band discrete-time/digital filter banks class is described below, in order to show the difference between the hybrid uniform-band analog/digital filter banks and hybrid uniform-band discrete-time/digital filter banks, in terms of the aliasing terms that each need to include and to illustrate how bandlimitation condition alters the equation of the CT HFB to have similar expression of distortion and aliasing function.

2.3 Hybrid Uniform-Band Discrete-Time/Digital Filter Banks

The M-channel uniform-band DT HFB ADC is shown in Fig. 1.22. The input signal for DT HFB ADC to the filter bank is a discrete-time signal which, in practice, is obtained by sampling the analog signal $x_a(t)$ with the effective sampling frequency given by $f_{sample} = \frac{1}{T}$. In DT HFB ADC, the sampling is thus performed with full sampling frequency f_{sample}, whereas the quantizations occurring on ADCs in the Fig. 1.22 takes place at the low rate $f_{sample} / M = \frac{1}{T_s}$, where $T_s = MT$ and T is the sampling period of the output signal. Ignoring the quantizations, the Fourier transform of the output signal $y(n)$ of the filter bank, can be written as follows:

$$Y(e^{j\omega T}) = \sum_{k=0}^{M-1} G_k(e^{j\omega T}) X_k(e^{jM\omega T}) \tag{2.16}$$

where

$$\begin{aligned} X_k(e^{jM\omega T}) &= X_k(e^{j\omega T_s}) \\ &= \frac{1}{M}\sum_{l=0}^{M-1} X(e^{j(\omega TM - 2\pi l)/M}) H_k(e^{j(\omega TM - 2\pi l)/M}) \end{aligned} \tag{2.17}$$

then (2.1) can be written as

$$Y(e^{j\omega T}) = \frac{1}{M}\sum_{l=0}^{M-1} V_l(e^{j\omega T}) X(e^{j(\omega TM - 2\pi l)/M}) \tag{2.18}$$

where

$$V_l(e^{j\omega T}) = \frac{1}{M}\sum_{k=0}^{M-1} G_k(e^{j\omega T}) H_k(e^{j(M\omega T - 2\pi l)/M}) \tag{2.19}$$

From equation (2.1.9), there are two components that are very important, the first one occurs when $V_0(e^{j\omega T})$ known as the frequency response of the distortion term and the second one occurs when $V_l(e^{j\omega T}), l = 0$ known as the frequency responses of the aliasing terms. The first component corresponds to the gain and phase of the filter bank, whereas the latter one corresponds to the aliasing errors in the filter bank.

In literature there are also four cases that could be realized with DT-HFB ADC, which are *perfect reconstruction* case, *perfect magnitude reconstruction* case, *near perfect reconstruction* case, and near *perfect magnitude reconstruction* case.

A perfect reconstruction (PR) DT HFB is only obtained only if

$$\begin{aligned} V_l(e^{j\omega T}) &= ke^{-j\omega Tc}, \quad l = 0 \\ V_l(e^{j\omega T}) &= 0, \quad l \neq 0 \end{aligned} \tag{2.20}$$

for an integer c and non-zero constant k. In this case, the output signal is a scaled and delayed version of the input signal, i.e. $y(n) = kx(n-c)$. A PMR case is obtained if the magnitude response of the distortion function is constant and the aliasing function is zero, therefore the condition is written as:

$$\begin{aligned} &\left|V_l(e^{j\omega T})\right| = k, \quad |\omega T| \le \pi \text{ and } l = 0 \\ &V_l(e^{j\omega T}) = 0, \quad l \ne 0 \end{aligned} \tag{2.21}$$

this implies, in this case, that there is no magnitude distortion, but there is phase distortion. The filter banks can also be designed in such a way that the PR and PMR are approximated. In this case, an approximated PR is termed NPR and is obtained by considering the following conditions.

$$\begin{aligned} &\left|V_l(e^{j\omega T})\right| \approx k, \quad l = 0, \quad |\omega T| \le \pi \\ &\arg\left[V_l(e^{j\omega T})\right] \approx \omega T c \\ &\left|V_l(e^{j\omega T})\right| \approx 0, \quad l \ne 0, \quad |\omega T| \le \pi \end{aligned} \tag{2.22}$$

If the requirement on the approximately linear phase response of the distortion term is relaxed, a near perfect magnitude reconstruction (NPMR) is obtained, which can be written as

$$\begin{aligned} &\left|V_l(e^{j\omega T})\right| \approx k, \quad l = 0, \quad |\omega T| \le \pi \\ &\left|V_l(e^{j\omega T})\right| \approx 0, \quad l \ne 0, \quad |\omega T| \le \pi \end{aligned} \tag{2.23}$$

Considering then (2.18 and 2.19) for DT HFB and (2.10 and 2.11) for CT HFB, one noticeable difference has to do with the number of terms that need to be considered for both classes, i.e. for DT HFB we only need $M-1$ terms, whereas for CT HFB we need $2(M-1)$ terms in the $-\pi \le \omega T \le \pi$. However, it is sufficient to only include M terms for CT HFB also, this is due to the fact that $X_B(j\omega)$ and $H_{Bk}(j\omega)$ are bandlimited as shown in subsection 2.2.1. Equation (2.9) can then be rewritten by introducing these two terms $X_B^s(j\omega)$ and $H_{Bk}^s(j\omega)$, which we define as a sum of two terms as follows:

$$X_B^s(j\omega) = X_B(j\omega) + X_B(j\omega + j2\pi/T) \tag{2.24}$$

and

$$H_{Bk}^{s}(j\omega) = H_{Bk}(j\omega) + H_{Bk}(j\omega + j2\pi/T) \tag{2.25}$$

Considering (2.5) and (2.6) the following holds,

$$X_B(j\omega)H_{Bk}(j\omega + j2\pi/T) = 0, \quad \forall\omega \text{ and } k = 0,1,...M-1 \tag{2.26}$$

and

$$H_{Bk}(j\omega)X_B(j\omega + j2\pi/T) = 0, \quad \forall\omega \text{ and } k = 0,1,...M-1 \tag{2.27}$$

as a result,

$$\begin{aligned} X_B^s(j\omega)H_{Bk}^s(j\omega) = {} & X_B(j\omega)H_{Bk}(j\omega) + \\ & X_B(j\omega + j2\pi/T)H_{Bk}(j\omega + j2\pi/T) \end{aligned} \tag{2.28}$$

then (2.9) becomes,

$$Y(e^{j\omega T}) = \frac{1}{T}\sum_{l=0}^{M-1} V_{Bl}^{s}(j\omega)X_B^s\left(j\omega - j\frac{2\pi l}{MT}\right), \quad -\pi \le \omega T \le \pi \tag{2.30}$$

where

$$V_{Bl}^{s}(j\omega) = \frac{1}{M}\sum_{k=0}^{M-1} G_k(e^{j\omega T})H_{Bk}^{s}\left(j\omega - j\frac{2\pi l}{MT}\right) \tag{2.31}$$

Equations (2.24) to (2.28) are introduced to maneuver the frequency responses in such a way that we get similar expression for distortion and aliasing function for both DT HFB and CT HFB, details are given in [10]. Then looking (2.9) and (2.30), we see that the two are very similar, when introducing (2.24) and (2.25). This offers a possibility to obtain similar expressions for the aliasing and distortion in both hybrid analog/digital filter banks and hybrid discrete-time/digital filter banks.

2.4 Distortion and Aliasing in HFB

Considering the frequency response of the output signal, it is clear that it depends on the distortion function $V_{l=0}(j\omega)$ and aliasing function $V_l(j\omega)$. Hence, it is vitally important to consider them when designing hybrid filter banks (HFBs). Equation (2.3) and (2.18), shows the dependence of the output signal on $V_{l=0}(j\omega)$ and $V_l(j\omega)$. The distortion function describes how the unshifted version of the input signal is distorted as it propagates through the system. On the other hand, aliasing function $V_l(j\omega)$, determines how much of the undesired, aliased versions of the input signal frequency response will appear in the output frequency response.

The requirement on combination of analysis filters $H_l(j\omega)$ and the synthesis filters $G_l(e^{j\omega T})$ during the design phase of HFBs is in such a way that the distortion function should have a small effect on desired output signal, while at the same time, it is important to control the undesired shifted versions of the input signal, the control part of the undesired shifted version is computed by aliasing function.

The main difference between the proposed scheme in this work, which is the continuous-time HFB and the discrete-time HFB ADC, can be described quite easily, in terms of what have been included in the summation as illustrated before in (2.10) and (2.18). In CT HFB, we require $2M-1$ terms in total, whereas in a DT HFB only $M-1$ terms are required in the frequency region. However, for each single frequency, the number of contributing aliasing terms is only M for CT HFB as well as DT HFB. Fig 2.2 illustrates the properties of (2.3) and the characteristics of the distortion and aliasing for CT HFB. Fig 2.2 can be used also for the case of DT HFB; the difference will be on the number of terms in the summation of the frequency response of the output signal.

The distortion term consists of the following $H_l(j\omega)G_l(e^{j\omega T})$, since $l=0$. This implies that such terms will be the product of two passband responses for frequencies where the individual filters have their passband and the product between two stopband responses elsewhere, except in transition regions, this is shown in Fig 2.2 (i) and (ii). (Fig 2.2 (iii) is a shifted version of the analog filter bank for $l=1$, then the aliasing term for $l=1$ is then obtained by taking the product of the magnitude response of Fig 2.2 (iii) and (ii) for every filter pair with index l, thereafter, the resulting result is shown in Fig 2.2 (iv) and (v), which illustrates that for every $l\neq 0$, in the frequency band of interest, in the region $\omega=[0,\pi/T]$, there exist always two $l=l_i,l_j$ where the product $H_l\left(j\omega-\frac{j2\pi}{MT}\right)G_l\left(e^{j\omega T}\right)$ have the overlapping transition regions). The remaining $M-2$ products have at least a passband response overlapping a stopband response or two overlapping stopbands. This is illustrated in Fig. 2.2 for $l=0,1$. In [10] it is stated that in

order to achieve small aliasing terms at the output of the hybrid filter bank ADC, the filter banks are to be designed in such a way that the overlapping transition regions in Fig. 2.2 (iv) and (v) are cancelled out. This implies that their magnitude responses are similar, but their phase responses differ by 180 degrees.

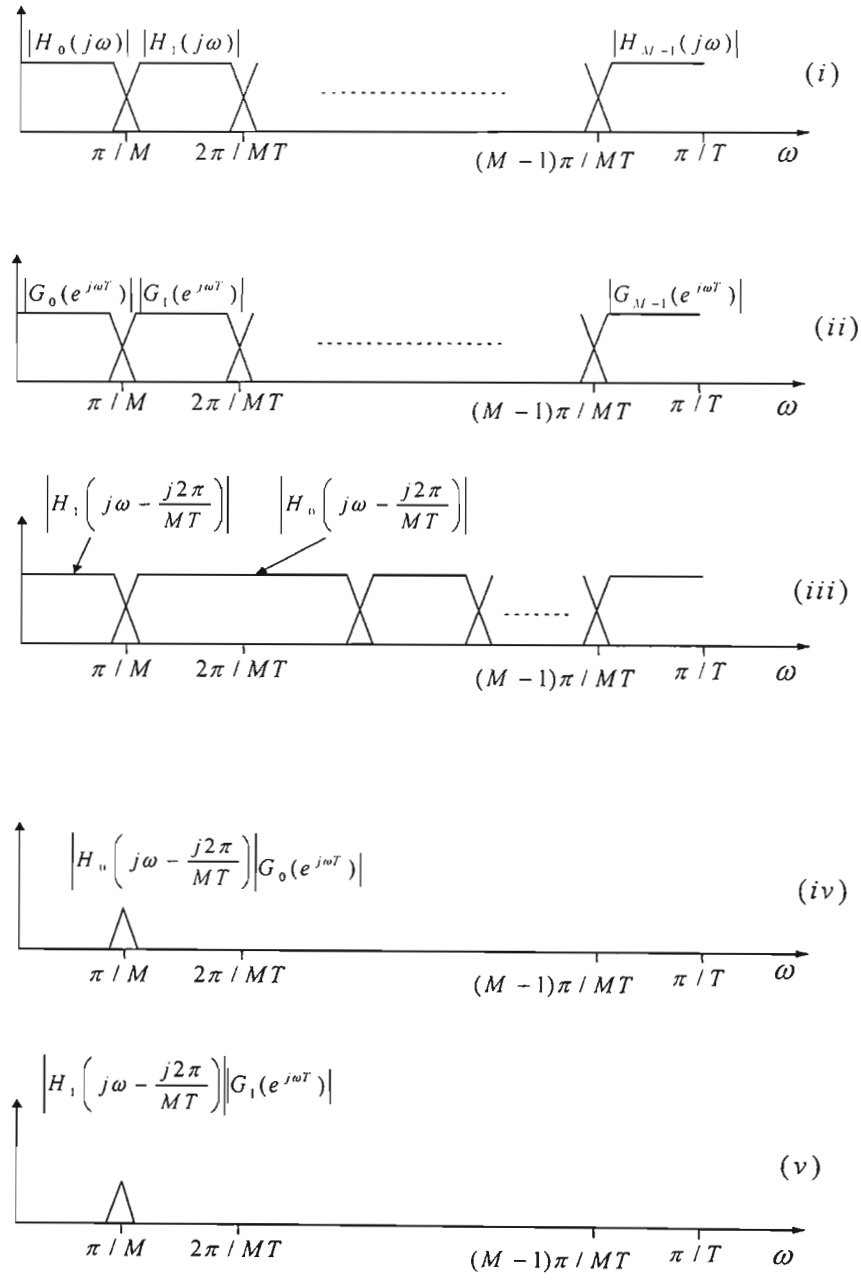

Figure 2.2: Magnitude responses of the M -channel uniform band CT HFB (i) Analysis filter bank. (ii) Synthesis filter bank. (iii) Shifted version of the analysis filter bank. (iv) The first overlapping transition regions. (v) The second overlapping transition regions [1,2,3].

2.5 Summary

Chapter 2 was a literature review on HFB. Firstly, we examined the importance of understanding the HFB transfer functions and its usefulness in designing and analyzing filter banks.

We then reviewed the design of DT HFB ADC and CT HFB ADC and showed how they differ from each.

Thirdly we investigated how we can use same functions for aliasing and distortion for DT HFB and CT HFB, by including the bandlimitation condition.

Finally, we discussed the properties of the distortion and aliasing occurring in HFB. This was also illustrated in Fig. 2.1, in particular for CT HFB, how many terms do we need to include in order to use similar aliasing function as for DT HFB.

CHAPTER 3

DESIGN OF HYBRID FILTER BANKS

3.1 Design of Continuous-Time Hybrid Filter Banks

In 1992, the first reported HFB ADC in literature was of a DT HFB and was designed employing a quadrature mirror filter bank known as QMF ADC [9]. This was followed by a thesis written by Velázquez on Hybrid quadrature mirror filter bank ADC (HQMF ADC) [2] in 1994. Recently, in [6, 11] three schemes were treated these including TI ADC, DT HFB ADC, and CT HFB ADC. For the DT HFB, the design problem is quite simple, since the design is the same as for purely maximally decimated filter banks, (see details on [6]).

The design of the CT HFB on the other hand is quite a challenging task. One of the reasons is that the frequency response of the analog filters are rational functions in $j\omega$, which is required to be matched with the frequency response of the digital filters, which are rational functions of $e^{j\omega T}$. This matching is very important and required in order to simultaneously minimize both distortion and aliasing.

Instead of designing the analog filters from digital prototypes as in [11], we design the system using design procedures in [6], where the analog part is designed independently of the digital filters. This is accomplished by first designing the analog filters, this way the complexity of these can be minimized, given that the frequency selective requirement due to the dynamic performance requirements of the HFB ADC are met. Then, with a fixed analysis filter bank, the digital filters can be designed in order to meet the requirements on distortion and aliasing. With the analog filters designed and fixed, the digital filters designed and optimized, by doing so, the minimization of the distortion and aliasing are achieved.

Another advantage of using this approach is that the complexity of optimization problem is reduced. Due to the possibility to minimize the complexity of the analog filters and the reduction of the number of design parameters.

All of the HFB structures proposed in this work are asymmetric as in [6], they are asymmetrical in the sense that the analysis and synthesis filter banks have different complexities.

3.2 Noise in the Filter Bank Based ADCs

In this section, we consider noise in the filter bank due to quantization, in literature there are two schemes that are treated, one is known as single rate and the other is multirate filter bank ADCs, here we only consider the latter. A single-rate ADC differs from the multirate in the sense of how sampling rate is

defined, in single-rate ADC scheme, all the subconverters work at the same sampling rate as the desired sampling rate, whereas in the multirate the converters work at a sampling rate which is M times lower than that of the effective sampling rate. In multirate ADCs the subconverters work in lower data rate as compared to single-rate ADCs. The purpose of this section is basically, to point out the difference between the multirate filter bank ADCs and the conventional one, in terms of quantization noise considering the narrowband signal as opposed to wideband signal. Different authors have worked on the effect of quantization noise in ADCs that consist of parallel arrays of analog-to-digital converters (including multirate ADCs), including Petraglia and Mitra (1991), Velazquez *e. al.* 1998 as well as in [10].

3.2.1 Conventional ADC

This subsection briefly gives A/D conversion and the quantization noise utilizing a conventional ADC. For a conventional ADC an input signal is assumed to be strictly bandlimited according to the following relation,

$$X_a(j\omega) = 0, \quad |\omega| \geq \pi / T \tag{3.1}$$

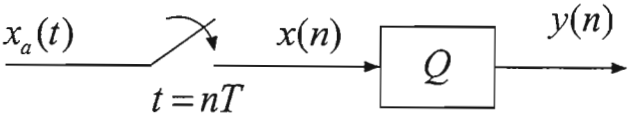

Figure 3.1: Conventional ADC showing Sampling and Quantization

Equation (3.1) shows that the Nyquist criterion for sampling with the desired sampling frequency of $1/T$ without aliasing is accomplished. A/D conversion consists of two important processes, namely sampling, which is followed by quantization, the sampling and quantization processes are depicted in Fig. 3.1. The sequence $x(n)$ is found by first sampling the analog input signal uniformly at the time instance, for all integers n as follows,

$$x(n) = x_a(t)\big|_{t=nT}, \quad n = \ldots, -1, 0, 1, \ldots \tag{3.2}$$

where T is the sampling period. The Fourier transforms of $x_a(t)$ and $x(n)$ are related to each other according to Poisson's summation formula as follows,

$$X(e^{j\omega T}) = \frac{1}{T}\sum_{k=-\infty}^{\infty} X_a\left(j\omega - j\frac{2\pi k}{T}\right) \tag{3.3}$$

One important fact to mention is that the spectrum of a sampled signal is always periodic with the periodicity of 2π. Hence, $X(e^{j\omega T})$ has the same periodicity with respect to ωT. This implies that it is sufficient to only consider the interval $-\pi \le \omega \le \pi$, and since the bandlimitation condition of (3.1) is considered, the following relation holds,

$$X(e^{j\omega T}) = \frac{1}{T}X_a(j\omega), \quad |\omega T| \le \pi \tag{3.4}$$

To do the analysis on the effect of the quantization, it is then customary to utilize the linear model of a conventional ADC depicted in Fig. 3.2,

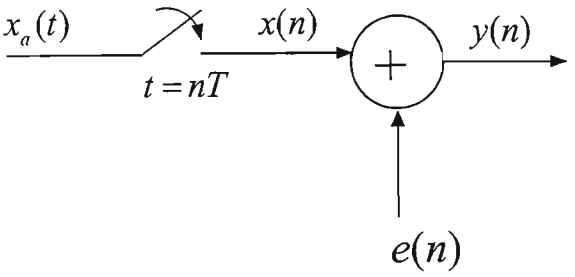

Figure 3.2: Conventional ADC showing linear model of Fig. 3.1.

where $e(n)$ is an error sequence that is modeled as stationary zero-mean white noise. The sequence $x(n)$ and $e(n)$ are assumed to be uncorrelated. The effect of quantization is usually measured by considering signal-to-noise ratio (SNR), which is given as:

$$SNR = 10\log_{10}(\sigma_x^2 / \sigma_e^2) \tag{3.5}$$

where σ_e^2 and σ_x^2 are variances of $e(n)$ and $x(n)$, respectively. This means σ_e^2 and σ_x^2 are the average noise power and signal power, respectively, provided the following assumption is made, that the average values of $e(n)$ and $x(n)$ are zero. Using Fig.3.2, the output sequence of the quantizer is given by

$$y(n) = x(n) + e(n) \tag{3.6}$$

The probability density function $p(e)$ is assumed to have a uniform distribution, for the uniform quantizer according to the following relation,

$$p(e) = \begin{cases} 1/Q, & |e| \le Q/2 \\ 0 & |e| > Q/2 \end{cases} \tag{3.7}$$

where Q represents the quantization step as given by

$$Q = X_p 2^{-(B-1)} \tag{3.8}$$

with $-X_p \le x(n) \le X_p - Q$ and B representing the number of bits of the quantizer. The values of X_p, which is known as full-scale (FS) level of the ADC, are determined in such a way that the overflow in the ADC does not occur. Hence, the variance of the error sequence $e(n)$ can be defined as

$$\sigma_e^2 = Q^2/12 \tag{3.9}$$

3.2.2 Multirate Filter Bank ADC

In this subsection, we are considering an M-channel multirate filter bank based ADC, according to the structure of CT HFB ADC with general quantizations. In this scheme the output sequence from the analysis filters are sampled and quantized at lower rates (M times lower), i.e. f_s/M, so as to attain the desired sampling rate, upsamplers are utilized after quantization.

In this scheme, the output signal $Y(e^{j\omega T})$ has a periodicity of 2π, with the input signal bandlimited according to (3.1). Ignoring the quantizations, the frequency response of output signal is given as

$$Y(e^{j\omega T}) = \frac{1}{T}\sum_{l=-(M-1)}^{M-1} V_l(j\omega)X_a\left(j\omega - j\frac{2\pi l}{MT}\right) \tag{3.10}$$

for $|\omega T| \le \pi$ where

$$V_l(j\omega) = \frac{1}{M}\sum_{i=0}^{M-1} G_i(e^{j\omega T})H_i\left(j\omega - j\frac{2\pi l}{MT}\right) \tag{3.11}$$

For multirate filter bank ADC, to obtain a perfect reconstruction condition, the following should be true:

$$V_l(j\omega) = ke^{-j\omega Tc} \quad l = 0$$
$$V_l(j\omega) = 0, \quad l \neq 0$$

for some constants k and c. For the sake of simplicity, we consider $k = 1$, and then to satisfy the perfect reconstruction, the following should be satisfied

$$e^{-jc\omega T} = \frac{1}{M}\sum_{i=0}^{M-1} G_i(e^{j\omega T})H_i(j\omega), \quad |\omega T| \le \pi \tag{3.12}$$

Then again for simplicity, we take the analysis filters $H_i(s)$ and synthesis filters $G_i(e^{j\omega T})$ as ideal lowpass and bandpass filters with gain constants equal to one and M, respectively. This is depicted in Fig 3.3 and Fig.3.4.

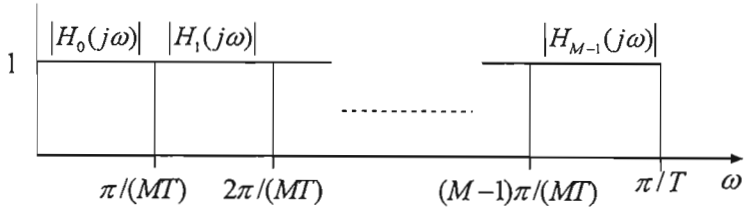

Figure 3.3: Magnitude response for analysis filters in the multirate case

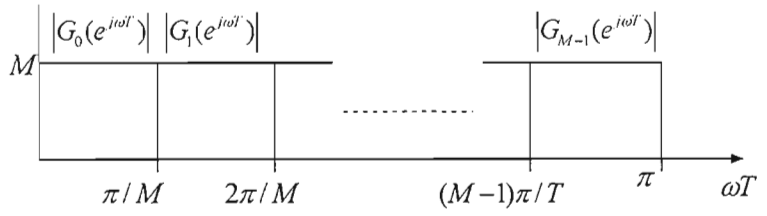

Figure 3.4: Magnitude response for synthesis filters in the multirate case

The main difference in terms of magnitude response of synthesis filters of the multirate filter bank based ADC, is that the gain is M times higher. This is due to the factor $1/M$ in (3.12), in this case the aliasing terms becomes zero, since we consider the case of perfect reconstruction.

Considering (3.6), and replacing the quantizers by the additive error sequences $e_i(n)$, where the error sequences are assumed to be stationary white noise uncorrelated to zero-mean and variances $\sigma_{e_i}^2$. In equation (3.6), $x(n) = x(nT)$ and $e(n)$ is the total error due to each $e_i(n)$. However, the error sequences $e_i(n)$ are propagated through a multirate system, as previously explained in [45]. For the case of time-varying system, the noise analysis becomes too complicated. This is because the output of a time-varying system is not stationary even if the input is stationary. Due to this fact, in [45] the synthesis filter bank was represented using polyphase realization, as shown in Fig. 3.5.

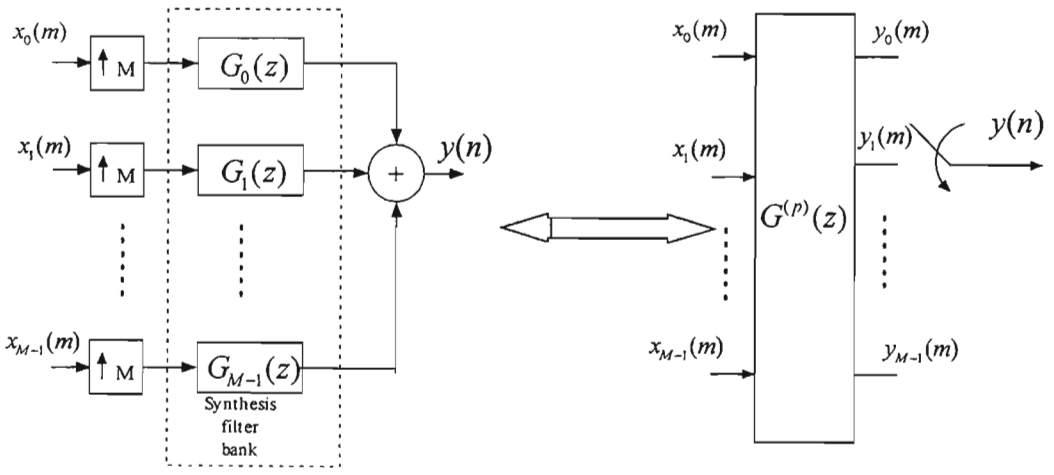

Figure 3.5: Synthesis filter bank with its corresponding polyphase representation

The transfer function of the output $y(n)$ is given by:

$$Y(z) = \sum_{k=0}^{M-1} z^{-k} Y_k(z^M) \tag{3.13}$$

where

$$Y(z) = G^p(z)X(z) \tag{3.14}$$

with $X(z)$ and $Y(z)$ defines as

$$X(z) = [X_0(z) \;\; X_1(z) \ldots X_{M-1}(z)]^T \tag{3.15}$$

$$Y(z) = [Y(z) \;\; Y_1(z) \ldots Y_{M-1}(z)]^T \tag{3.16}$$

and

$$G^{(p)}(z) = \begin{bmatrix} G_{00}(z) & \cdots & G_{0,M-1}(z) \\ \vdots & \ddots & \vdots \\ G_{M-1,0}(z) & \cdots & G_{M-1,M-1}(z) \end{bmatrix} \tag{3.17}$$

the $G_{jk}(z)'s$ are the polyphase components of $G_k(z)$ according to the following relation

$$G_k(z) = \sum_{j=0}^{M-1} z^{-j} G_{jk}(z^M) \tag{3.18}$$

since $G^p(z)$ describes a linear and time-invariant system, this implies that the outputs $y_k(m)$, $k = 0,1,....,M-1$ are also stationary noise with zero mean. However, the variances of the errors in $y_k(m)$ (denoted by $\sigma^2_{e_{y_k}}$) are generally different, even when $\sigma^2_{e_i}$ are equal. The errors may also be correlated. The total error $e(n)$, at the output, will therefore generally not be stationary noise. The variance $\sigma^2_e(n)$ of the total error is time-varying and periodic with the period of M. This is due to the following fact:

$$\sigma^2_e(nM+i) = \sigma^2_{ey_k} \tag{3.19}$$

we can then define the average variance as shown in [2]

$$(\sigma_e^2)_{av} = \frac{1}{M}\sum_{k=0}^{M-1}\sigma_{ey_k}^2 \tag{3.20}$$

Knowing the synthesis filter bank and equation (3.17), $(\sigma_e^2)_{av}$ can be computed as follows,

$$\begin{aligned}(\sigma_e^2)_{av} &= \frac{1}{M}\sum_{k=0}^{M-1}\sigma_{ey_k}^2 \\ &= \frac{1}{M}\sum_{k=0}^{M-1}\sum_{l=0}^{M-1}\sigma_{el}^2\sum_{n=-\infty}^{\infty}\left|g_{kl}(n)\right|^2 \\ &= \frac{1}{M}\sum_{l=0}^{M-1}\sigma_{el}^2\sum_{n=-\infty}^{\infty}\left|g_{l}(n)\right|^2 \\ &= \frac{1}{M}\sum_{l=0}^{M-1}\sigma_{el}^2\sum_{n=-\infty}^{\infty}\left|g_{l}(n)\right|^2\end{aligned} \tag{3.21}$$

Considering Fig.3.4, $\sum_{n=-\infty}^{\infty}\left|g_l(n)\right|^2$ can be written as

$$\sum_{n=-\infty}^{\infty}\left|g_l(n)\right|^2 = \frac{1}{2\pi}\int_{-\pi}^{\pi}\left|G_i(e^{j\omega T})\right|^2 d\omega T = M \tag{3.22}$$

substituting (3.22) in to (3.21), we get

$$(\sigma_e^2)_{av} = \sum_{i=0}^{M-1}\sigma_{ei}^2 \tag{3.23}$$

An alternative to (3.21) is to use a paraunitary matrix for $G^{(p)}(z)$ as in [9, 45]. Hence, all the variances of $y_k(m)$ are equal. Then there is no need to compute $(\sigma_e^2)_{av}$ using (3.21). For general cases however (3.21) method is very useful. One important measure again, is to check the output quantization noise variance for both narrow band signal and wideband signal. This assists in determining if the output quantization noise variance is the same as the conventional ADC. The variance of the error sequence $e(n)$ of the conventional ADC is given by (3.9). Then for narrow band signal the following is assumed $X_{pl} = X_p$ and $B_l = B$, and for wide band signal $X_{pl} = X_p/\sqrt{M}$ and $B_l = B$.

In the case of case for narrow band signal, we consider an input signal, which is sinusoidal signal, where the amplitude is X_p, this implies the overflow will not occur. Whereas for wide band, the input signal is assumed to be gaussian and the input range is assumed to be in this range $\left[-X_p, X_p\right]$. Assuming that the subconverters in the system occur with equal probabilities, the following relation holds,

$$\frac{\sqrt{M}}{\sqrt{2\pi\sigma_x}} \int_{-X_p/\sqrt{M}}^{X_p/\sqrt{M}} e^{-\sigma_y^{-2} y^2/2} dy = \frac{1}{\sqrt{2\pi\sigma_x}} \int_{-X_p}^{X_p} e^{-\sigma_x^{-2} x^2/2} dx \tag{3.24}$$

Equation (3.24) show us the fact that the filters remove noise power according to

$$\sigma_y^2 = \sigma_x^2 / M \tag{3.25}$$

where the input ranges are scaled with a factor $1/\sqrt{M}$. For wide band signal the quantizations can be defined as

$$\begin{aligned} Q_l &= X_{pl} 2^{-(B_l - 1)} \\ &= X_p 2^{-(B-1)} / \sqrt{M} = Q/\sqrt{M} \end{aligned} \tag{3.26}$$

The variance of $e_l(n)$ then becomes,

$$\sigma_{e_l}^2 = Q^2 / 12M \tag{3.27}$$

substituting (3.27) into (3.21), the variance of $(\sigma_e^2)_{av}$ is found to be

$$(\sigma_e^2)_{av} = \sum_{i=0}^{M-1} \sigma_{ei}^2 = Q^2/12 \tag{3.28}$$

This shows that the noise variance of the wide band signal is equal to that of a conventional ADC, see (3.9). For a narrow band signal, the quantizations can be written as

$$\begin{aligned} Q_l &= X_{pl} 2^{-(B_l - 1)} \\ &= X_p 2^{-(B-1)} = Q \end{aligned} \tag{3.29}$$

then the variance of $e_l(n)$ becomes

$$\sigma_{e_l}^2 = Q^2/12 \tag{3.30}$$

substituting (3.27) into (3.21), the variance of $(\sigma_e^2)_{av}$ is found to be

$$(\sigma_e^2)_{av} = \sum_{i=0}^{M-1} \sigma_{ei}^2 = MQ^2/12 \tag{3.31}$$

Equation (3.31), implies that the noise variance is M times higher than that of a conventional ADC.

3.3 Channel Mismatch error and Spurious Free Dynamic Range

The filters in the hybrid filter bank (HFB) isolate the converters in the array from each other, which makes the HFB ADC concept more effective as opposed to time-interleave ADC (TI ADC). The drawback with the interleaved structure is that, due to the manufacturing process, all the ADCs are not identical and mismatch errors are introduced into the system. Three kinds of mismatch errors are introduced:

- *Time errors (static jitter)*

  The delay times of the clock between the different ADCs are not equal. This means that the signal will be periodically, but non-uniformly sampled.

- *Amplitude offset errors*

  The ground level differs between the different ADCs. This means that there is a constant amplitude offset in each ADC.

- *Gain errors*

  The gain, from analog input to digital output, differs between the different ADCs.

In the HFB structures, filters in HFB attenuate the effect of gain and phase mismatches, which severely limit the resolution in TI ADCs. In [9] it is shown that filters do not attenuate the effect of DC-offset errors. The simulations in [9] showed that the HFB ADC architectures attenuate gain, phase errors by 21 [dB]. Furthermore, in the HFB (with 30 [dB] stopband attenuation) than in the time-interleaving system. In literature, two measures for resolution are used to analyze the performance of the system, which is spurious

free dynamic range (SFDR[3]), and total spurious distortion (TSD[4]). The definition of SFDR and TSD are given mathematically as the footnote. The reasons for using SFDR and TSD instead of SNR and THD are given in details in [9]. Major results and analysis of the effects of gain and phase mismatch errors, respectively, were also presented [9]. Recently in [44], only SFDR was used for numerical analysis for a typical filter bank design. In this dissertation, only the numerical analysis is considered for a typical filter bank design with slightly different values from [44]. Considering the equations that were derived in both [9, 44] for SFDR. It is easy to note that the derived equations are not similar. In [9] the equations given are for calculating the minimum SFDR that could be obtained based on the stopband attenuation. Furthermore, $\mathrm{E}\{x\}$ which denotes the expected value of random variable x (x could be either gain tolerance error or phase tolerance error) as well as for the typical SFDR, on the other hand in [44], the SFDR is computed for both passband and stopband, details are shown later in this section, for the later case. However, the equations derived in [9, 44] are valuable since they give the information about how we can design the filter bank that could give desired SFDR and TSD, depending on the specification of the application at hand. In this section, the only derivation that would be considered is the one presented in [44], since they are more relevant to our work and since the conditions considered are for approximated PR as opposed to PR conditions, (details for PR cases are given in [9]). Gain, phase delay, and DC offset error model of an ADC is diagrammatically given as shown in Fig. 3.6

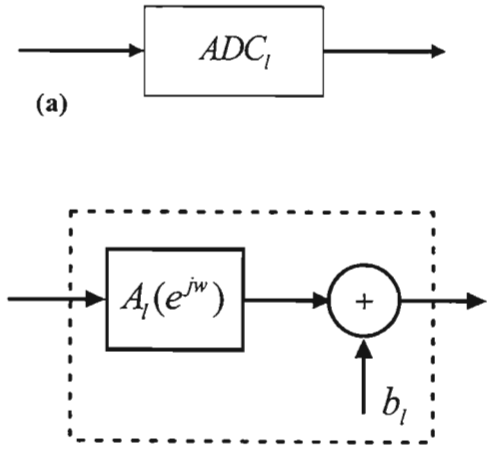

Figure 3.6: (a) ADC, (b) model of an ADC

---

[3] $SFDR = \dfrac{\mathrm{E}\left\{\left|desired\ signal\right|^2\right\}}{\max\left(\mathrm{E}\left\{\left|undesired\ signal\right|^2\right\}\right)}$

[4] $TSD = \dfrac{\mathrm{E}\left\{\left|desired\ signal\right|^2\right\}}{\sum\left(\mathrm{E}\left\{\left|undesired\ signal\right|^2\right\}\right)}$

where $A_l(e^{j\omega}) = (1 + a_l(\omega))e^{-j\omega d_l(\omega)}$ and $a_l(\omega)$[5] is a gain error, b_l is a dc-offset error, and $d_l(\omega)$[6] is a phase delay error, details on each of these error is given in [9]. The above model of an ADC does not consider errors such as ADC quantization errors, and ADC harmonic distortion errors. This is because quantization and harmonic distortion errors are not limiting errors in both time-interleaving and HFB systems. The derived equations in [9] are based on the model illustrated in Fig. 3.6, and are given below for SFDR and TSD, considering only typical HFB ADC designs,

$$SFDR_{typ} = \frac{1}{E\{\hat{a}^2\}2(\delta_s)^2} \tag{3.32a}$$

$$TSD_{typ} = \frac{1}{(M-1)E\{\hat{a}^2\}2(\delta_s)^2} \tag{3.32b}$$

where equations (3.32a) and (3.32b) are for computing the SFDR and TSD with gain mismatch error and δ_s and $\hat{a}$ are stopband and gain error, respectively. Equations (3.32c) and (3.32d) are for calculating SFDR and TSD with phase mismatch error.

$$SFDR_{typ} = \frac{1}{\pi^2 E\{\hat{a}^2\}2(\delta_s)^2} \tag{3.32c}$$

$$TSD_{typ} = \frac{1}{\pi^2 (M-1)E\{\hat{a}^2\}2(\delta_s)^2} \tag{3.32d}$$

The equations (3.32a-d) were all derived based on the traditional perfect reconstruction conditions, which simply states that the output signal is a scaled, delayed version of the input signal. In fact, equations (3.32a-d) are the first equations derived for HFB ADC system in [9], and they were published in 1997. Previously, it was shown in [19 ,44] that it is possible for digital filter banks including discrete-time HFBs (DT HFBs) to achieve a PR and PMR, but it appears to be impossible for CT HFBs, if analog filter bank is assumed to

---

[5] where $a_l(\omega)$ is the frequency-dependent gain error and

[6] $d_l(\omega)$ is the frequency-dependent phase delay error. The periodicity of the ADC transfer function $A_l(e^{j\omega})$ can be shown explicitly using the mod function as follows:

$$A_l(e^{j\omega}) = (1 + a_l(\omega \bmod 2\pi))e^{-j(\omega \bmod 2\pi)d_l(\omega \bmod 2\pi)}$$

be realized utilizing only lumped elements. On the other hand, if the transmission lines are used as components it would be possible to obtain CT HFBs with PR and PMR, since in this work we are considering approximated PMR, i.e. we are considering the conditions utilized in [44] for lumped element assumption. Moreover, it was also stated that if the processing unit between the analysis and synthesis filter bank is not lossless, it is unnecessary to impose the filter bank not to introduce any errors at all. This has been shown in literature that introducing small errors in the filter bank can significantly reduce arithmetic complexity. In this work, NPMR is considered, this implies that, in terms of the magnitude distortion and aliasing functions, they would approximate one and zero, respectively. Therefore, equations (3.32a-d) would not be relevant to our filter bank design, in other words, in this work the procedures used in [44] will be used to determine the bounds on SFDR for typical CT HFB designs.

In [44], the following errors gain and time-skew errors in HFB ADCs are considered. The bound on SFDR is very important in filter bank design for HFB ADC systems, since the specification of the filters in the filter bank based ADC can be determined easily, so that a certain requirement on SFDR of the converter is met, provided the maximum gain and time-skew error magnitudes are given.

The gain and time-skew error model used in this dissertation is the same as in [44]. Considering that quantization characteristics of the ADCs normally exhibit different gain as function of input signal. Therefore, ignoring quantization noise does not have any impact. The model for the quantization in each channel, i.e. channel l can be given as

$$A_l = 1 + \Delta a_l \tag{3.33}$$

where Δa_l is a small static gain error and where A_l includes gain errors as well as the ones that are introduced in the sampling circuitry. Time-skew errors on the other side come from deterministic errors in the sampling instants of the sampling circuitry. The main difference between the TI systems and HFB systems, in terms of the sampling, is that for TI-ADCs the sampling instants are distributed uniformly in time. This implies that each converter in TI ADC architecture works with samples taken at uniformly delayed instants, whereas in the HFB ADC architecture, all channels are sampled simultaneously. Ignoring random sampling time uncertainty due to noise in the sampling switches, the sampling instants in TI ADC and HFB ADC will deviate to some extent from ideal ones. Hence, the sampling instants will be periodically non-uniformly distributed in time. This can be illustrated as shown in Fig. 3.7 for only $M = 2$ for simplicity, where $t_l = lT + \Delta t_l$.

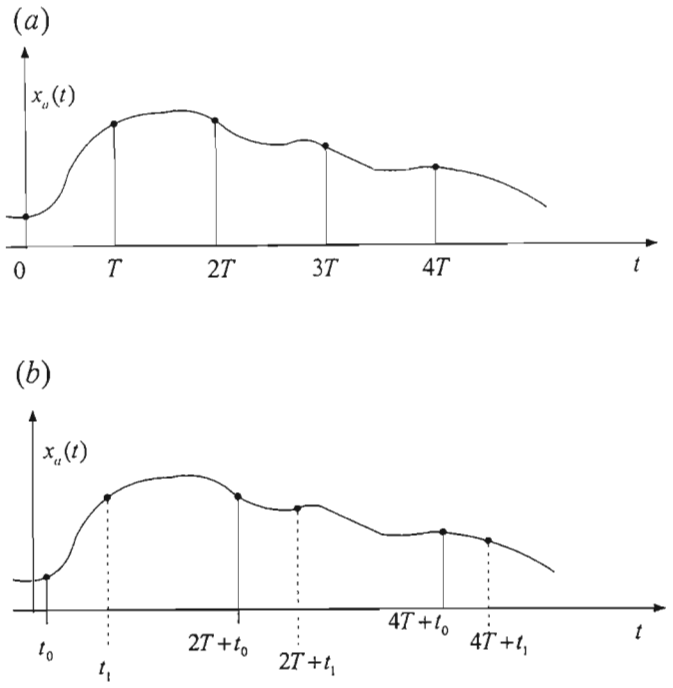

Figure 3.7: (a) uniform sampling and (b) periodic non-uniform sampling.

The time-skew error can be either modeled by delaying the signals incident to the samplers or by skewing the sampling instants. The model used here is

$$C_l(j\omega) = e^{j\omega\Delta t_l} \tag{3.34}$$

where Δt_l are small static time-shifts of the signals in channel l before sampling. Considering the gain and time-skew error models, the input and output relation can be easily derived, the steps for such derivations is shown below.

When designing the hybrid filter bank the bandlimitation assumption should always be considered. Another important note is that, if the filter bank has a PR, this implies that the actual aliasing in the overall ADC is determined by the anti-aliasing filter that must precede the filter bank. Thus, the aliasing is identical to that of a conventional ADC that utilizes the same anti-aliasing filter. However, this is not the case for our system, due to the presence of channel errors. This implies that the output signal will be somewhat distorted. Taking into consideration the error model of gain and time-skew errors and ignoring quantization. The frequency response of input and output relations becomes:

$$
\begin{aligned}
Y(e^{j\omega T}) &= \sum_{l=0}^{M-1} G_l(e^{j\omega T}) A_l X_l(e^{jM\omega T}) \\
&= \sum_{l=0}^{M-1} G_l(e^{j\omega T}) A_l X_l(e^{jMT_1}) \\
&= \frac{1}{MT} \sum_{r=-\infty}^{\infty} X_a\left(j\omega - j\frac{2\pi r}{MT}\right) H_l\left(j\omega - j\frac{2\pi r}{MT}\right) C_l\left(j\omega - j\frac{2\pi r}{MT}\right)
\end{aligned} \tag{3.35}
$$

It was shown in chapter 2 subsection 2.2 that $r \in [-(M-1), M-1]$ and $\omega T \in [-\pi, \pi]$, with (3.33) and (3.34), (3.35), $Y(e^{j\omega T})$ can be restructured and be given as

$$
Y(e^{j\omega T}) = \frac{1}{T} \sum_{r=-(M-1)}^{M-1} \hat{V}_r(j\omega) X_a\left(j\omega - j\frac{2\pi r}{MT}\right) \tag{3.36}
$$

where

$$
\hat{V}_r(j\omega) = \frac{1}{M} \sum_{l=0}^{M-1} H_l\left(j\omega - j\frac{2\pi r}{MT}\right) G_l(e^{j\omega T})(1+\Delta a_l) e^{\left(j\omega - j\frac{2\pi r}{MT}\right)\Delta t_l} \tag{3.37}
$$

If we ignore gain and time-skew errors, equation (3.37) becomes equation (2.11). Considering the usual way of designing the CT HFB (this is given below)

$$
\begin{aligned}
&1-\delta_0 \le |V_0(j\omega)| \le 1+\delta_0, \quad |r| = 0 \\
&|V_r(j\omega)| \le \delta_1, \quad |r| = 1, \ldots, M-1
\end{aligned} \tag{3.38}
$$

this means that the magnitude of the output signal frequency response is deviated from the magnitude of the input signal frequency response with less than δ_0 and the magnitude of the aliasing terms also deviates with less than δ_1. One of the known ways in literature that could be used to expand (3.35), which is the time-skew error model, is to use the Taylor series expansion. Then (3.37) can be rewritten as:

$$
\hat{V}_r(j\omega) = \frac{1}{M} \sum_{l=0}^{M-1} H_l\left(j\omega - j\frac{2\pi r}{MT}\right) G_l(e^{j\omega T})(1+c(\Delta a_l, \Delta t_l)) \tag{3.39}
$$

where $c(\Delta a_l, \Delta t_l)$ is defined as

$$c(\Delta a_l, \Delta t_l) = \Delta a_l + (1+\Delta a_l)\sum_{n=1}^{\infty}\frac{1}{n!}\left[j\left(\omega T - \frac{2\pi l}{M}\right)\frac{\Delta t_l}{T}\right]^n \tag{3.40}$$

Expanding (3.39), it can be rewritten as

$$\begin{aligned}\hat{V}_r(j\omega) = &\frac{1}{M}\sum_{l=0}^{M-1} H_l\left(j\omega - j\frac{2\pi r}{MT}\right)G_l(e^{j\omega T}) + \\ &\frac{1}{M}\sum_{l=0}^{M-1} H_l\left(j\omega - j\frac{2\pi r}{MT}\right)G_l(e^{j\omega T})c(\Delta a_l, \Delta t_l))\end{aligned} \tag{3.41}$$

Therefore this expansion of (3.41) illustrates that $\hat{V}_r(j\omega)$ can be defined in terms of (2.11) as follows,

$$\hat{V}_r(j\omega) = V_r(j\omega) + \frac{1}{M}\sum_{l=0}^{M-1} H_l\left(j\omega - j\frac{2\pi r}{MT}\right)G_l(e^{j\omega T})c(\Delta a_l, \Delta t_l)) \tag{3.42}$$

where $V_r(j\omega)$ is exactly (2.11) as shown in (3.43)

$$V_r(j\omega) = \frac{1}{M}\sum_{l=0}^{M-1} H_l\left(j\omega - j\frac{2\pi r}{MT}\right)G_l(e^{j\omega T}) \tag{3.43}$$

Based on the above derivation of $\hat{V}_r(j\omega)$, the bounds on $\hat{V}_r(j\omega)$ can also be derived. In this work, the considered CT HFB divides the frequency range of the input signal uniformly; we do not consider the octave case. Since the magnitude responses of the filters are very important in the design of HFB, they are also part of the equations of the bounds on $\left|\hat{V}_r(j\omega)\right|$, this is required in order to be able to derive the bounds on the minimum SFRD. First of all, let us introduce Δ_r which is defined in terms of the Taylor expansion represented by (3.40) as follows,

$$\Delta_r = \left|c(\Delta a_l, \Delta t_l)\right|, \quad l = 0,\ldots,M-1 \tag{3.43}$$

Ignoring all terms above of order two, Δ_r can be now defined as

$$\Delta_r \le \Delta_{r\max} = \left(\left|\Delta a_l\right|^2_{\max} + q(r)\right)^{1/2} \tag{3.44}$$

where $q(r)$ is given by,

$$q(r)=\begin{cases}\dfrac{|\Delta t_l|^2_{\max}}{T^2}\pi^2, & r=0\\ \dfrac{|\Delta t_l|^2_{\max}}{T^2}\dfrac{\pi^2}{M}(3M-2)^2, & r=1,\ldots,M-1\end{cases} \tag{3.45}$$

even this term $\frac{1}{M}\sum_{l=0}^{M-1}H_l\left(j\omega-j\frac{2\pi r}{MT}\right)G_l(e^{j\omega T})c(\Delta a_l,\Delta t_l))$, in (3.42). It can be

bounded in terms of $\Delta_{r\max}$ as follows:

$$\begin{aligned}&\left|\frac{1}{M}\sum_{l=0}^{M-1}H_l\left(j\omega-j\frac{2\pi r}{MT}\right)G_l(e^{j\omega T})c(\Delta a_l,\Delta t_l))\right|\le\\ &\Delta_{r\max}\left|\frac{1}{M}\sum_{l=0}^{M-1}H_l\left(j\omega-j\frac{2\pi r}{MT}\right)G_l(e^{j\omega T})c(\Delta a_l,\Delta t_l))\right|\\ &=\Delta_{r\max}D(\omega T,r)\end{aligned} \tag{3.45}$$

where $\Delta_{r\max}$ is defined in (3.44). The values of $D(\omega T,r)$ depends on r. For instance, if $r=0$ this means, we are left with the unshifted version of $H_l(j\omega)$. This gives information about the passband frequencies, i.e. $D(\omega T,0)$ illustrates that for any passband frequency there is one term, for which the filters $H_l(j\omega)$ and $G_l(e^{j\omega T})$ have their passbands simultaneously and, hence the maximum value of their product can be given as

$$\max\left\{\left|H_l(j\omega)G_l(e^{j\omega T})\right|\right\}-1=\delta_2 \tag{3.47}$$

where $\omega T\in$ of passband and $l=0,\ldots,M-1$. The other $M-1$ terms have also their stopband simultaneously. Thus, if $r=0$, we have

$$\Delta_{0\max}D(\omega T,0)\le(1+\delta_2+(M-1)\delta_s^2)\Delta_{0\max} \tag{3.48}$$

where δ_s is the stopband ripple of the filters.

Then, for transition band it's slightly different because it involves two terms from $D(\omega T, 0)$ for which the filters, $H_l(j\omega)$ and $G_l(e^{j\omega T})$ have transition bands simultaneously. The maximum value of the sum of their product is given as

$$\max\left\{\left|H_l(j\omega)G_l(e^{j\omega T})\right|+\left|H_i(j\omega)G_i(e^{j\omega T})\right|\right\}-1=\delta_3 \tag{3.49}$$

where $l,i=0,\ldots,M-1,\quad i\neq l$ and $\omega T\in$ of transition band. The other $M-2$ terms have also their stopband simultaneously. Thus, if $r=0$, we have

$$\Delta_{0\max}D(\omega T,0)\leq(1+\delta_3+(M-2)\delta_s^2)\Delta_{0\max} \tag{3.50}$$

(3.49) and (3.50) means that for any passband frequency there will be two terms, which are product of a passband and a stopband response, while the other $M-2$ terms will be the products of two stopband responses. Thus,

$$\Delta_{r\max}D(\omega T,r)\leq(2\delta_s(1+\delta_c)+(M-2)\delta_s^2)\Delta_{r\max} \tag{3.51}$$

where $\omega T\in$ of passband and δ_c is the passband ripple of the filters. Again for any frequency in the transition band there are two terms in $D(\omega T,r)$ (for which it is for $r\neq 0$), this implies that the shifted version of $H_l(j\omega)$ and $G_l(e^{j\omega T})$ have the transition bands simultaneously and the maximum value can be computed by the following relation

$$\begin{aligned}&\max\left\{\begin{array}{l}\left|H_l\left(j\omega-\dfrac{2\pi r}{MT}\right)G_l(e^{j\omega T})\right|+\\ H_l\left(j\omega-\dfrac{2\pi r}{MT}\right)\left|H_i(j\omega)G_i(e^{j\omega T})\right|\end{array}\right\}-1\\&=\delta_4\end{aligned} \tag{3.52}$$

where $l,i=0,\ldots,M-1,\quad i\neq l$ and $\omega T\in$ of transition band, while the other $M-2$ terms simultaneously have their stopbands. Thus,

$$\Delta_{r\max} D(\omega T, r) \le (1 + \delta_4 + (M-2)\delta_s^2)\Delta_{r\max} \tag{3.53}$$

Using triangle inequality, considering (3.39) to (3..53), for $\hat{V}_r$, then applying triangle inequality, the following holds,

$$|V_r|_{\min} - \Delta_{r\max} D(\omega T, r) \le \left|\hat{V}_r(j\omega)\right| \le |V_r|_{\min} + \Delta_{r\max} D(\omega T, r) \tag{3.54}$$

(3.54) implies that $\left|\hat{V}_r\right|$ can, then be bounded according to

$$\begin{aligned} 1 - \delta_0 - \xi_0 &\le \left|\hat{V}_0(j\omega)\right| \le 1 + \delta_0 + \xi_0, \quad |r| = 0 \\ \left|\hat{V}_r(j\omega)\right| &\le \delta_1 + \xi_r, \quad |r| = 1, \ldots, M-1 \end{aligned} \tag{3.55}$$

for every angular frequency ω, where ξ_0 , ξ_r in (3.55) can be defined explicitly for passband and transition band as in (3.56) which is for $r = 0$ and (3.57) is for $r \neq 0$

$$\begin{aligned} \xi_{0p} &= (1 + \delta_2 + (M-1)\delta_s^2)\Delta_{0\max} \qquad \omega T \in \textit{passband} \\ \xi_{0t} &= (1 + \delta_3 + (M-2)\delta_s^2)\Delta_{0\max} \qquad \omega T \in \textit{transtion band} \end{aligned} \tag{3.56}$$

$$\begin{aligned} \xi_{rp} &= (2\delta_s(1+\delta_c) + (M-2)\delta_s^2)\Delta_{r\max} \qquad \omega T \in \textit{passband} \\ \xi_{rt} &= (1 + \delta_4 + (M-2)\delta_s^2)\Delta_{r\max} \qquad \omega T \in \textit{transtion band} \end{aligned} \tag{3.57}$$

where $\delta_2, \delta_3, \delta_4$ are given by (3.47), (3.49), (3.52), respectively, and δ_s and δ_c are the stopband and passband ripples of the filters, respectively. Using (3.55) to (3.57), the lower bounds on the SFDR of hybrid filter bank ADCs can be obtained for passband and transition band frequencies. Minimum SFDR for HFB ADCs, for passband can be found as follows,

$$10^{0.05SFDR} \geq \frac{\min\left\{\left|\hat{V}_{r=0}(j\omega)\right|\right\}}{\max\left\{\left|\hat{V}_{r}(j\omega)\right|\right\}} \geq \frac{1-\delta_0-\xi_{0p}}{\delta_1+\xi_{rp}} \tag{3.58}$$

and the minimum SFDR for HFB ADCs, for transition band can be obtained as

$$10^{0.05SFDR} \geq \frac{\min\left\{\left|\hat{V}_{r=0}(j\omega)\right|\right\}}{\max\left\{\left|\hat{V}_{r}(j\omega)\right|\right\}} \geq \frac{1-\delta_0-\xi_{0t}}{\delta_1+\xi_{rt}} \tag{3.59}$$

to illustrate the numerical approximated values, we only consider to a first order the SFDR expressions, which can for HFB ADC can be approximated as

$$10^{0.05SFDR} \geq \frac{\min\left\{\left|\hat{V}_{r=0}(j\omega)\right|\right\}}{\max\left\{\left|\hat{V}_{r}(j\omega)\right|\right\}} \geq \frac{1-\delta_0-\Delta_{0\max}}{\delta_1+2\delta_s\Delta_{r\max}} \tag{3.60}$$

Equation (3.60) is for passband case and (3.61) is for the transition band case.

$$10^{0.05SFDR} \geq \frac{\min\left\{\left|\hat{V}_{r=0}(j\omega)\right|\right\}}{\max\left\{\left|\hat{V}_{r}(j\omega)\right|\right\}} \geq \frac{1-\delta_0-\Delta_{0\max}}{\delta_1+\Delta_{r\max}} \tag{3.61}$$

Table 3.1 gives typical design case for a hybrid filter bank system.

Table 3.1: Numerical values for typical CT HFB Designs

parameter	Case A	Case B	Case C	Case D
M	2	2	2	2
δ_0	0.05	0.05	0.05	0.05
δ_1	0.00011	0.00011	0.00011	0.00011
δ_2	0.0012	0.0012	0.0012	0.0012
δ_3	0.0012	0.0012	0.0012	0.0012
δ_4	0.0012	0.0012	0.0012	0.0012
$\lvert\Delta t_l\rvert_{max}/T$	0.0029	0.0029	0.0029	0.0029
$\lvert\Delta a_l\rvert_{max}$	0.018	0.018	0.018	0.018
δ_c	0.01	0.01	0.01	0.005
δ_s	0.01	0.02	0.03155	0.01
$SFDR_t[dB]$	> 31.161679	> 31.161679	> 31.161679	> 31.161679
$SFDR_p[dB]$	> 63.488657	> 58.271861	> 54.626383	> 63.488659

The numerical values in table 3.1 illustrate that as we decrease the stopband ripple of the filters, the increase SFDR (denoted in the table 3.1 as $SFDR_p$) is achieved at the passband frequencies by utilizing the HFB ADCs, whereas at the crossover point in the transition band the worst case SFDR (denoted in the table 3.1 as $SFDR_t$) is the same. In order to decrease effect of mismatch errors in general systems, incorporating parallel ADCs, tuning, offline or online can be done. This has significant advantage, since for TI ADCs, tuning needs to be performed in the whole frequency band of interest, whereas for HFB ADCs, tuning is only required at some few frequency points in the transition regions, only if the improvement in SFDR is sufficient in passband regions. Moreover, in the HFB ADCs, the sampling in the channels takes place simultaneously, which has a significant advantage in comparison to TI ADCs system, which requires the generation of uniformly distributed sampling instants. This fact implies that the HFB ADC system will always have smaller sampling instant errors, thus, achieving smaller time-skew errors in HFB ADCs as compared to TI ADCs. Case D in table 3.1 is for our specification.

3.4 Summary

We discussed in this chapter efficient design procedures for CT HFB. Thereafter we investigated different methods that were used previously in literature to match the frequency response of analog filters with the digital ones. This matching if it is not done properly, would cause the complexity of the filters in terms of the order of analog filter to becomes too high and unacceptable. We also discussed the noise in the filter bank due to quantization, considering the case of multirate filter bank ADC, in comparison to conventional

ADC. Lastly, we discussed the types of mismatch errors, and showed that they are attenuated in HFB ADC. We derived then and showed how we can attain lower bound of SFDR of HFB ADCs for passband and transition band frequencies. We concluded the chapter by presenting the numerical values for typical design of CT HFB. In the subsequent chapters we will present our proposed system. The conclusions of chapter 4 together with the conclusions of chapter 5 are presented in a table form at the section that gives the summary of results. Since chapter 4 forms the basis of comparison for our proposed system.

CHAPTER 4

PROPOSED HYBRID ANALOG/DIGITAL FILTER BANKS STRUCTURES FOR SDR

Hybrid analog/digital multirate filter bank incorporates an analysis filter bank and a synthesis filter bank. In our case however, the analysis filter bank is analog filters and the synthesis filter bank is discrete time. The two-channel hybrid analog/digital filter bank ADC is shown in Fig. 4.1. This filter bank finds applications in high-speed and high-resolution analog-to-digital converters. This scheme is a generalization of time-interleaved ADCs, where the utilization of filter banks is to reduce the distortion, mainly caused by gain and time-skew mismatch errors [9, 10, 19, 44, 45]. In this dissertation the analog filters are to be implemented using lumped elements as in [10]. When using such analog filters, it is not known at this point in time how to achieve PR and PMR. There are also no known literature, which deals with analog filters utilizing lumped elements that achieve PR and PMR. Therefore, in this work, we are considering approximated PMR. According to [10] there is no reason to use exact PR and PMR filter banks, since the desired frequency response of the analog filters cannot be implemented exactly. In addition to that, we cannot rely on the design procedures of digital filter banks as shown in chapter 2. In the case of CT HFB ADC, only a few publications dealing with hybrid analog/digital filter banks exist. This causes a lot of difficulties in deriving efficient design procedures. Some of the design techniques, such as the ones given in [9], results in analog filters of much higher order and complexity than necessary. This is because the analog filters are designed after the digital filters have been optimized and fixed. It is shown in [10] that this will cause problems, since it is very difficult to implement wide band analog filters with high accuracy, especially for high order filters. Design approaches where the synthesis filters are designed after analysis filters have been designed and fixed, have been addressed in [9], however, only approximated PR filter banks were considered. This results in digital synthesis filters of higher order and complexity than necessary if the specifications of an application at hand allow phase distortion. This was also addressed in [10] in detail. The authors of [10] concluded that digital filters designed by using non-linear optimization methods straightforwardly, may cause problems. In particular, it may be difficult to find good solutions in terms of small distortion and aliasing since locally optimal solutions can be obtained that are far from the global optimal solutions. Recently, a case of approximated PMR was published but it suffered the problem of having digital filters of higher order. Moreover, the proposed approximated PMR in [10] didn't consider the case where the filters have sharp roll-off; this results in digital synthesis filters of higher order again.

From the above discussion, it is clear that there is a need for new filter banks and design techniques for hybrid analog/digital filter banks. In this section we are considering a conventional two-channel hybrid analog/digital filter bank, for approximately PMR (or near PMR) which is denoted in literature as NPMR.

In the next chapter, the proposed structures based on FRM are presented, which deals with the problem of reducing the order of digital filter bank as well as its complexity in general.

In our work, as in [10], the filter bank design is performed by first optimizing the analog and then with the analysis filters fixed, optimizing the digital synthesis filters. By designing the analysis filters and synthesis filters separately, it is possible to obtain analysis filters of very low order and complexity, which is the method followed in this work. This way of designing the analysis and synthesis filters separately produces low overall complexity. In this work the analysis filters are equiripple filters. In [10], it is stated that for approximated PMR hybrid analog/digital filter banks, the synthesis filters can be designed using linear programming, which ensures optimal synthesis filters. We follow however another design procedure when designing and optimizing the synthesis filters, the procedure we are using will be explained in detail under filter bank design in subsequent sections.

4.1 Two-Channel Hybrid Analog and Digital (FIR) Filter Bank

For two-channel hybrid analog/digital filter banks, it is assumed that the input signal is bandlimited to $|\omega| < \pi / T$. This simply means that the Nyquist criterion for sampling with effective sampling frequency of $1/T$ without aliasing is accomplished.

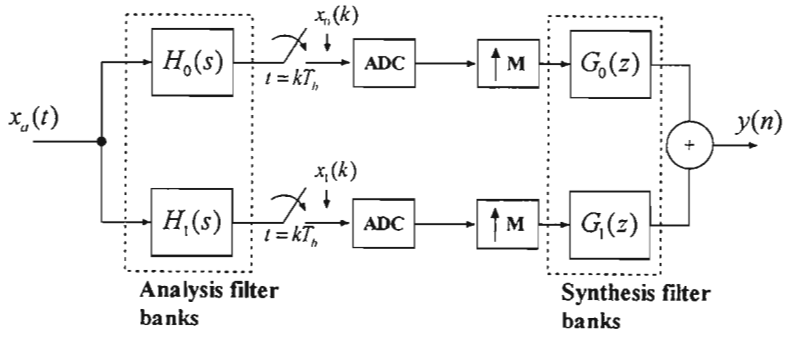

Figure 4.1: Two-channel hybrid analog/digital filter bank ADC

Ignoring the quantizations, the frequency responses of the input and output signals of M -channel filter bank is given as follows:

$$Y(e^{j\omega T}) = \frac{1}{T}\sum_{l=-\infty}^{\infty} V_l(j\omega) X\left(j\omega - j\frac{2\pi l}{MT}\right) \tag{4.1}$$

$$V_l(j\omega)=\frac{1}{M}\sum_{k=0}^{M-1}G_k(e^{j\omega T})H_k\left(j\omega-j\frac{2\pi l}{MT}\right) \tag{4.2}$$

For two-channel $(M=2)$ filter bank as shown in Fig. 4.1, the input and output signals of the filter bank are then given as

$$Y(e^{j\omega T})=\frac{V_0(j\omega)X(j\omega)+V_1(j\omega)X\left(j\omega-j\frac{\pi}{T}\right)}{T},\quad \omega T\in[0,\pi] \tag{4.3}$$

where

$$V_0(j\omega)=\frac{H_0(j\omega)G_0(e^{j\omega T})+H_1(j\omega)G_1(e^{j\omega T})}{2} \tag{4.4}$$

$$V_1(j\omega)=\frac{H_0(j\omega-j\frac{\pi}{T})G_0(e^{j\omega T})+H_1(j\omega-j\frac{\pi}{T})G_1(e^{j\omega T})}{2} \tag{4.5}$$

The functions $V_0(j\omega)$ and $V_1(j\omega)$ are distortion and aliasing frequency responses, respectively.

A perfect magnitude reconstruction (PMR) case is obtained if the magnitude response of the distortion function is constant and the aliasing function is zero as shown in equation (2.6), therefore the condition is written as

$$\begin{aligned}|V_0(j\omega)|&=k,\quad |\omega T|\le\pi\\ V_1(j\omega)&=0,\quad |\omega T|\le\pi\end{aligned} \tag{4.6}$$

PMR filter bank is possible with discrete-time HFB, but it is not yet known how this (PMR filter bank) can be accomplished or achieved for continuous-time HFB, when the analog analysis filter bank are implemented using lumped elements. Therefore, approximated PMR or NPMR has a different condition for distortion function as shown in equation (4.7), provided the requirement on the approximately linear phase response of the distortion term is relaxed, then a NPMR is obtained according to

$$\begin{aligned}|V_0(j\omega)|&\approx k,\quad |\omega T|\le\pi\\ |V_1(j\omega)|&\approx 0,\quad |\omega T|\le\pi\end{aligned} \tag{4.7}$$

This section introduces CT HFBs, and thoroughly gives some expressions for the frequency responses which are very useful in the filter design. The analysis filters, as well as the synthesis filters, follows similar design procedures as in [10].

4.1.1 Analysis Filters

Let us express the transfer functions of the analog lowpass and highpass analysis filters as follows

$$H_0(s)=\frac{A_0(s)+A_1(s)}{2}, \qquad H_1(s)=\frac{A_0(s)-A_1(s)}{2} \tag{4.8}$$

where $A_0(s)$ and $A_1(s)$ are stable all-pass filters with orders denoted by N_{LP} and N_{HP}. The order of $H_0(j\omega)$ and $H_1(j\omega)$ is then given by $N=N_{LP}+N_{HP}$, where $H_0(j\omega)$ and $H_1(j\omega)$ has real-valued polynomial coefficients each. Moreover, one of N_{LP} and N_{HP} is always odd and the other always even, which simply means N is odd. The transfer functions of $A_0(s)$ and $A_1(s)$ can then be expressed as follows:

$$A_k(s)=\frac{\Pi_{r=0}^{N_k}(-s-s_k)}{\Pi_{r=0}^{N_k}(s-s_k)}, \qquad k=0,1 \tag{4.9}$$

Letting the analog filters be expressible as a sum and difference of two all-pass filters is not a severe restriction, since, it is known that the standard approximations i.e. Elliptic, Chebyshev in odd-order case can be expressed in this way. In fact, all analog filters with odd characteristics function, can be written in this way [10, 46]. The frequency responses of $H_0(j\omega)$ and $H_1(j\omega)$ can then be given as:

$$\begin{aligned} H_0(j\omega) &= e^{j\left(\frac{\Phi_0(\omega)+\Phi_1(\omega)}{2}\right)}H_{0R}(\omega) \\ H_1(j\omega) &= je^{j\left(\frac{\Phi_0(\omega)+\Phi_1(\omega)}{2}\right)}H_{1R}(\omega) \end{aligned} \tag{4.10}$$

where $H_{0R}(\omega)$ and $H_{1R}(\omega)$ are real-valued functions, and can be given as follows

$$H_{0R}(\omega) = \cos\left(\frac{\Phi_0(\omega) - \Phi_1(\omega)}{2}\right)$$
$$H_{1R}(\omega) = \sin\left(\frac{\Phi_0(\omega) - \Phi_1(\omega)}{2}\right) \tag{4.11}$$

where $\Phi_0(\omega)$ and $\Phi_1(\omega)$ represent the phase responses of $A_0(s)$ and $A_1(s)$, respectively.

4.1.2 Synthesis Filters

Let us express the transfer functions of the analog lowpass and highpass synthesis filters as follows

$$G_0(e^{j\omega T}) = 2F_{eq}(e^{j\omega T})F_0(e^{j\omega T})$$
$$G_1(e^{j\omega T}) = 2F_{eq}(e^{j\omega T})F_1(e^{j\omega T}) \tag{4.12}$$

where in general for approximated PR, the filter $F_{eq}(e^{j\omega T})$ is an N_{eq} th order non-linear phase finite-impulse response (FIR) filter and $F_0(e^{j\omega T})$ and $F_1(e^{j\omega T})$ are N_F th order linear phase FIR filters. The basic role of $F_{eq}(e^{j\omega T})$ is to equalize the phase distortion, hence, it is known as the phase equalizer, whereas $F_0(e^{j\omega T})$ and $F_1(e^{j\omega T})$ are normally used to shape the magnitude response. The frequency response of $F_0(e^{j\omega T})$ and $F_1(e^{j\omega T})$ can then be given as

$$F_0(e^{j\omega T}) = e^{-j\left(\frac{N_F \omega T}{2}\right)} F_{0R}(\omega T)$$
$$F_1(e^{j\omega T}) = je^{-j\left(\frac{N_F \omega T}{2}\right)} F_{1R}(\omega T) \tag{4.13}$$

where $F_{0R}(\omega T)$ and $F_{1R}(\omega T)$ are zero-phase frequency responses, respectively and can be written as

$$F_{0R}(\omega T) = \sum_{n=0}^{(N_F-1)/2} 2h_{F_0}(n, N_F)\cos\left(\left[n+\frac{1}{2}\right]\omega T\right)$$
$$F_{1R}(\omega T) = \sum_{n=0}^{(N_F-1)/2} 2h_{F_1}(n, N_F)\sin\left(\left[n+\frac{1}{2}\right]\omega T\right) \quad (4.14)$$

with $h_{F_0}(n, N_F) = h_{F_0}[(N_F-1)/2-n]$ and $h_{F_1}(n, N_F) = h_{F_1}[(N_F-1)/2-n]$, respectively. The frequency response of $F_{eq}(e^{j\omega T})$ can be written as

$$F_{eq}(e^{j\omega T}) = e^{j\Phi_{eq}(\omega T)}\left|F_{eq}(e^{j\omega T})\right| \quad (4.15)$$

where $\left|F_{eq}(e^{j\omega T})\right|$ and $\Phi_{eq}(\omega T)$ are the magnitude and phase response of $F_{eq}(e^{j\omega T})$, respectively. Equation (4.12) is a general case for designing for approximated PR. Since we are working on approximated PMR in this work, $F_{eq}(e^{j\omega T})$ must be taken as $F_{eq}(e^{j\omega T}) = 1$, by doing so NMPR can easily be achieved. In such case, equation (4.12) becomes,

$$G_0(e^{j\omega T}) = 2F_0(e^{j\omega T})$$
$$G_1(e^{j\omega T}) = 2F_1(e^{j\omega T}) \quad (4.16)$$

for NPMR HFB class.

4.1.3 Distortion and Aliasing

With analysis and synthesis filters as given in (4.8) to (4.14) in the previous subsections, the distortion and aliasing function can be given as

$$V_0(j\omega) = e^{j\left(\frac{\Phi_0(\omega)+\Phi_1(\omega)-N_F\omega T}{2}\right)}V_{0R}(\omega)$$
$$V_1(j\omega) = e^{j\left(\frac{\Phi_0(\omega-\pi/T)+\Phi_1(\omega-\pi/T)-N_F\omega T}{2}\right)}V_{1R}(\omega) \quad (4.17)$$

where $V_{0R}(\omega)$ and $V_{1R}(\omega)$ are real functions, derived as follows

$$\begin{aligned} V_{0R}(\omega) &= H_{0R}(\omega)F_{0R}(\omega T) - H_{1R}(\omega)F_{1R}(\omega T) \\ V_{1R}(\omega) &= H_{0R}(\omega - \pi/T)F_{0R}(\omega T) \\ &\quad -H_{1R}(\omega - \pi/T)F_{1R}(\omega T) \end{aligned} \tag{4.18}$$

Due to our class of filter bank, which is NPMR CT HFB, and taking (4.7) into consideration, we can consider $V_{0R}(\omega)$ and $V_{1R}(\omega)$ instead of $V_0(j\omega)$ and $V_1(j\omega)$. This implies that if, for example, $|V_{0R}(\omega)|$ and $|V_{1R}(\omega)|$, approximate one and zero, respectively, so do $|V_0(\omega)|$ and $|V_1(\omega)|$. Therefore, from (4.17), we get the following

$$|V_0(j\omega)| = |V_{0R}(\omega)|, \qquad |V_1(j\omega)| = |V_{1R}(\omega)| \tag{4.19}$$

4.2 Filter Bank Design

4.2.1 Design of the Analog Analysis Filters

In our case the requirements on $H_0(j\omega)$ and $H_1(j\omega)$ in terms of frequency selectivity, passband and stopband attenuations are normally set by the desired ADC performance. Since $H_0(j\omega)$ and $H_1(j\omega)$ are designed by taking the sum and the difference of two stable all-pass filters $A_0(s)$ and $A_1(s)$ as mentioned in previous subsection, it is enough to just design either $H_0(j\omega)$ or $H_1(j\omega)$. However, the chosen one must be designed in such a way that both filters satisfy their respective requirements, i.e. the two filters $H_0(j\omega)$ and $H_1(j\omega)$ should be complementary filters. This means that the absolute value of the sum of $H_0(j\omega)$ and $H_1(j\omega)$ frequency response equals one, i.e.

$$\left|H_0(e^{j\omega}) + H_1(e^{j\omega})\right| = 1 \tag{4.20}$$

Furthermore, since low filter order is of high priority, the filters used in filter bank design are equiripple filters. For analysis filter bank, the specifications of $H_0(j\omega)$ and $H_1(j\omega)$ are as follows

$$
\begin{aligned}
&1-\delta_s^2 \le \left|H_0(j\omega)\right|^2 \le 1, \qquad \omega \in \left[0, \pi/T - \omega_s\right] \\
&\left|H_0(j\omega)\right|^2 \le \delta_s^2, \qquad \omega \in \left[\omega_s, \pi/T\right]
\end{aligned} \tag{4.21}
$$

and

$$
\begin{aligned}
&1-\delta_s^2 \le \left|H_1(j\omega)\right|^2 \le 1, \qquad \omega \in \left[\omega_s, \pi/T\right] \\
&\left|H_1(j\omega)\right|^2 \le \delta_s^2, \qquad \omega \in \left[0, \pi/T - \omega_s\right]
\end{aligned} \tag{4.22}
$$

The approximation problem of finding suitable or reasonable $H_0(j\omega)$ and $H_1(j\omega)$ can be solved in various methods. One method is to use standard tabulated filters with suitable passband and stopband attenuation which could be done easily using MATLAB. Then, if there is a requirement of finding a filter that would achieve transmission zero pair at, for instance $\pm j\pi/T$ a frequency transformation can be performed to achieve such condition.

4.2.2 Design of the Digital Synthesis Filters

For synthesis filters, let's suppose the following specifications of distortion $V_0(j\omega)$ and aliasing terms $V_1(j\omega)$,

$$
\begin{aligned}
&1-\delta_1 \le \left|V_0(j\omega)\right|^2 \le 1+\delta_1, \qquad \omega \in \left[0, \pi/T\right] \\
&\left|V_1(j\omega)\right|^2 \le \delta_2, \qquad \omega \in \left[0, \pi/T\right]
\end{aligned} \tag{4.23}
$$

The synthesis filters $F_0(e^{j\omega T})$ and $F_1(e^{j\omega T})$ are then optimized or designed in such a way that distortion $V_0(j\omega)$ and aliasing terms $V_1(j\omega)$ meet the requirements of (4.23). To optimize $F_0(e^{j\omega T})$ and $F_1(e^{j\omega T})$, the relations given by (4.19) are considered, which restates the specifications of (4.23), since NPMR is considered. Thus, (4.23) becomes

$$
\begin{aligned}
&1-\delta_1 \le V_{0R}(\omega T) \le 1+\delta_1, \qquad \omega T \in \left[0, \pi\right] \\
&-\delta_2 \le V_{1R}(\omega T) \le \delta_2, \qquad \omega T \in \left[0, \pi\right]
\end{aligned} \tag{4.24}
$$

Therefore, if $V_{0R}(\omega T)$ and $V_{1R}(\omega T)$ satisfy equation (4.24), then $\left|V_0(e^{j\omega T})\right|$ and $\left|V_1(e^{j\omega T})\right|$ are also satisfying (4.24). The filters $F_0(e^{j\omega T})$ and $F_1(e^{j\omega T})$ can for a given filter order, be easily designed such that the distortion and aliasing functions satisfy (4.24). This can be achieved by solving the following linear programming (LP) problem

minimize η_{N+1}

subject to

$$\begin{aligned}
&-\eta_{N+1}\delta_1/\delta_2 + \sum_{l=0}^{N}\eta_l R_1(l,\omega_k T)R_2(l,\omega_k T) \le 1\\
&-\eta_{N+1}\delta_1/\delta_2 - \sum_{l=0}^{N}\eta_l R_1(l,\omega_k T)R_2(l,\omega_k T) \le -1\\
&-\eta_{N+1} + \sum_{l=0}^{N}\eta_l R_1(l,\omega_k T)R_3(l,\omega_k T) \le 0\\
&-\eta_{N+1} - \sum_{l=0}^{N}\eta_l R_1(l,\omega_k T)R_2(l,\omega_k T) \le 0
\end{aligned} \tag{4.25}$$

where all η_l's $l=0,1,\ldots,N+1$ are free unknown parameters, and with $R_2(l,\omega_k T)$ and $R_3(l,\omega_k T)$ given by

$$R_2(l,\omega_k T)=\begin{cases}\cos\left(\dfrac{\Phi_0(\omega)-\Phi_1(\omega)}{2}\right), & 0\le l\le\dfrac{N-1}{2}\\ -\sin\left(\dfrac{\Phi_0(\omega)-\Phi_1(\omega)}{2}\right), & \dfrac{N+1}{2}\le l\le N\end{cases} \tag{4.26}$$

$$R_3(l,\omega_k T)=\begin{cases}\cos\left(\dfrac{\Phi_0(\omega-\pi/T)-\Phi_1(\omega-\pi/T)}{2}\right), & 0\le l\le\dfrac{N-1}{2}\\ -\sin\left(\dfrac{\Phi_0(\omega-\pi/T)-\Phi_1(\omega-\pi/T)}{2}\right), & \dfrac{N+1}{2}\le l\le N\end{cases} \tag{4.27}$$

The above expressions for LP problem are the special case that occurs when there are no requirements on the phase response of the distortion function. The linear programming in (4.25) can be efficiently solved with the help of simplex method, which is implemented in MATLAB's optimization toolbox by **linprog.m**. In general, the problem in (4.25) must be solved a number of times, with increasing or decreasing values of N in order to find the minimum-order filter that satisfies (4.25). Another alternative method to LP is to utilize the well-known techniques such as the windowing method and the frequency-sampling method- the details of these techniques are given in [2, 3, 4]. However, they also have some minor disadvantages. A major problem is a lack of precise control of the critical frequencies, such as cut off frequencies of stopband and passband. In other words, these techniques, in particular windowing method, do not permit individual control over the approximation errors in different bands. For many applications, better filters result from a minimax strategy (minimization of the maximum error). Such designs can be achieved utilizing algorithmic techniques. In this work we consider a particular effective and widely used algorithmic procedure for the design of FIR filters with a generalized linear phase. It is convenient first to consider the design of a zero-phase filter, i.e. $h_k[n] = h_k[-n]$, the corresponding frequency response is given then by

$$A_k(e^{j\omega}) = h_k[0] + \sum_{n=1}^{N/2} 2h_k[n]\cos(\omega n) \tag{4.28}$$

A casual system can thereafter be obtained from $h_k[n]$ by delaying it by $N/2$ samples. The resulting system has impulse response

$$h[n] = h_k[n - N/2] = h[N - n] \tag{4.29}$$

and a frequency response

$$H(e^{j\omega}) = A_k(e^{j\omega})e^{-j\omega N/2} \tag{4.30}$$

Let's consider the case of a lowpass filter with a real function $A_k(e^{j\omega})$, where zero is to be approximated in the band $\omega_s \le |\omega| \le \pi$ with a maximum absolute error of δ_2, and unity is approximated in the band $0 \le |\omega| \le \omega_p$ with a maximum absolute error δ_1 (ω_s and ω_p denote stopband edge frequency and passband edge frequency, respectively). An algorithmic technique for designing a filter to meet these specification for lowpass filter must, in effect, systematically vary the $(N/2+1)$ unconstrained impulse response values $h_k[n]$, where $0 \le n \le N/2$. Design algorithms have been developed in literature e.g. [4]

(see chapter 7 section 7.4 for details). In this work we consider only the Parks-McClean algorithm, the details of this algorithm can be found at [2, 3, 4]. Basically, Parks-McClean algorithm is based on reformulating the filter design problem as a problem in polynomial approximation. The term $\cos(\omega n)$ in (4.28) can be expressed as a sum of powers of $\cos(\omega)$ in the form of

$\cos(\omega n) = T_n(\cos\omega)$ where $T_n(x)$ is an n^{th} -order polynomial given as

$$T_n(x) = \cos(n\cos^{-1}x) \tag{4.31}$$

where $T_n(x)$ is a Chebyshev polynomial. Equation (4.28) can then be expressed as an L^{th} – order polynomial in $\cos(\omega)$, namely,

$$A_k(e^{j\omega}) = \sum_{l=0}^{L} \alpha_l (\cos\omega)^l \tag{4.32}$$

where α_l's are constants that are related to $h_k[n]$, the values of the impulse response with the substitution $x = \cos\omega$, and $L = N/2$. We can express (4.32) as

$$A_k(e^{j\omega}) = \mathrm{P}(x)\big|_{x=\cos\omega} \tag{4.33}$$

where $\mathrm{P}(x)$ is the L^{th} – order polynomial

$$\mathrm{P}(x) = \sum_{l=0}^{L} \alpha_l x^l \tag{4.34}$$

The key to gaining control over ω_p and ω_s is to fix them at their desired values and let δ_1 and δ_2 vary. To formalize the approximation problem let us define an approximation error function

$$E(\omega) = W(\omega)[H_d(e^{j\omega}) - A_k(e^{j\omega})] \tag{4.35}$$

where the weighting function $W(\omega)$ incorporates the approximation error parameters into the design process. In this design technique, the error function $E(\omega)$, the weighting function $W(\omega)$, the desired

frequency response $H_d(e^{j\omega})$ are defined only over closed subintervals of $0 \le \omega \le \pi$. The approximating function $A_k(e^{j\omega})$ is not constrained in the transition region(s), and it may take any shape necessary to achieve the desired response in the other subintervals. Assume as an example, we want to obtain an approximation for a lowpass filter, i.e.

$$H_d(e^{j\omega}) = \begin{cases} 1, & 0 \le \omega \le \omega_p \\ 0, & \omega_s \le \omega \le \pi \end{cases} \tag{4.36}$$

the weighting function allows us to weight the approximation error differently in the different approximation intervals. For the lowpass filter approximation problem, the weighting function is

$$W(\omega) = \begin{cases} \delta_2 / \delta_1, & 0 \le \omega \le \omega_p \\ 1, & \omega_s \le \omega \le \pi \end{cases} \tag{4.37}$$

with this weighting, the maximum weighted absolute approximation error is $\delta = \delta_2$ in both bands. The criterion utilized in this procedure is known as Minimax or Chebyshev criterion, where within the frequency intervals of interest, that is the passband and stopband. We seek a frequency response $A_k(e^{j\omega})$ that minimizes the maximum weighted approximation error of equation (4.35), stated more formally, the best approximation is to be found in the sense of

$$\min_{\{h_k[n]:0 \le n \le N/2\}} \left(\max_{\omega \in F} \left| E(\omega) \right| \right)$$

where F is the closed subset of $0 \le \omega \le \pi$ such that $0 \le \omega \le \omega_p$ and $\omega_s \le \omega \le \pi$. This algorithmic design utilizes alternation theorem (details in [4]). The alternation theorem gives necessary and sufficient conditions on the error for optimality in the Chebyshev or minimax sense. In this work, instead of using LP as in [10], we are using this alternative approach (as explained above). Standard MATLAB functions are used from the filter design toolbox to optimize the filters used in our system.

4.3 Design Example

In this section, we demonstrate by means of a design example the proposed filter banks. This example considers the design of a two-channel NPMR CT hybrid filter bank. We start by designing the analysis filters to meet (4.21) and (4.22). The specifications of the analysis filters in terms of the stopband edge

frequency and stopband attenuation is $\omega_s = 0.501\pi / T$ and $\delta_s = 0.01$, where the transition width is $\Delta = 0.002$. The specifications are satisfied by using a seventeenth-order filter pair. The magnitude response of the analysis filters are shown in Fig. 4.4. With the analysis filters fixed, the synthesis filters are optimized by using the method described in section 4.2 under *Design of the digital Synthesis Filters* with $F_{eq}(e^{j\omega T}) = 1$, so that the distortion and aliasing satisfy the conditions for the NPMR filter bank design. The specifications are satisfied using a filter pair of order $N = 1945$. The magnitude responses of the synthesis filters are shown in Fig. 4.4 and the resulting magnitude responses of the distortion and aliasing functions are shown in Fig. 4.5.

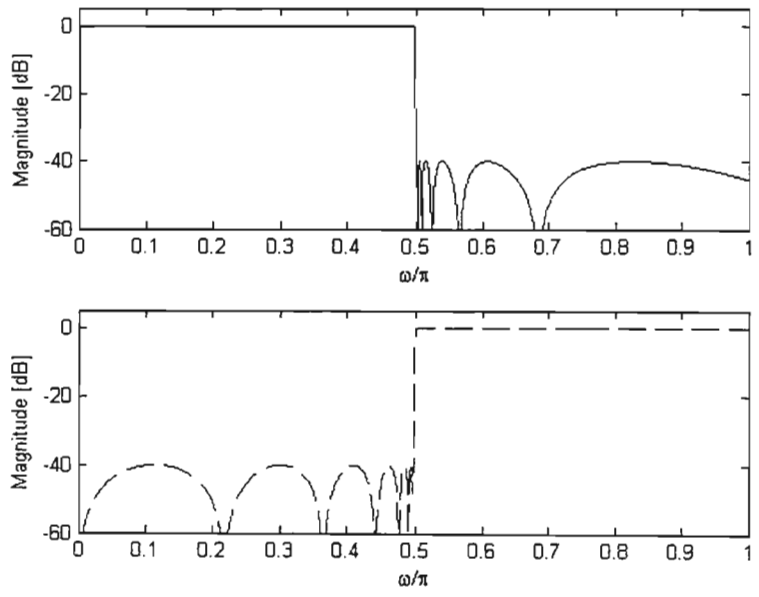

Figure 4.2: Magnitude responses of the Lowpass (top) and Highpass (bottom) of analog analysis filters

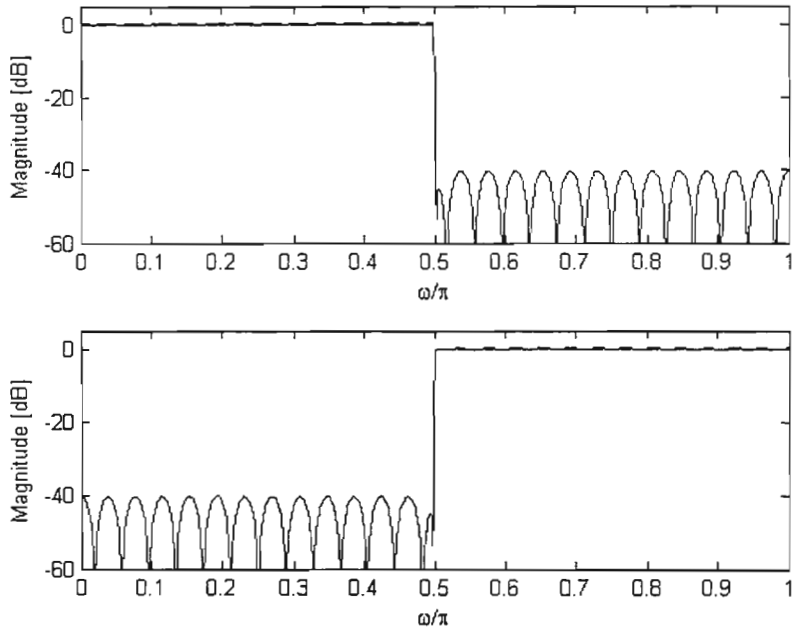

Figure 4.3: Magnitude responses of the Lowpass (top) and Highpass (bottom) of digital synthesis filters

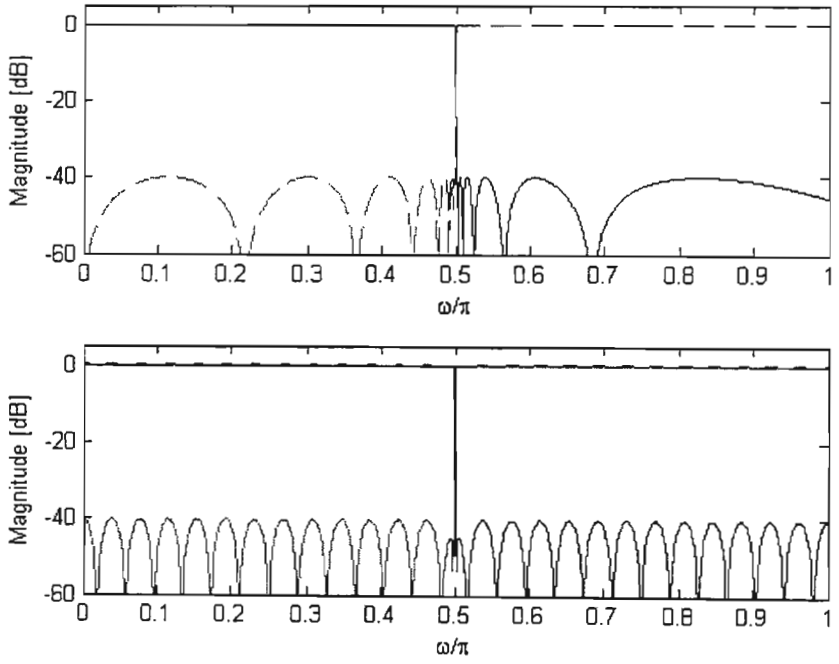

Figure 4.4: Magnitude responses of the analog analysis filters (top) and digital synthesis filters (bottom)

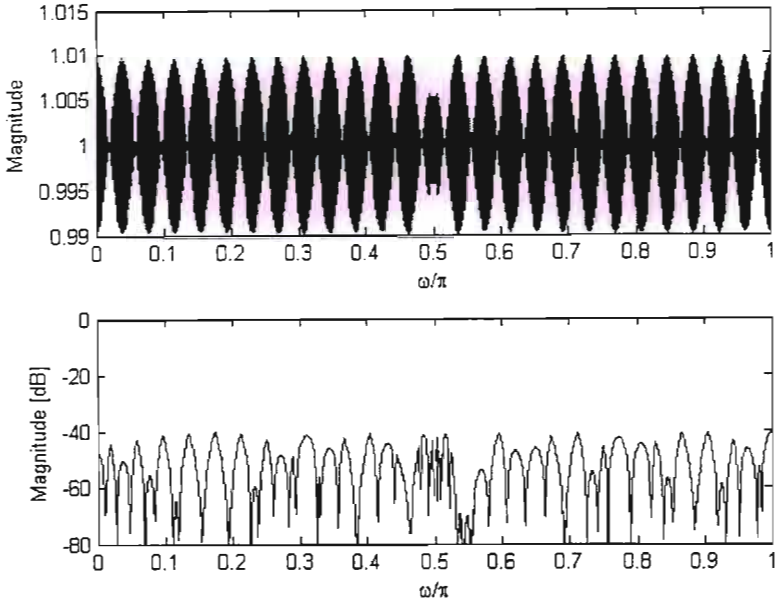

Figure 4.5: Magnitude responses of the distortion function (top) and aliasing function (bottom)

4.4 Two-Channel Hybrid Analog and Digital (IIR) Filter Bank

This section introduces another class of two-channel NMPR HFB that uses IIR synthesis filter bank. It utilizes the same analysis filter bank as the previous one in section 4.1 but uses IIR synthesis filters instead of FIR for the synthesis filter bank. Utilizing IIR filters instead of FIR, is another way of reducing the computational complexity. The transfer functions of the analysis filter are exactly the same as in section 4.1. We consider the same equations from 4.8 till 4.11 for analysis filter bank.

4.4.1 Synthesis Filters

Let's express the transfer functions of the digital lowpass and highpass synthesis filters as follows

$$G_0(e^{j\omega T}) = \frac{F_{0n}(e^{j\omega T})}{F_D(e^{j\omega T})}, \qquad G_1(e^{j\omega T}) = \frac{F_{1n}(e^{j\omega T})}{F_D(e^{j\omega T})} \tag{4.42}$$

where $F_{0n}(e^{j\omega T}), F_{1n}(e^{j\omega T})$ and $F_D(e^{j\omega T})$ can be represented as

$$F_0(e^{j\omega T}) = \sum_{k=0}^{N_n} f_0(k)e^{-j\omega Tk}, \quad F_1(e^{j\omega T}) = \sum_{k=0}^{N_n} f_1(k)e^{-j\omega Tk}$$

$$F_D(e^{j\omega T}) = \sum_{k=0}^{N_D} f_D(k)e^{-j\omega Tk} \tag{4.43}$$

In (4.43) the numerator polynomial order denoted as N_n is always odd, and $f_0(k)$ and $f_1(k)$ are symmetric and antisymmetric, respectively, i.e. $f_0(k) = f_0(N_n - k)$ and $f_1(k) = -f_1(N_n - k)$, $k = 0, 1, ..., N_n$. The frequency response of $F_0(e^{j\omega T})$, $F_1(e^{j\omega T})$ and $F_D(e^{j\omega T})$ can therefore be represented as

$$\begin{aligned} F_0(e^{j\omega T}) &= e^{-j\left(\frac{N_n \omega T}{2}\right)} F_{0R}(\omega T) \\ F_1(e^{j\omega T}) &= je^{-j\left(\frac{N_n \omega T}{2}\right)} F_{1R}(\omega T) \\ F_D(e^{j\omega T}) &= e^{j\Phi_{F_D}(\omega T)} \left| F_D(e^{j\omega T}) \right| \end{aligned} \tag{4.44}$$

where $\Phi_{F_D}(\omega T)$ is the phase response of $F_D(e^{j\omega T})$ and $F_{0R}(\omega T)$ and $F_{1R}(\omega T)$ are the real-valued zero-phase functions as given in [2].

4.4.2 Distortion and Aliasing

With analysis and synthesis filters as given in (4.40) to (4.44) in the previous subsections, the distortion and aliasing function can be given as

$$\begin{aligned} V_0(j\omega) &= e^{j\left(\frac{\Phi_0(\omega)+\Phi_1(\omega)-N_n\omega T}{2} - \Phi_{F_D}(\omega T)\right)} V_{0R}(\omega) \\ V_1(j\omega) &= e^{j\left(\frac{\Phi_0(\omega-\pi/T)+\Phi_1(\omega-\pi/T)-N_n\omega T}{2} - \Phi_{F_D}(\omega T)\right)} V_{1R}(\omega) \end{aligned} \tag{4.45}$$

where $V_{0R}(\omega)$ and $V_{1R}(\omega)$ are real functions, which can be expressed as follows

$$V_{0R}(\omega) = H_{0R}(\omega)\frac{F_{0R}(\omega T)}{\left|F_D(e^{j\omega T})\right|} - H_{1R}(\omega)\frac{F_{1R}(\omega T)}{\left|F_D(e^{j\omega T})\right|}$$

$$V_{1R}(\omega) = H_{0R}(\omega - \pi/T)\frac{F_{0R}(\omega T)}{\left|F_D(e^{j\omega T})\right|} \qquad (4.46)$$

$$-H_{1R}(\omega - \pi/T)\frac{F_{1R}(\omega T)}{\left|F_D(e^{j\omega T})\right|}$$

Due to our class of filter bank, which is NPMR HFB, and taking (4.7) into consideration, we can consider $V_{0R}(\omega)$ and $V_{1R}(\omega)$ instead of $V_0(j\omega)$ and $V_1(j\omega)$. This implies that if, for example, $|V_{0R}(\omega)|$ and $|V_{1R}(\omega)|$, approximates one and zero, respectively, so do $|V_0(\omega)|$ and $|V_1(\omega)|$. Therefore from (4.46), we obtain the following

$$|V_0(j\omega)| = |V_{0R}(\omega)|, \qquad |V_1(j\omega)| = |V_{1R}(\omega)| \qquad (4.47)$$

4.5 Filter Bank Design

4.5.1 Design of the digital Synthesis Filters

The design of the analog analysis filters is exactly the same as in section 4.2. For synthesis filters let's assume the following specifications of distortion $V_{0R}(\omega)$ and aliasing terms $V_{1R}(\omega)$

$$1-\delta_1 \le V_{0R}(\omega T) \le 1, \qquad \omega T \in [0,\pi]$$
$$-\delta_2 \le V_{1R}(\omega T) \le \delta_2, \qquad \omega T \in [0,\pi] \qquad (4.34)$$

If $V_{0R}(\omega T)$ and $V_{1R}(\omega T)$ satisfy equation (4.34), then $|V_0(e^{j\omega T})|$ and $|V_1(e^{j\omega T})|$ are also satisfied.

In this work, instead of using linear programming (LP) and non-linear programming (NLP) as in [5], we use recently developed IIR Halfband filters, details of the design of these IIR Halfband filter is given in [47-51]. This is due to the limitations with the use of standard MATLAB functions like **ellip.m**, which comes from the fact that, this function is based on the Jacobi elliptic sn function given as follows in MATLAB, [sn,cn,dn]=ellipj(U,M), where M is a parameter $0 < M < 1$ and U is a real argument. The function **ellipj (U, M)** is accurate to *eps* = 2.220446049250313e-016 in MATLAB. Then for larger stopband attenuation, **ellipj.m** returns an error because some parameters may become too small in the

optimization routines, and the argument U becomes a complex number. Hence, that is the reason we are using the design procedure given in [47-51].

4.6 Design Example

In this section, we demonstrate by means of a design example, the proposed filter bank. This example considers the design of a two-channel NPMR CT hybrid filter bank with the IIR synthesis filters.

First, a seventeenth-order power complementary analog filters pair is designed with minimized and equal stopband attenuation and with stopband edges at $\omega_s = 0.501\pi / T$ and stopband attenuation $\delta_s = 0.01$, where the transition width is $\Delta = 0.002$. To design and optimize the IIR synthesis filters, we used a different approach. Instead of using design approach available on MATLAB for discrete-time IIR filters, which resulted with high orders of the numerator and denominator polynomials, yielding the lowest overall complexity, turned out to be 17, we used efficient IIR halfband filters as mentioned before. With such efficient halfband filters we obtained the magnitude response of synthesis filters as shown in Fig 4.7. The orders of the numerator and denominator polynomials, yielding the lowest overall complexity, turned out to be 9 for the lowpass filter and 8 for the highpass filter. The magnitude responses of the synthesis filters are shown in Fig. 4.7 and the resulting magnitude responses of the distortion and aliasing functions are shown in Fig. 4.8.

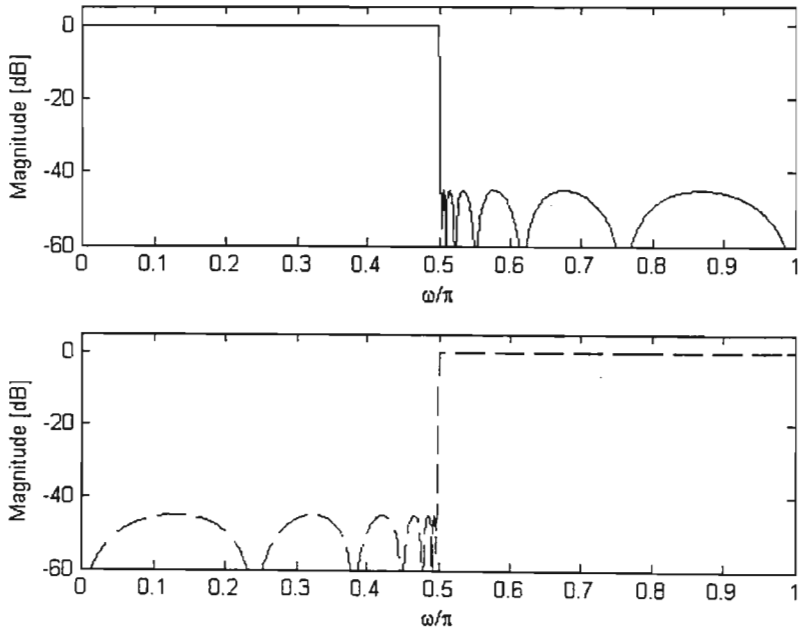

Figure 4.6: Magnitude responses of the Lowpass (top) and Highpass (bottom) of digital synthesis filters

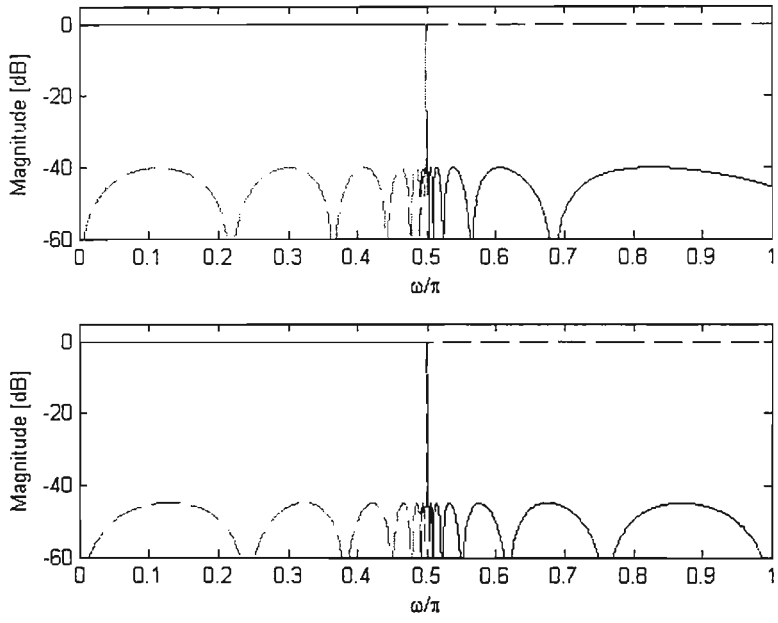

Figure 4.7: Magnitude responses of the analog analysis filters (top) and digital synthesis filters (bottom)

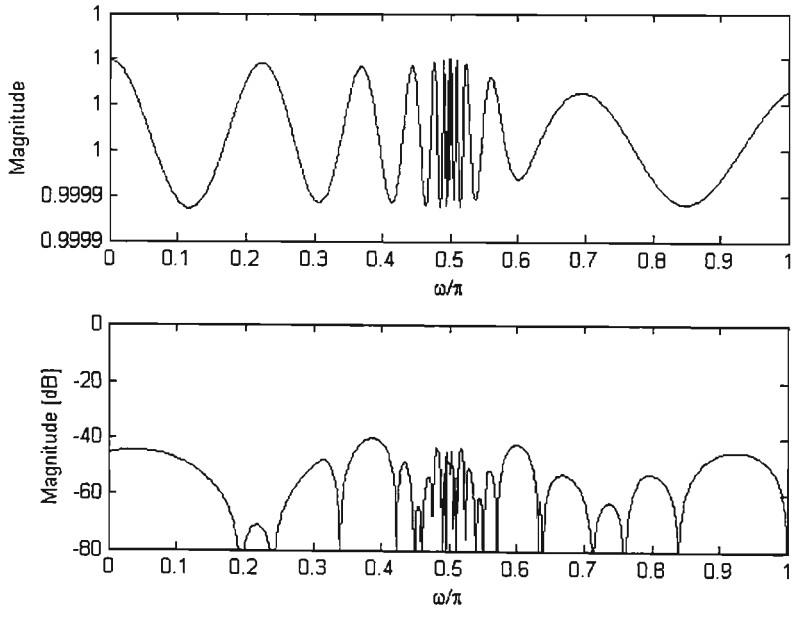

Figure 4.8: Magnitude responses of the distortion function (top) and aliasing function (bottom)

CHAPTER 5

FREQUENCY-RESPONSE MASKING APPROACH (FRM) TECHNIQUE

The multirate approach is normally used to improve the computational efficiency of digital filters. In this chapter, the basics of the FRM approach are described in detail. Firstly the simple case when the filter is restricted to be a narrow-banded is described, and then the more general case for arbitrary bandwidth design, which is used in our design procedures. For multirate systems half-band filters are of particular importance, in the proposed system, halfband filters are used for two-channels.

Digital filters with sharp transition bands are difficult and sometimes impossible to implement using conventional structures. Finite-impulse response (FIR) filters are well known to have good properties, like stability and possibility to have exact linear-phase. However, there is one major drawback, namely a rapidly increasing filter order for filters with narrow transition band. The filter order can be estimated using the formula

$$N = q/(\omega_s T - \omega_c T) \tag{5.1}$$

where $\omega_c T$ is the passband edge, $\omega_s T$ is the stopband edge of the filter, and q is a constant depending on the tenth logarithm of the square root of the stopband and passband ripples

$$q = 2\pi \frac{-20\log(\sqrt{(\delta_c \delta_s)}) - 13}{14.6} \tag{5.2}$$

Equation (5.1) implies that the filter order N is inversely proportional to the width of the transition band. Therefore, for filter specifications with sharp cutoff, the cost of a regular FIR filter might be very expensive. One solution to this problem is to use the FRM approach. The application of the frequency-response masking technique for implementing a sharp FIR with arbitrary bandwidth was first introduced in Lim (1986) for FIR filters. The aim of the approach was to reduce the complexity of the FIR filter. FRM technique was later extended to recursive filters in Johansson and Wanhammar (1997, 2000), respectively.

5.1 Narrow-Band Filter Design

The principle of a narrow-band filter design utilizing the FRM technique is shown in Fig. 5.2. and the structure is illustrated in Fig. 5.1. $G(z^M)$ and $G_m(z)$ are known in literature as periodic model filter and

masking filter, respectively. According to Fig. 5.1, $G(z^M)$ is modified to have a periodicity of $2\pi/M$ instead of 2π. This is similar to inserting $M-1$ zeros between the impulse response values of $g(n)$, resulting in the transfer function $G(z^M)$. The images produced by $G(z^M)$ are eliminated by the masking filter. For the lowpass filter the masking filter is lowpass, for the bandpass the masking filter is bandpass and for the narrow-band filter the transfer function is expressed in the form [11, 12, 52]

$$H(z) = G(z^M)G_m(z) \tag{5.3}$$

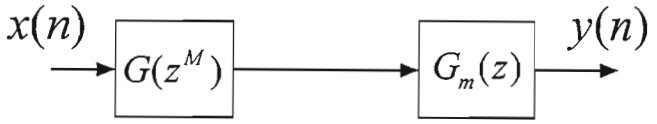

Figure 5.1: Block diagram of narrow-band filter design utilizing the FRM technique

Typical magnitude response of a narrow-band filter design is illustrated in Fig. 5.2. The overall filter represented by equation (5.3) is restricted to have a narrow-band bandwidth. For instance, for a lowpass filter, the stopband edges is restricted as

$$\omega_s T < \pi/M \tag{5.4}$$

Fig. 5.2 shows a method of deriving sharp filters from filters with much wider transition bands. This simple FRM approach suffers a serious difficulty, while replacing every delay in $G(z)$ by M delays, which reduces the transition width by a factor of M, the passband bandwidth is also reduced by the same factor. It is thus only suitable for narrow-band design. It can also be illustrated that the interpolated FIR (IFIR) is a special case of this FRM technique where the frequency response of the interpolator belongs to the same category as that of Fig. 5.2(c) [12, 52].

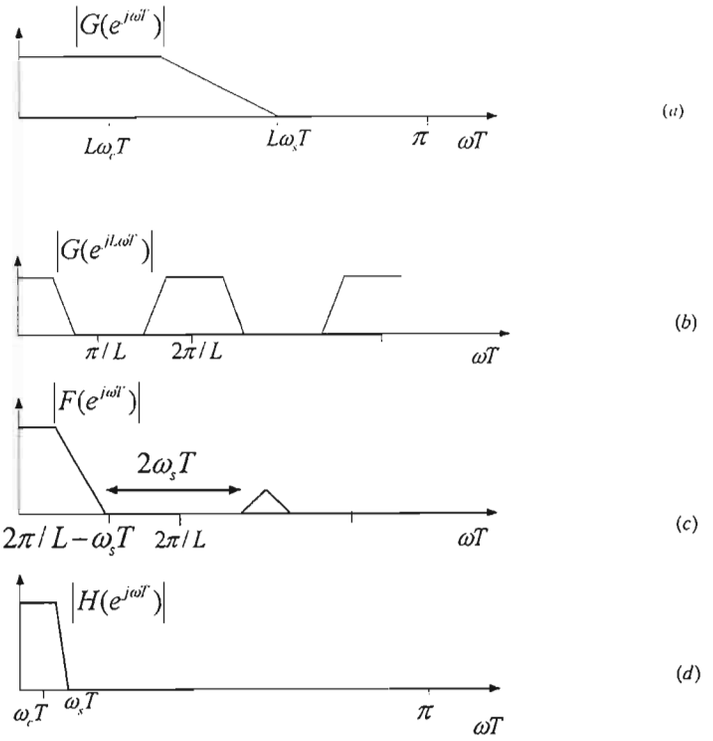

Figure 5.2 Frequency response masking technique; for narrow-band filter design

5.2 Arbitrary Bandwidth Filter Design

It is necessary to first discuss the concept of complementary filters, in order to explain the principle of obtaining an arbitrary bandwidth filter design. Taking the complement of a transfer function can be easily shown using systems with a real frequency response. Fig. 5.3 illustrates a structure whose inner system, with transfer function $H(e^{j\omega})$, is used to form a complementary transfer function [2, 4, 6, 11, 12, 52].

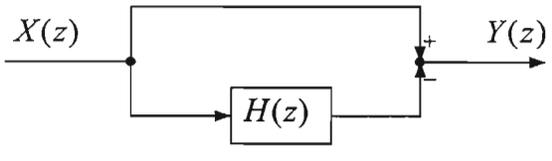

Figure 5.3: Block diagram illustrating complementary concept

Doing the analysis of Fig.5.3, the following is always true

$$\begin{aligned} Y(e^{j\omega}) &= [1 - H(e^{j\omega})] \cdot X(e^{j\omega}) \\ &= H_c(e^{j\omega}) \cdot X(e^{j\omega}) \end{aligned} \tag{5.5}$$

Therefore, the complementary transfer function is

$$H_c(e^{j\omega}) = [1 - H(e^{j\omega})]$$

This means, it is the 1's complement of the transfer function $H(e^{j\omega})$. Complementing can be used to derive a new transfer function from an old transfer function. This process will be used in explaining the design of arbitrary bandwidth design utilizing FRM technique. The following is then true, two filters $G(z)$ and $G_c(z)$ are said to be complementary only if the absolute sum of their frequency response equals one,

$$\left|G(e^{j\omega}) + G_c(e^{j\omega})\right| = 1$$

To present the principle of FRM approach for arbitrary case, Fig. 5.4 is used. Lim (1986) introduced a more general FRM technique based on the structure shown in Fig.5.4, which can handle filters with any bandwidth. The basic idea is to compose the overall filter using several subfilters with very low orders, namely, model filter, which is a bandedge shaping filter, its complementary and two masking filters. In this structure a complementary filter in the second branch of the structure is included. This complementary filter can be derived using Fig. 5.3 as shown in equation (5.5). $G_c(z^M)$ is known as complementary periodic model filter and $G(z^M)$ as periodic model filter. $G_m(z)$ and $G_{mc}(z)$ are called masking filters.

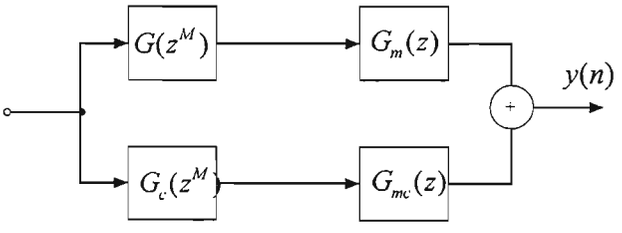

Figure 5.4 General structure of the FRM approach

The transfer function of the overall filter can be expressed as

$$H(z) = G(z^M)G_m(z) + G_c(z^M)G_{mc}(z) \qquad (5.6)$$

where $G_c(z^M)$ is the complementary of $G(z^M)$ and $G_m(z)$ and $G_{mc}(z)$ are masking filters. The filters $G_m(z)$ and $G_{mc}(z)$ are actually masking out the wanted images of the periodic model filter. Typical magnitude responses for model, periodic model, masking filters and overall filters are illustrated in Fig. 5.5 (a, b, c, d). The choice of model filter is dependent on the authors, based on the application they have at the hand. For the proposed system in this dissertation, the model filter $G(z)$ is a halfband filter as well as $G_c(z)$. Replacing each delay in the model filter $G(z)$ and its complementary filter pair by M delays,

periodic model filters are obtained respectively, as shown in Fig. 5.5(b). The boundary frequencies for the masking filters and the overall filters are indicated in Fig. 5.5(c and d). The overall filter is obtained by adding the outputs of the first and the second branch of Fig. 5.4.

Fig. 5.5 (c) illustrates the case when $G_{m0}(z)$ determines the transition band, this case is referred to as *Case 1* and Fig. 5.5(d) shows the case when $G_{m1}(z)$ determines the transition band, this case is referred to as *Case 2*. Table-I and Table-II show the boundary frequencies for *Case 1* and for *Case 2*.

TABLE 5.1: CASE 1: BOUNDARY FREQUENCIES

FILTER	ω_p	ω_s
$G_m(z)$	$(2k\pi + \omega_{c,G}T)/M$	$(2(k+1)\pi - \omega_{s,G}T)/M$
$G_{mc}(z)$	$(2k\pi - \omega_{c,G}T)/M$	$(2k\pi + \omega_{s,G}T)/M$
$H(z)$	$(2k\pi + \omega_{c,G}T)/M$	$(2k\pi + \omega_{s,G}T)/M$

TABLE 5.2: CASE 2: BOUNDARY FREQUENCIES

FILTER	ω_p	ω_s
$G_m(z)$	$(2(k-1)\pi + \omega_{s,G}T)/M$	$(2k\pi - \omega_{c,G}T)/M$
$G_{mc}(z)$	$(2k\pi - \omega_{s,G}T)/M$	$(2k\pi - \omega_{c,G}T)/M$
$H(z)$	$(2k\pi - \omega_{s,G}T)/M$	$(2k\pi + \omega_{c,G}T)/M$

In Tables 5.1 and 5.2, ω_p and ω_s denote passband and stopband edges and k is a constant given

$$k = \left\lfloor \frac{M\omega_{c,G}}{2\pi} \right\rfloor \tag{5.7}$$

for *Case 1*, and for *Case 2* by

$$k = \left\lceil \frac{M\omega_{s,G}}{2\pi} \right\rceil \tag{5.8}$$

In the filter design problem, ω_p and ω_s are always given and k, M, $\omega_{s,G}$, $\omega_{c,G}$ must be determined. For M there is no known closed form of analytic expression for finding the optimum M [52]. However, a good choice of M can still be obtained by simply estimating the filter complexity for each value and then

finally choose the M, which corresponds to the lowest estimate (or which gives the minimum overall complexity).

For proper filter design, the group delay of the masking filters must always be equal. In case if they are not equal, leading delays must be added to the masking filter that has less length in comparison to the other masking filter, to equalize their group delays. Another important point note is that the lengths of masking filters must be either both even or both odd. To avoid the half sample delays, i.e. if the delay is given as Z^{-x}, x can be anything depending on the choice of the complementary filter, $(n-1)M$ must be even. The transition width of the overall filter can then be chosen to equal one of the transition bands of either periodic model filter or periodic complementary filter. Choosing the case which will give the minimum overall complexity for ω_p and ω_s and M, only one of Fig. 5.5(c) or (d), however, not both Fig. 5.5(c) and (d) will yield a set of ω_p and ω_s satisfying the constraint $\omega_s < \pi$.

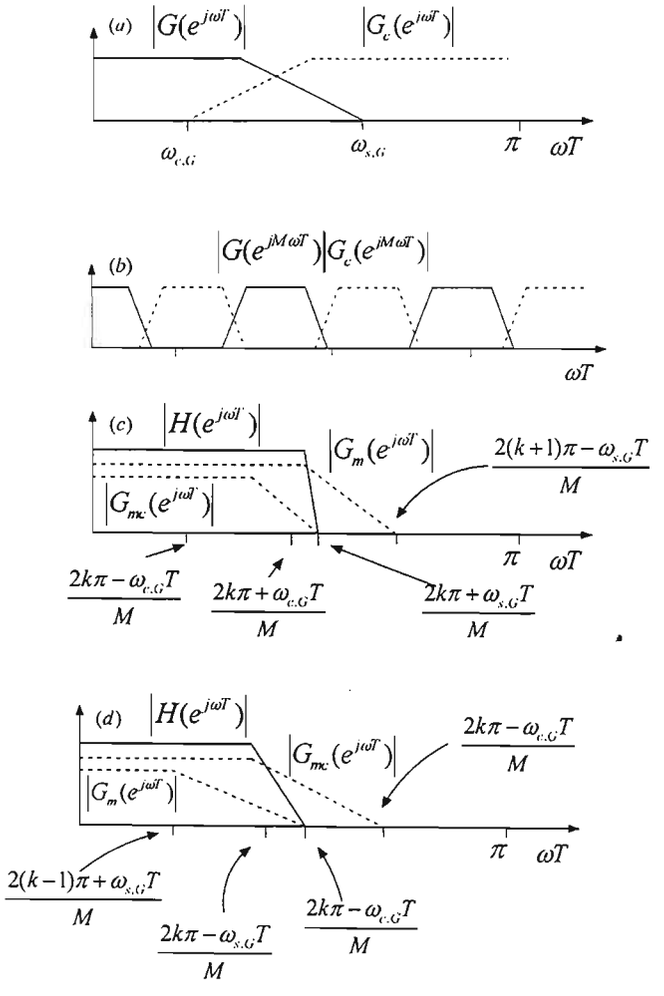

Figure 5.5: Illustration of magnitude responses in the FRM

Complementary filter choices depend on the choice of authors, for instance, $G_c(z)$ can be selected as one of the following

$$G_c(z) = z^{-(N_G/2)} - G(z) \tag{5.9}$$

$$G_c(z) = G(-z) \tag{5.10}$$

$$G_c(z) = z^{-M(N_G-1)/2} - G(z) \tag{5.11}$$

In [11] a lot of information is given about the choice of a complementary filter. The important note to extract from [11] is the following; for filter bank design the case where $G(z)$ and $G_c(z)$ are power complementary is favorable property and this can be show easily by using (5.10). For instance, N_G , which is the order of $G(z)$, can either be chosen as even or odd. In the case that it is even, the following is true:

$$\left|G(e^{j\omega T}) + G_c(e^{j\omega T})\right| \approx 1 \tag{5.12}$$

and in the case that it is odd:

$$\left|G(e^{j\omega T})\right|^2 + \left|G_c(e^{j\omega T})\right|^2 \approx 1 \tag{5.13}$$

(5.13) is preferred in filter bank design, due to its desired power complementary property.

5.3 Proposed HFB Structures for SDR Utilizing FRM

In this section we are using the FRM technique to implement the FIR synthesis filters. This is a class of two-channel NMPR HFB class with FIR synthesis filter bank synthesized using frequency-response masking (FRM) technique. This class utilizes same analysis filter bank as in section 4.1 and 4.2. The synthesis filters are designed using similar halfband filters as in section 4.2 and McClellan-Parks-Rabiner's algorithm is widely used in the design of the masking filters.

When designing linear-phase FIR filters, the most common approach to determine the filter coefficients $h(n)$, is to employ the McClellan-Parks-Rabiner's (MPR) algorithm. Instead of the filter coefficients, the extreme frequencies are optimized (the frequencies corresponding to the largest deviations from the desired

function). This algorithm is very efficient from the complexity point of view, but has some restrictions regarding the optimization constraints compared to the more general linear programming (LP). The MPR algorithm gives the equiripple solution, which means that all ripples in a passband or stopband have the same size and that the solution is a global optimum for a given filter order and specification.

In the frequency-response masking (FRM) approach, the transfer function of the overall filter can be given as in [12, 52]

$$H(z) = G(z^M)G_m(z) + G_c(z^M)G_{mc}(z) \tag{5.14}$$

FRM technique was first introduced as a means to reduce the arithmetic complexity of linear-phase FIR filters with narrow transition bands. In this case, $G(z)$ and $G_c(z)$ are even-order linear-phase filters of equal delays and form a complementary filter pair, whereas both $G_m(z)$ and $G_{mc}(z)$ are either even or odd-order linear-phase filters of equal delays. These filters can be utilized directly to generate the synthesis filters in the proposed filter bank scheme.

The configuration illustrated by Fig. 4.1 is taken as the conventional case as was explained in chapter 4, in this section instead of using $G_0(z)$, lowpass filter and $G_1(z)$, highpass filter as in Fig 4.1, we are synthesizing these filter ($G_0(z)$ and $G_1(z)$) utilizing FRM technique. In other words, $G_0(z)$ is designed or synthesized by the structure given by Fig. 5.4, as well as $G_1(z)$. In simple terms we can say $H(z)$ is an equivalent filter to either $G_0(z)$ and $G_1(z)$, provided the overall filter $H(z)$ is designed to be either lowpass or highpass.

5.4 Proposed Filter Banks for Two-Channel Hybrid Analog and Digital (FIR FRM) Filter Bank

This section gives some expressions for the frequency responses which are very useful in the filter design, the analysis filter as well as the synthesis filters of the proposed filter banks, where the analysis and synthesis filters are generated, based on the use of the frequency-response masking technique. This proposed class utilizes same analysis filter bank as the previous one in section 4.1. The transfer functions of the analysis filter are exactly the same as in section 4.1. We consider the same equations from 4.8 till 4.11 for analysis filter bank.

5.4.1 Synthesis Filters

The design of the synthesis filters corresponding to Fig. 4.1 are given in details in section 4.1. In this subsection we present the case where the synthesis filters are synthesized using FRM. It is necessary to first

give the equation of the conventional case as shown in section 4.1. Since we are considering the NPMR HFB, the corresponding equations for Fig.4.1 are given as

$$G_0(e^{j\omega T}) = 2F_0(e^{j\omega T})$$
$$G_1(e^{j\omega T}) = 2F_1(e^{j\omega T}) \tag{5.18}$$

Then instead of $G_0(e^{j\omega T})$ as in (5.18), we synthesize this lowpass filter by replacing $2F_0(e^{j\omega T})$ of (5.18) with (5.14), which can be written as

$$\begin{aligned} G_0(e^{j\omega T}) &= H(e^{j\omega T}) \\ &= G(e^{j\omega MT})G_m(e^{j\omega T}) + G_c(e^{j\omega MT})G_{mc}(e^{j\omega T}) \end{aligned} \tag{5.19}$$

where $G(e^{j\omega T})$, and $G_c(e^{j\omega T})$ are model and complementary model filters, respectively and $G_m(e^{j\omega T})$, and $G_{mc}(e^{j\omega T})$ are masking filters. The frequency response of model, complementary and masking filters can be written as

$$\begin{aligned} G(e^{j\omega T}) &= e^{-j\left(\frac{N_G \omega T}{2}\right)} G_R(\omega T) \\ G_c(e^{j\omega T}) &= je^{-j\left(\frac{N_G \omega T}{2}\right)} F_{cR}(\omega T) \\ G_m(e^{j\omega T}) &= e^{-j\left(\frac{N_{G_m} \omega T}{2}\right)} G_{mR}(\omega T) \\ G_{mc}(e^{j\omega T}) &= e^{-j\left(\frac{N_{G_m} \omega T}{2}\right)} G_{mcR}(\omega T) \end{aligned} \tag{5.20}$$

where $G_R(\omega T)$, $G_{cR}(\omega T)$, $G_{mR}(\omega T)$, and $G_{mcR}(\omega T)$ represent the zero-phase frequency response of $G(e^{j\omega T})$, $G_c(e^{j\omega T})$, $G_m(e^{j\omega T})$, and $G_{mc}(e^{j\omega T})$, respectively.

- N_G denotes the order of $G(e^{j\omega T})$
- N_{G_m} is the order of $G_m(e^{j\omega T})$

To obtain $G_1(e^{j\omega T})$ would be trivial because, we don't need to change the model filter and complementary filter, we are only required to change the masking filters from lowpass to highpass. In other words, we change $G_m(e^{j\omega T})$ and $G_{mc}(e^{j\omega T})$ to be highpass filters, then we end up with a corresponding highpass filter to $G_0(e^{j\omega T})$. Given the passband and stopband edges of the model filter $G(e^{j\omega T})$, denoted here by $\omega_{c,G}T$ and $\omega_{s,G}T$, respectively

$$\omega_c T = \frac{2k\pi + \omega_{c,G}T}{M}, \qquad \omega_s T = \frac{2k\pi + \omega_{s,G}T}{M} \tag{5.21}$$

$$\omega_c T = \frac{2k\pi - \omega_{s,G}T}{M}, \qquad \omega_s T = \frac{2k\pi - \omega_{c,G}T}{M} \tag{5.22}$$

where (5.21) is for *Case 1 design* and (5.22) *Case 2 design*. The transition band of the model filter $G(e^{j\omega T})$ and complementary model filter $G_c(e^{j\omega T})$ always include $\pi/2$ since these filters are to be approximately power complementary. It is thus practical to let the sum of the passband and stopband edges for these filters, as well as for the analysis and synthesis filters, to be equal to π. This implies the following

$$\omega_c T + \omega_s T = \omega_{c,G}T + \omega_{s,G}T = \pi \tag{5.23}$$

In this work, M and subfilters are selected to satisfy the following rules:

- M is an odd integer, since $\pi M/2 = 2\pi k \pm \pi/2$. This gives $M = k+1$ and $M = k-1$ for *Case 1* and *Case 2,* respectively. This can easily be deduced from (5.21) and (5.22).
- The model and its complementary filter, $G(e^{j\omega T}), G_c(e^{j\omega T})$ are of even order N_G and linear phase FIR filters, with $G_c(e^{j\omega T})$ being related to $G(e^{j\omega T})$ as $G_c(z) = G(-z)$
- The masking filters $G_m(e^{j\omega T})$ and $G_{mc}(e^{j\omega T})$ can be of even order N_{G_m} and linear phase FIR filters or sometimes odd.

5.4.2 Distortion and Aliasing

With analysis and synthesis filters as given in (5.15) to (5.20) in the previous subsections, the distortion and aliasing function can be given as

$$V_0(j\omega) = e^{j\left(\frac{\Phi_0(\omega)+\Phi_1(\omega)-2(MN_G\omega T+N_G\omega T)}{2}\right)}V_{0R}(\omega)$$
$$V_1(j\omega) = e^{j\left(\frac{\Phi_0(\omega-\pi/T)+\Phi_1(\omega-\pi/T)-2(MN_G\omega T+N_G\omega T)}{2}\right)}V_{1R}(\omega) \qquad (5.24)$$

where $V_{0R}(\omega)$ and $V_{1R}(\omega)$ are real functions. To obtain the real function of the distortion and aliasing as in (5.24), let's take masking filters in (5.19), which are lowpass filters given as $G_m(e^{j\omega T})$ and $G_{mc}(e^{j\omega T})$, and introduce a new subscript for clarity lm and lmc instead of m and mc, which stands for lowpass masking filters, i.e.

$$G_m(e^{j\omega T}) = G_{lm}(e^{j\omega T}), \qquad G_{mc}(e^{j\omega T}) = G_{lmc}(e^{j\omega T}) \qquad (5.25)$$

We can now denote the highpass masking filters as

$$G_m(e^{j\omega T}) = G_{hm}(e^{j\omega T}), \qquad G_{mc}(e^{j\omega T}) = G_{hmc}(e^{j\omega T}) \qquad (5.26)$$

and write the real function of $V_0(j\omega)$ and $V_1(j\omega)$ as

$$\begin{aligned} V_{0R}(\omega) &= H_{0R}(\omega)[G(M\omega T)G_{lm}(\omega T) + G_c(M\omega T)G_{lmc}(\omega T)] - \\ &\quad H_{1R}(\omega)[G(M\omega T)G_{hm}(\omega T) + G_c(M\omega T)G_{hmc}(\omega T)] \\ V_{1R}(\omega) &= H_{0R}(\omega-\pi/T)[G(M\omega T)G_{lm}(\omega T) + G_c(M\omega T)G_{lmc}(\omega T)] \\ &\quad - H_{1R}(\omega-\pi/T)[G(M\omega T)G_{hm}(\omega T) + G_c(M\omega T)G_{hmc}(\omega T)] \end{aligned} \qquad (5.25)$$

Due to our class of filter bank, which is NPMR HFB, and taking (4.7) into consideration, we can consider $V_{0R}(\omega)$ and $V_{1R}(\omega)$ instead of $V_0(j\omega)$ and $V_1(j\omega)$. This implies that if $|V_{0R}(\omega)|$ and $|V_{1R}(\omega)|$, say they approximate one and zero, respectively, so do $|V_0(\omega)|$ and $|V_1(\omega)|$. Therefore, from (4.17), we obtain the following:

$$|V_0(j\omega)| = |V_{0R}(\omega)|, \qquad |V_1(j\omega)| = |V_{1R}(\omega)| \qquad (5.26)$$

5.5 Filter Bank Design

Design of the analog analysis filters in this proposed class (as delineated in section 5.4) utilizes same analysis filter bank as in section 4.1. The transfer functions of the analysis filter are exactly the same as in section 4.1. We consider the same equations from 4.8 till 4.11 for analysis filter bank.

Design of the digital Synthesis Filters

For synthesis filters, let the specification of $G_0(e^{j\omega T})$ be

$$\begin{aligned} 1-\delta_c \le \left|G_0(e^{j\omega T})\right| \le 1+\delta_c, \quad \omega T \in [0, \omega_c T] \\ \left|G_0(e^{j\omega T})\right| \le \delta_s, \quad \omega T \in [\omega_s T, \pi] \end{aligned} \tag{5.27}$$

with $\omega_c T$ and $\omega_s T$ satisfying the frequency symmetry condition, i.e. $\omega_c T + \omega_s T = \pi$. Furthermore, the magnitude of the distortion and aliasing is to meet

$$\begin{aligned} 1-\delta_0 \le \left|V_{0R}(j\omega)\right| \le 1 \\ -\delta_1 \le \left|V_{1R}(j\omega)\right| \le \delta_1 \end{aligned} \tag{5.28}$$

Then to meet the above specifications, we optimize $G(e^{j\omega T})$ as follows

$$\begin{aligned} 1-\delta_{c,G} \le \left|G(e^{j\omega T})\right| \le 1+\delta_{c,G}, \quad \omega T \in [0, \omega_{c,G} T] \\ \left|G(e^{j\omega T})\right| \le \delta_{s,G}, \quad \omega T \in [\omega_{s,G} T, \pi] \end{aligned} \tag{5.29}$$

with

$$1-\delta_p \le \left|G(e^{j\omega T})\right|^2 + \left|G_c(e^{j\omega T})\right|^2 \le 1+\delta_p, \quad \omega T \in [0, \omega_{c,G} T] \tag{5.30}$$

according to Fig. 5.6, and $G_m(e^{j\omega T})$ to meet the following criteria:

$$\begin{aligned} 1-\delta_{c,G_m} \le \left|G_m(e^{j\omega T})\right| \le 1+\delta_{c,G_m}, \quad \omega T \in [0, \omega_{c,G_m} T] \\ \left|G(e^{j\omega T})\right| \le \delta_{s,G}, \quad \omega T \in [\omega_{c,G_m} T, \pi] \end{aligned} \tag{5.31}$$

with $\omega_{c,G_m}T$ and $\omega_{s,G_m}T$ given by

$$\begin{aligned}\omega_{c,G_m}T &= \omega_s T \\ \omega_{s,G_m}T &= \frac{2(k+1)\pi - \omega_{s,G}T}{L}\end{aligned} \tag{5.32}$$

and

$$\begin{aligned}\omega_{c,G_m}T &= \frac{2(k-1)\pi - \omega_{s,G}T}{L} \\ \omega_{s,G_m}T &= \omega_c T\end{aligned} \tag{5.33}$$

for *Case 1* and *Case 2* designs, respectively.

5.6 Design Example

In this section, we demonstrate by means of a design example the properties and advantages of the proposed filter banks. This example considers the design of a two-channel NPMR filter bank with the FIR FRM synthesis filters. To design and optimize the FIR synthesis filters synthesized using FRM technique, we use a different approach. Instead of using design approach available on MATLAB for designing and optimizing FIR filters, we again use halfband filters as explained in section 5.2. These halfband filters are more efficient than using standard **remez.m** from MATLAB. We considered the following specifications: stopband edges at $\omega_s = 0.501\pi/T$ and stopband attenuation $\delta_s = 0.01$, and transition width is $\Delta = 0.002$, according to (5.27) to (5.31). In order to reduce the computational complexity, we optimized the model filter and masking filters simultaneously. The orders of the FIR masking filters are roughly inversely proportional to their transition width. Therefore, as M increases (see (5.14) for M), the complexity of the model filter decreases, roughly, linearly with M whereas that of masking filters increases. Generally, the trend is that the overall complexity will therefore reach a minimum for a certain value of M that needs not be $M = 1$. Utilizing these filters, we thus obtained an increased speed as well as a reduced complexity. We used the proposed structure with $M = 15$, and as a consequence, a Case 2 design. The overall filter length is $N = 269$, with the order of model filter $N = 143$, masking filters having the order of $N = 63$ each (we used two masking filters). The magnitude responses of the synthesis filters are shown in Fig. 5.7, and the resulting magnitude responses of the distortion and aliasing functions are shown in Fig. 5.8.

As a comparison, using instead a regular linear-phase FIR (conventional linear-phase FIR, $M = 1$) filter, the required order is estimated to be 1945, this order resulted from using halfband filters. However, if standard linear-phase FIR filters other than halfband FIR filters, the required order goes above 1945.

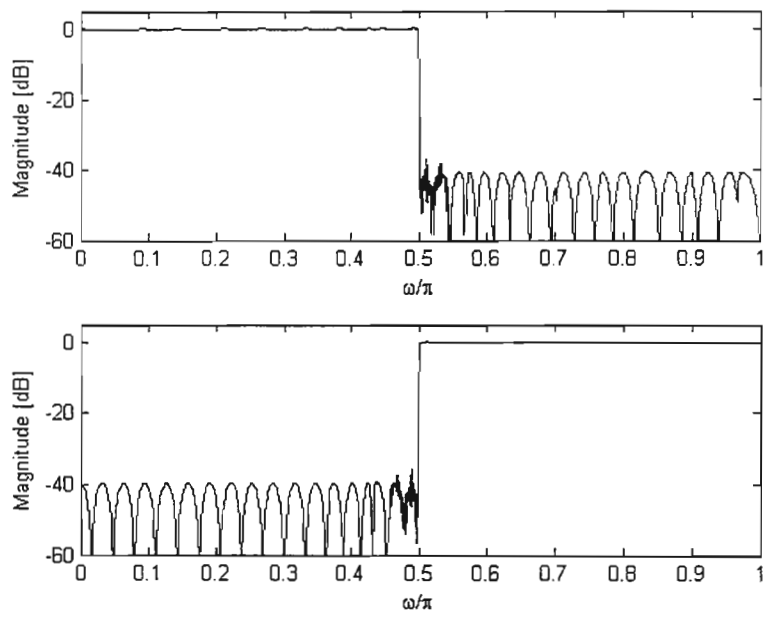

Figure 5.6: Magnitude responses of the Lowpass (top) and Highpass (bottom) of digital synthesis filters

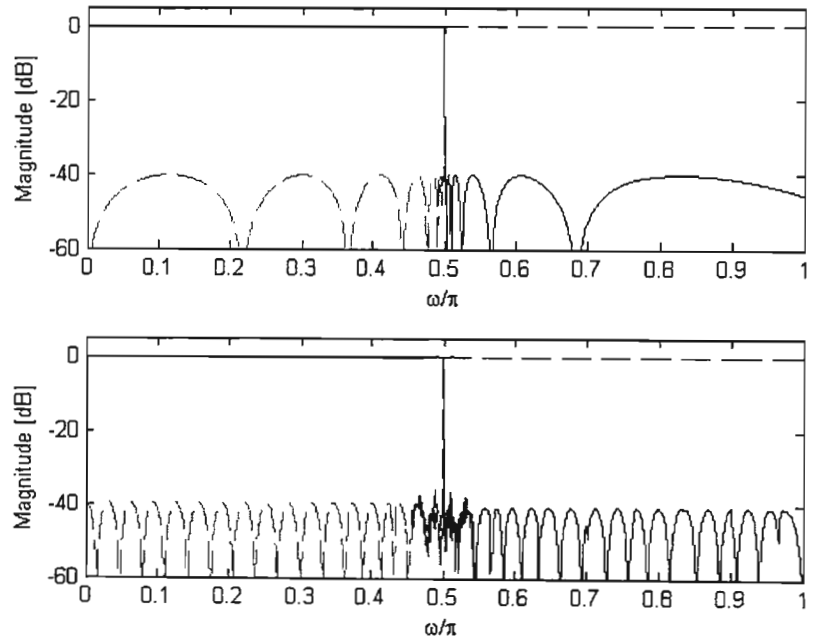

Figure 5.7: Magnitude responses of the analog analysis filters (top) and digital synthesis filters (bottom)

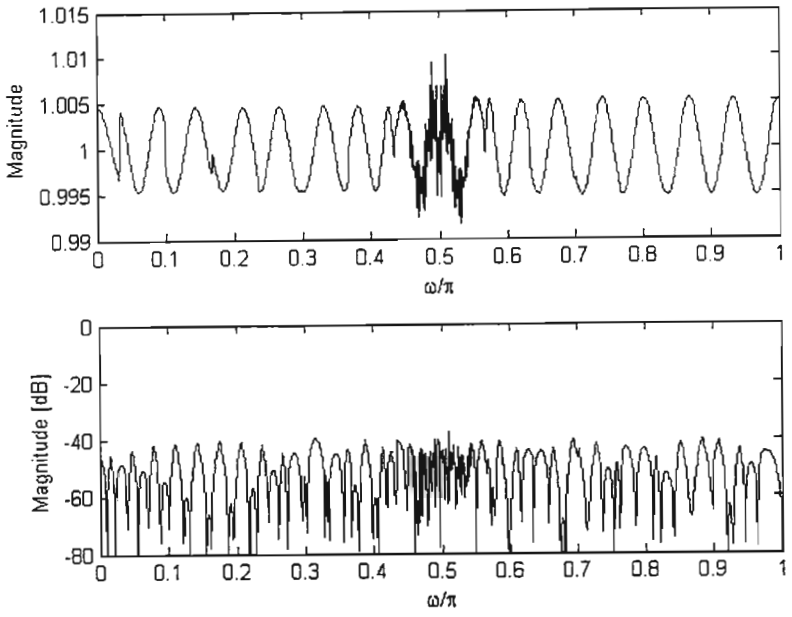

Figure 5.8: Magnitude responses of the distortion function (top) and aliasing function (bottom)

5.7 Proposed Hybrid Filter Banks for Two-Channel Hybrid Analog and Digital (IIR FRM) Class

This section introduces another class of two-channel NMPR HFB class with IIR synthesis filter bank utilizing FRM technique. It utilizes same analysis filter bank as the previous one in section 5.3 but uses IIR synthesis filters instead of FIR filter as in previous section. Utilizing IIR filters instead of FIR is another way of reducing the computational complexity.

A combination of a complementary filter pair and a properly designed pair of masking filters may result in a digital filter with an arbitrary bandwidth. Let us first recapitulate on the concept of complementary IIR filter, (details given in section 5.2). Two IIR filters are said to be power complementary if their square magnitudes satisfy the relation

$$|G(z)|^2 + |G_c(z)|^2 = 1 \tag{5.34}$$

The complimentary filter pair is then obtained if the parallel connection of two all-pass networks is utilized. The complementary filter pair $G(z)$ and $G_c(z)$ can easily be represented as a sum or difference of two all-pass functions as follows:

$$G(z)=\frac{G_0(z)+G_1(z)}{2},\qquad G_c(z)=\frac{G_0(z)-G_1(z)}{2},\tag{5.35}$$

where $G_0(z)$ and $G_1(z)$ are all-pass functions determined by the poles of $G(z)$, the all-pass implementation of the complementary filter pair is shown in Fig. 5.9. If $G(z)$ is a lowpass filter, then Fig. 5.9 implies that $G_c(z)$ is a highpass filter.

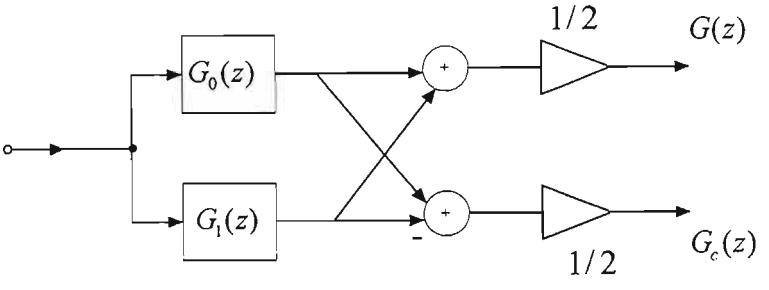

Figure 5.9: All-pass configuration of the power complementary IIR filter pair

In the frequency-response masking (FRM) approach, the transfer function of the overall filter is given by (see section 5.2 & 5.2)

$$H(z)=G(z^M)G_m(z)+G_c(z^M)G_{mc}(z)\tag{5.36}$$

where $G(z)$ and $G_c(z)$ are referred to as the model filter and complementary model filter, respectively. The filters $G_m(z)$ and $G_{mc}(z)$ are referred to as the masking filters which extract one or several passbands of the periodic model filter $G(z^M)$ and periodic complementary model filter $G_c(z^M)$. The structure of the FRM technique for IIR FRM is illustrated in Fig. 5.5. For a lowpass filter, typical magnitude responses for the model, masking and overall filters, are as shown in Fig. 5.5. The transition band of $H(z)$ can be chosen to be one of the transition bands provided by either $G(z^M)$ or $G_c(z^M)$. The FRM technique was first introduced as a means to reduce the arithmetic complexity of linear-phase FIR filters with narrow transition bands. In this case, the model filters are power complementary IIR filters being realizable as a parallel connection of two all-pass filters as in Fig. 5.4, whereas both $G_m(z)$ and $G_{mc}(z)$ are either even or odd-order linear-phase FIR filters of equal delays. These filters can be utilized directly to generate the synthesis filters in the proposed filter bank scheme to be considered in the following section. Fig. 5.10 illustrates the realization structure that implements the FRM expressed by equation (5.36)

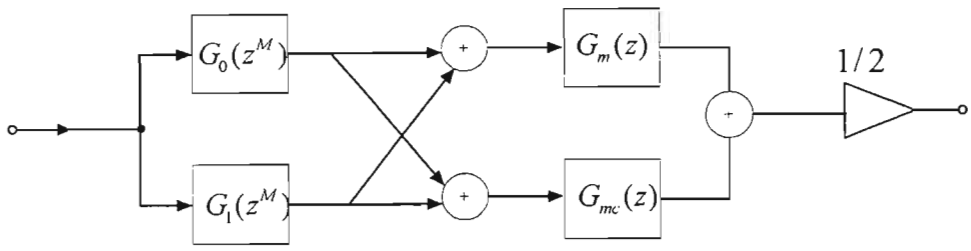

Figure 5.10: Block diagram of IIR filter synthesized utilizing the FRM technique

Then, the structure from Fig. 5.7 can be re-arranged in the following manner. Utilizing (5.35), the overall transfer function (5.36) can be given as:

$$H(z) = \frac{G_0(z^M) + G_1(z^M)}{2} G_m(z) + \frac{G_0(z^M) - G_1(z^M)}{2} G_{mc}(z) \qquad (5.37)$$

5.7.1 Analysis Filters

The transfer functions of the analysis filter are exactly the same as in 5.4, then letting the analog filters be expressible as a sum and difference of two all-pass filters is not a severe restriction, since standard approximations i.e. Elliptic, Chebyshev in odd-order case can be expressed in this way. In fact, all analog filters with odd characteristics function can be written in this way. The transfer functions of the analysis filter are exactly the same as in section 4.1. We consider the same equations from 4.8 till 4.11 for analysis filter bank.

5.7.2 Synthesis Filters

In this subsection we present the case where the synthesis filters are synthesized using FRM based on (5.37). It is necessary to first give the equation of the conventional case as shown is section 4.1. Since we consider the NPMR HFB, the corresponding equations for Fig.5.8 are given as:

$$G_0(e^{j\omega T}) = 2F_0(e^{j\omega T})$$
$$G_1(e^{j\omega T}) = 2F_1(e^{j\omega T}) \qquad (5.40)$$

Instead of $G_0(e^{j\omega T})$ as in (5.40), we synthesize this lowpass filter by replacing $2F_0(e^{j\omega T})$ of (5.40) with (5.37), which can be written as

$$\begin{aligned} G_{IIR0}(e^{j\omega T}) &= H(e^{j\omega T}) \\ &= G(e^{j\omega MT})G_m(e^{j\omega T}) + G_c(e^{j\omega MT})G_{mc}(e^{j\omega T}) \end{aligned} \tag{5.41}$$

where

$G(e^{j\omega MT}) = \frac{G_0(e^{j\omega MT}) + G_1(e^{j\omega MT})}{2}$, and $G_c(e^{j\omega T}) = \frac{G_0(e^{j\omega MT}) - G_1(e^{j\omega MT})}{2}$ are a periodic model filter and complementary periodic model filter, respectively and $G_m(e^{j\omega T})$, and $G_{mc}(e^{j\omega T})$ are masking filters. Again, to obtain the highpass of $G_{IIR0}(e^{j\omega T})$ is very trivial because, we don't need to change the model filter and complementary filter. We only change the masking filters, which were lowpass filters for $G_{IIR0}(e^{j\omega T})$ i.e. in (5.41), we just change $G_m(e^{j\omega T})$ and $G_{mc}(e^{j\omega T})$ to be highpass filters, then we end up with a corresponding highpass filter to $G_{IIR0}(e^{j\omega T})$. Given the passband and stopband edges of the model filter $G(e^{j\omega T})$, denoted here by $\omega_{c,G}T$ and $\omega_{s,G}T$, respectively, (see Fig. 5.4).

$$\omega_c T = \frac{2k\pi + \omega_{c,G}T}{M}, \qquad \omega_s T = \frac{2k\pi + \omega_{s,G}T}{M} \tag{5.42}$$

$$\omega_c T = \frac{2k\pi - \omega_{s,G}T}{M}, \qquad \omega_s T = \frac{2k\pi - \omega_{c,G}T}{M} \tag{5.43}$$

where (5.42) is for *Case 1 design* and (5.43) *Case 2 design*. The transition band of the model filter $G(e^{j\omega T})$ and complementary model filter $G_c(e^{j\omega T})$ always include $\pi/2$ since these filters are to be approximately power complementary. Thus, it is practical to let the sum of the passband and stopband edges for these filters as well as for the analysis and synthesis filters to be equal to π. This implies the following:

$$\omega_c T + \omega_s T = \omega_{c,G}T + \omega_{s,G}T = \pi \tag{5.44}$$

In this work to be able to compare the different techniques, M and subfilters are selected here to satisfy the same rules considered with FIR i.e.:

- M is an odd integer, since $\pi M/2 = 2\pi k \pm \pi/2$. This gives $M = k+1$ and $M = k-1$ for *Case 1* and *Case 2*, respectively. This can easily be deduced from (5.42) and (5.43).

- The model and its complementary filter, $G(e^{j\omega T}), G_c(e^{j\omega T})$ are even order N_G and complementary IIR filters, with $G_c(e^{j\omega T})$ being related to $G(e^{j\omega T})$ as $G_c(z) = G(-z)$
- The masking filters $G_m(e^{j\omega T})$ and $G_{mc}(e^{j\omega T})$ can be of even order N_{G_m} and linear phase FIR filters or odd.

5.7.3 Distortion and Aliasing

With analysis and synthesis filters as given in (5.40) to (5.44) in the previous subsections, the distortion and aliasing function can be exactly as in section 5.4. Where

$$G(\omega MT) = \frac{G_0(\omega MT) + G_1(\omega MT)}{2}, \text{ and } G_c(\omega MT) = \frac{G_0(\omega MT) - G_1(\omega MT)}{2}$$

Due to our class of filter bank, which is NPMR HFB, and taking (4.7) into consideration, we can consider $V_{0R}(\omega)$ and $V_{1R}(\omega)$ instead of $V_0(j\omega)$ and $V_1(j\omega)$. This implies that if $|V_{0R}(\omega)|$ and $|V_{1R}(\omega)|$, say , approximates one and zero, respectively, so do $|V_0(\omega)|$ and $|V_1(\omega)|$. Therefore from (4.17), we obtain the following

$$|V_0(j\omega)| = |V_{0R}(\omega)|, \qquad |V_1(j\omega)| = |V_{1R}(\omega)| \tag{5.45}$$

5.8 Filter Bank Design

5.8.1 Design of the Analog Analysis Filters

One of the ways of determining the requirements on $H_0(j\omega)$ and $H_1(j\omega)$ in terms of frequency selectivity, passband and stopband attenuations, is normally set by the desired ADC performance. Since $H_0(j\omega)$ and $H_1(j\omega)$ are designed by taking the sum and the difference of two stable all-pass filters $A_0(s)$ and $A_1(s)$ (as mentioned in previous subsection). It then suffices just to design either $H_0(j\omega)$ or $H_1(j\omega)$. However, the chosen one must be designed in such a way that both filters satisfy their respective requirements, i.e. a satisfying condition, which states that two filters $H_0(j\omega)$ and $H_1(j\omega)$ should be complementary filters, this means that the absolute sum of $H_0(j\omega)$ and $H_1(j\omega)$ frequency response

equals one, according to the relation (4.20). Furthermore, since low filter order is of high priority, the filters used in filter bank design are equiripple filters. For analysis filter bank, the specifications of $H_0(j\omega)$ and $H_1(j\omega)$ here are as in subsection 4.1.2 under *design of the analog analysis filters.*

5.8.2 Design of the Digital Synthesis Filters

In this work, again, instead of using linear programming (LP) and non-linear programming (NLP), we use recently developed halfband filters to design $G_{IIR0}(e^{j\omega T})$ and $G_{IIR1}(e^{j\omega T})$, details of the design of these Halfband filter is given in [53-62]. In this subsection we are using elliptic minimal Q factors (EMQF) filters in FRM technique. There are several reason to consider EMQF filters:

- An EMQF filter exactly satisfies the passband and stopband relations required for model and complementary filters [54, 56, 61].
- An EMQF transfer function can be efficiently implemented utilizing wave lattice digital filters (WDF's), or generally, structures consisting of two all-pass networks in parallel [60].
- Multiplierless IIR filters can be designed using EMQF transfer functions and all-pass implementations.

The limitations with the use of standard MATLAB functions like **ellip.m** come from the fact that, this function is based on the Jacobi elliptic sn function given as follows in MATLAB, **[sn,cn,dn]=ellipj(U,M)**, where M is a parameter $0 < M < 1$ and U is a real argument. The function **ellipj (U, M)** is accurate to eps = 2.220446049250313e-016 in MATLAB. Then for larger stopband attenuation **ellipj.m** returns an error because some parameters may become too small in the optimization routines, and the argument U becomes a complex number.

The passband ripple $G(e^{j\omega T})$ is the stopband ripple of $G_c(e^{j\omega T})$ and vice versa, this is due to the fact that they are power complementary. Furthermore, the frequency-response masking technique is based on the power complementary filter pair. Another remarkable advantage of the EMQF transfer function is that, it's an analytical solution for FRM technique for IIR filters. Furthermore, it was shown in [60] that the most sensitive coefficients in the lattice WDF can be directly controlled by filter parameters, i.e. (f_p, f_s, a_p, a_a). This way, a half of the multiplier coefficients can be implemented without quantization leaving the filter characteristics strictly elliptic. The EQMF filters have two important properties [53]:

- The square magnitude response has equal ripples in the passband and stopband.
- The passband attenuation is very small.

Let the specification of $G_{IIR0}(e^{j\omega T})$ then be

$$
\begin{aligned}
&1-\delta_c \le \left|G_{IIR0}(e^{j\omega T})\right| \le 1+\delta_c, \quad \omega T \in [0, \omega_c T] \\
&\left|G_{IIR0}(e^{j\omega T})\right| \le \delta_s, \quad \omega T \in [\omega_s T, \pi]
\end{aligned}
\tag{5.46}
$$

with $\omega_c T$ and $\omega_s T$ satisfying the frequency symmetry condition, i.e. $\omega_c T + \omega_s T = \pi$. Furthermore, the magnitude of the distortion and aliasing is to meet

$$
\begin{aligned}
&1-\delta_0 \le \left|V_{0R}(j\omega)\right| \le 1 \\
&-\delta_1 \le \left|V_{1R}(j\omega)\right| \le \delta_1
\end{aligned}
\tag{5.47}
$$

To meet the above specifications, we then optimize $G(e^{j\omega T})$ as follows

$$
\begin{aligned}
&1-\delta_{c,G} \le \left|G(e^{j\omega T})\right| \le 1+\delta_{c,G}, \quad \omega T \in [0, \omega_{c,G} T] \\
&\left|G(e^{j\omega T})\right| \le \delta_{s,G}, \quad \omega T \in [\omega_{s,G} T, \pi]
\end{aligned}
\tag{5.48}
$$

with

$$
1-\delta_p \le \left|G(e^{j\omega T})\right|^2 + \left|G_c(e^{j\omega T})\right|^2 \le 1+\delta_p, \quad \omega T \in [0, \omega_{c,G} T]
\tag{5.49}
$$

according to Fig. 5.4, and $G_m(e^{j\omega T})$ to meet the following criteria:

$$
\begin{aligned}
&1-\delta_{c,G_m} \le \left|G_m(e^{j\omega T})\right| \le 1+\delta_{c,G_m}, \quad \omega T \in [0, \omega_{c,G_m} T] \\
&\left|G(e^{j\omega T})\right| \le \delta_{s,G}, \quad \omega T \in [\omega_{c,G_m} T, \pi]
\end{aligned}
\tag{5.50}
$$

with $\omega_{c,G_m} T$ and $\omega_{s,G_m} T$ given by

$$
\begin{aligned}
&\omega_{c,G_m} T = \omega_s T \\
&\omega_{s,G_m} T = \frac{2(k+1)\pi - \omega_{s,G} T}{L}
\end{aligned}
\tag{5.51}
$$

and

$$\omega_{c,G_m} T = \frac{2(k-1)\pi - \omega_{s,G} T}{L}$$
$$\omega_{s,G_m} T = \omega_c T \tag{5.52}$$

for *Case 1* and *Case 2* designs, respectively.

5.9 Design Example

In this section, we demonstrate by means of a design example the properties and advantages of the proposed filter banks. This example considers the design of a two-channel NPMR filter bank with the IIR FRM synthesis filters. To design and optimize the IIR synthesis filters synthesized using FRM technique, we use a different approach, instead of using design approach available on MATLAB for designing and optimizing FIR filters, we again use EMQF halfband filters as explained above under section titled *Design of the Digital Synthesis Filters*. These halfband filters are more efficient than using standard **ellip.m** from MATLAB and standard halfband filters available in MATLAB. We consider the following specifications: stopband edges at $\omega_s = 0.501\pi / T$ and stopband attenuation $\delta_s = 0.01$, and transition width is $\Delta = 0.002$, according to (5.46) to (5.50). In order to reduce the computational complexity, we optimized the model filter and masking filters simultaneously. The orders of the IIR masking filters are roughly inversely proportional to their transition width. Therefore, as M increases (see (5.14) for M), the complexity of the model filter decreases, roughly linearly with M whereas that of masking filters increases. Generally, the trend is that the overall complexity will therefore reach a minimum for a certain value of M that need not be $M = 1$. Utilizing these filters, we thus obtain an increased speed as well as a reduced complexity. We use the proposed structure with $M = 21$, and as a consequence, a Case 2 design. The overall filter length is $N = 188$, with the FIR masking filters of order $N = 90$ each (note, we have two masking filters). With such efficient EMQF halfband filters we obtained the magnitude response of synthesis filters as shown in Fig. 5.12. The orders of the numerator and denominator polynomials, yielding the lowest overall complexity, turned out to be 9 for the lowpass filter and 8 for the highpass filter. The magnitude responses of the synthesis filters are shown in Fig. 5.12, and the resulting magnitude responses of the distortion and aliasing functions are shown in Fig. 5.13.

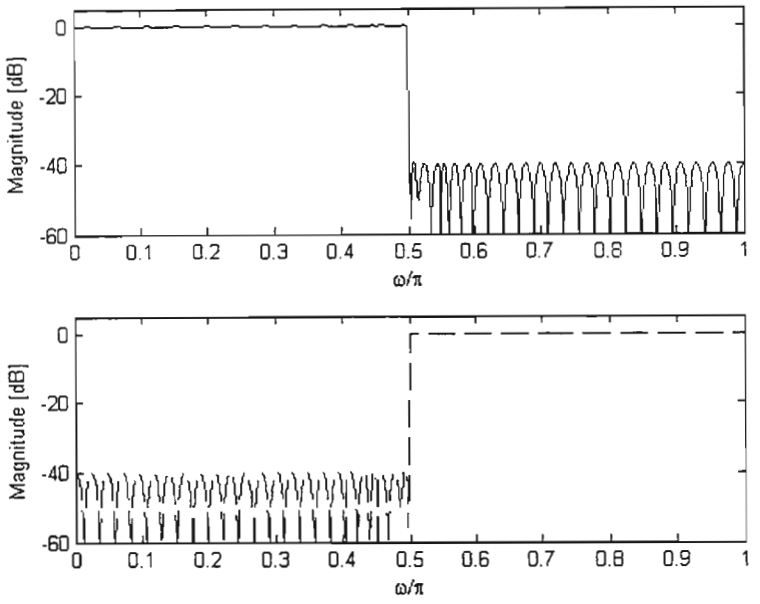

Figure 5.11: Magnitude responses of the Lowpass (top) and Highpass (bottom) of digital synthesis filters

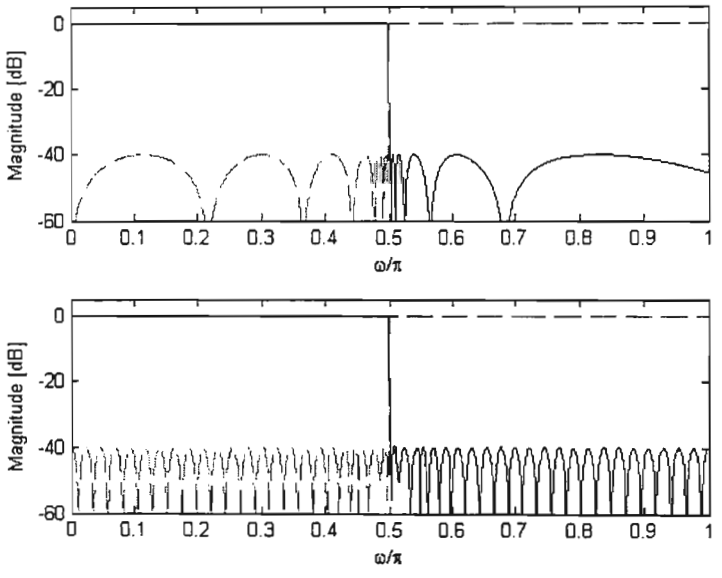

Figure 5.12: Magnitude responses of the analog analysis filters (top) and digital synthesis filters (bottom)

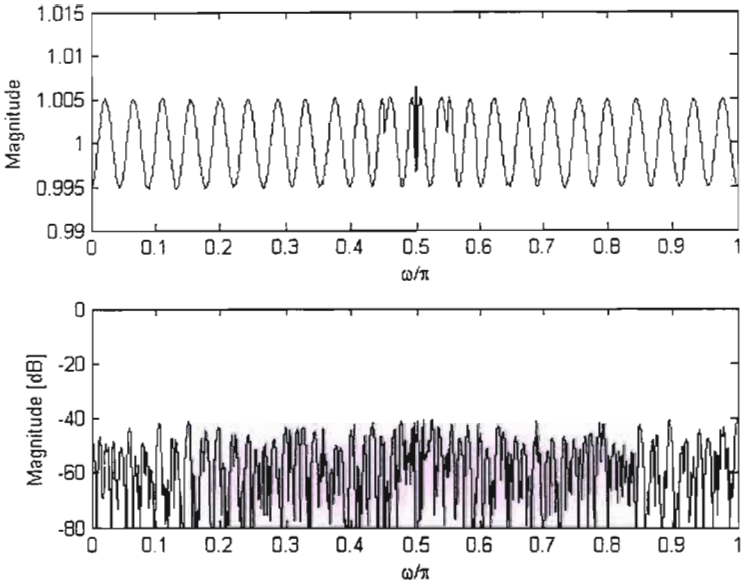

Figure 5.13: Magnitude responses of the distortion function (top) and aliasing function (bottom)

As a comparison, using FIR masking filter instead, the required order is estimated to $N = 188$, this order resulted from using a FIR masking filters. However, if IIR masking filters are used other than FIR masking filters, the required overall filter length becomes $N = 27$. With the orders of the numerator and denominator polynomials (of model, and IIR masking filters), yielding the lowest overall complexity, turned out to be 9 for the lowpass filter and 8 for the highpass filter. The magnitude responses of the synthesis filters are shown in Fig. 5.15 and the resulting magnitude responses of the distortion and aliasing functions are shown in Fig. 5.16.

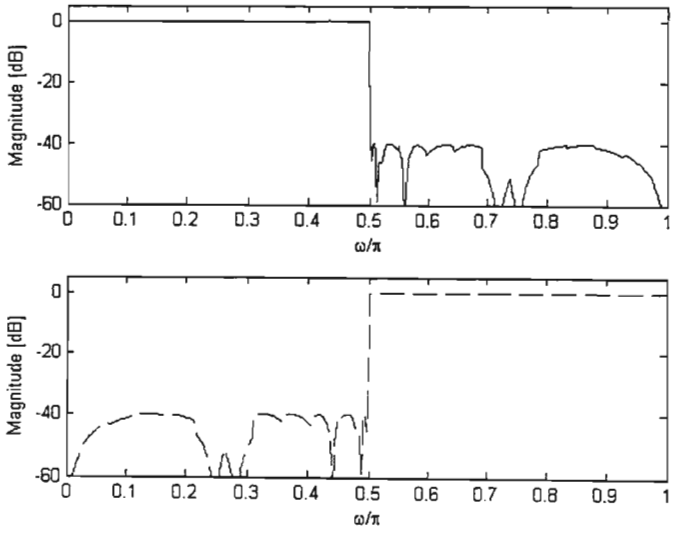

Figure 5.14: Magnitude responses of the Lowpass (top) and Highpass (bottom) of digital synthesis filters

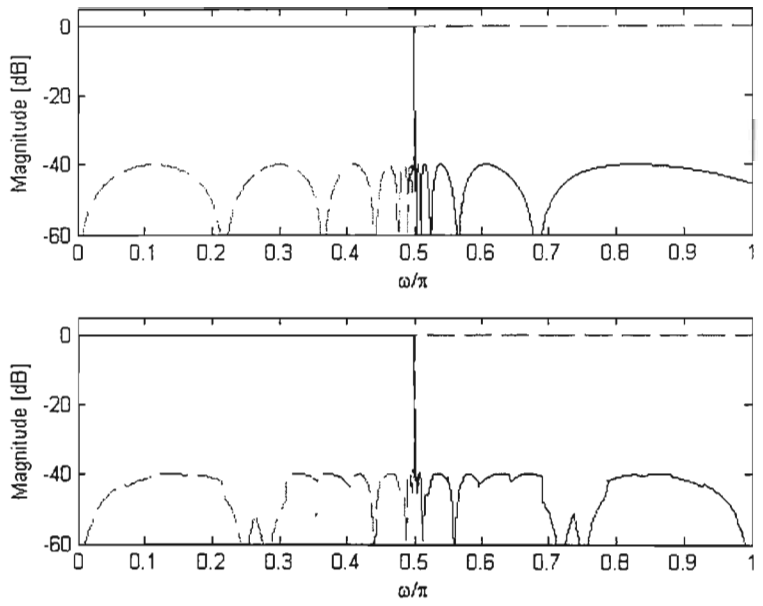

Figure 5.15: Magnitude responses of the analog analysis filters (top) and digital synthesis filters (bottom)

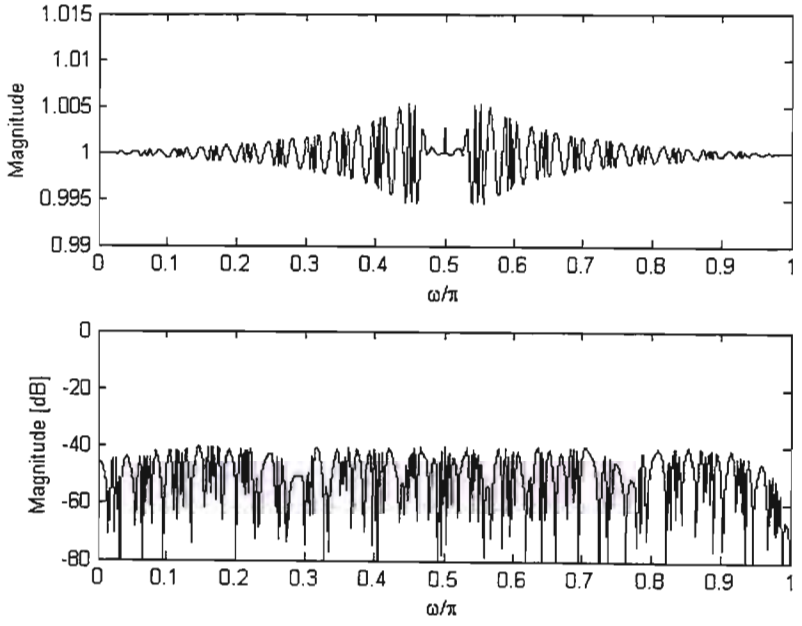

Figure 5.16: Magnitude responses of the distortion function (top) and aliasing function (bottom)

5.10 Summary

In our proposed system we considered from chapter 4 to chapter 5 the same specification(s), with the exception of the parameter M, as clearly indicated in table 5.1. For M, there is no closed form analytic expression for finding optimum M. However, a good choice can be obtained by estimating the filter complexity for each M and then selecting M which corresponds to the lowest estimate. We found that for our specifications, for FIR FRM the good choice can be obtained when $M=15$, whereas for IIR FRM, $M=21$ the distortion and aliasing for all cases listed in table 5.1, distortion is approximately one and aliasing is approximately zero. From the table it is clear that FIR FRM case is the preferable case, since the order of the conventional case was reduced from 1945 to 269. This is a huge improvement; this surely shows that the FRM technique is effective and efficient.

Table 5.3: Summary of the results

TECHNIQUE	ORDER OF THE MODEL FILTER	ORDER OF MASKING FILTERS EACH	OVERALL FILTER ORDER	M
Conventional FIR			1945	1
FIR FRM (with FIR masking Filters)	143	63	269	15
Conventional IIR			17	1
IIR FRM (with FIR masking filters)	9	90	188	21
IIR FRM (with IIR masking filters)	9	9	27	21

CHAPTER 6

DISCUSSIONS AND CONCLUSIONS

This dissertation was concerned with the use of frequency-response masking technique in designing A/D converter for any industrial application that requires ADC that has very high performance, i.e. high resolution (greater than 14-bits of resolution) at the same time attaining high sampling rate over 100 MSa/s. In this dissertation, we use the specification that SDR imposes on A/D conversion, which covers the worst case scenario, but the designed ADC is not limited to SDR applications only, requirements imposed by future wideband communication systems is inclusive. Moreover, this dissertation uses the concept of asymmetric filter bank based techniques for alleviating mismatch errors in the proposed system, which is CT HFB ADC. The filter banks are mainly used in our system to attenuate the aliasing introduced by channel mismatch errors.

One of the main problems we encountered is that there exist very few papers dealing with CT HFB, for instance there is only one paper that deals with NPMR filter bank system. This implies that it's quite difficult to do comparisons for NPMR CT HFB system at the moment with other available systems, i.e. DT HFB's. However, our system showed great potential, since we include the condition that was left out in the available paper, which deals with NPMR CT HFB. The condition can be stated as follows: for HFB based ADCs, the filters should have a sharp frequency response roll-off so that the transition regions are as narrow as possible and maximum stopband attenuation. Hence minimum spurious free dynamic range (SFDR) is achieved across as much of the band as possible. If this condition is left out, asymmetric HFB will achieve reasonable results. But if it's embraced the synthesis filter bank complexity becomes too high and sometimes unacceptably high. This implies that there is a need for good design procedures that will reduce the complexity of synthesis filter bank, at the same time retaining low order for analysis filter bank. In this dissertation, we combat the problem by using frequency-response masking technique to reduce the complexity of the synthesis filters, which resulted due to the mentioned condition. The objective is then to find good design procedures that will offer reasonable results, even in the case of filters having a sharp frequency response roll-off. The work presented in this dissertation is only designated to continuous-time hybrid analog/digital filter bank (CT-HFB).

The filter bank design is performed by first optimizing the analysis filters and then design, with the analysis filters fixed, optimizing the digital synthesis filters. By designing the analysis and synthesis filters separately, it is possible to obtain analysis filters of very low order and complexity.

In chapter 1, we reviewed different available techniques for designing A/D converters, gave details (motivation) for doing this work, basic building blocks with terminology used in subsequent chapters, an introduction to software radio stating the reason why we use the requirements on ADC imposed by software radio applications. In chapter 2, the dissertation gives a thorough analysis of HFB ADCs that is essential for understanding and designing hybrid filter banks, reason for giving such analysis is because

there are very few publications on CT HFB. This analysis gives the correct frequency response expression for CT HFBs. Distortion and aliasing is also investigated in this chapter.

In chapter 3, we focused on the design of Hybrid filter banks, but only dedicated on CT HFB ADC, we investigated one of the fundamental aspects to the ADC performance, which is the noise (quantization) in the filter bank based ADCs, comparing the case of the conventional case with the multirate filter bank ADC. This has recently been done in [10], we extended that analysis for our case based on our specifications, we focused on the numerical values for typical design for CT HFB, the spurious free dynamic range was investigated in the presence of static gain and time-skew errors, the results showed that our system achieves a better SFDR, this implies that as we consider the case where we use sharp frequency response roll-off filters, the SFDR is improving. Therefore, we concluded that FRM technique is one of the efficient techniques that produces filters with very sparse coefficients and so the resulting filter has very low complexity and CT HFB ADC is one of the potential ADC for any application that requires high performance ADC.

In this dissertation, five different classes of near perfect magnitude reconstruction (NPMR) continuous-time Hybrid filter banks (CT HFBs) are proposed. In each of the five cases, two filter banks are designed; analysis filter bank and synthesis filter bank. Since the systems are hybrid, continuous time IIR filter are used to implement the analysis filter bank and digital filters are used for the synthesis filter bank. To optimize the system, we use a new technique, known as frequency response masking (FRM), to design the synthesis filter bank. In this technique, the sharp roll-off characteristics can be achieved while keeping the complexity of the filter within practical range, by splitting the filter into two filters in cascade; model filter with relaxed roll-off characteristics followed by a masking filter.
One of the main factors controlling the overall complexity of the filter is the way of designing the model filter and that of designing the masking filter.

In chapter 4 and 5, we focused on designing two-channels of CT HFB ADC, one with the FIR synthesis filter bank and the other with the IIR synthesis filters. The dissertation proposed three combinations: use of IIR model filter and IIR masking filter, IIR model filter/FIR masking filter and FIR model filter/FIR masking filter (presented in chapter 5). To show the advantages of our designs, we consider the cases of designing the synthesis filter as one filter, either FIR or IIR. These two filters are used as basis for comparison to our proposed designs (the use of masking response filter).
The results showed the following:

- Asymmetric hybrid filter banks alone are not sufficient for filters with sharp frequency response roll-off, especially for IIR/FIR class.
- All classes that utilize FRM in their synthesis filter banks gave a good performance in general as compared to conventional classes, such as the reduction of the order of filters.

- IIR/IIR FRM gave better performance compared to IIR/FIR FRM.
- Comparing IIR/IIR FRM using FIR masking filters and IIR/IIR FRM using IIR masking filters, the later gave better performance (the performance is in general measured in terms of reduced filter order).
- All classes that use the FRM approach have a very low complexity, in terms of reduced filter order. Our target was to design a system with the following overall characteristics: pass band ripple of -0.01 dB, stop band minimum attenuation of – 40 dB and of response roll-off of 0.002. Our calculations showed that the order of the conventional IIR/FIR filter that achieves such characteristics is about $N = 2000$. Using the FRM technique, the order N reduced to about $N = 269$, $N = 188$ for IIR/FIR and IIR/IIR classes, respectively, this shows that the technique is very effective in reducing the filter complexity.
- The magnitude distortion and the aliasing noise are calculated for each design proposal and compared with the theoretical values. The comparisons show that all our proposals result in approximately PMR (Perfect Magnitude Reconstruction).

In conclusion, we can say that our proposal of using frequency-response masking technique to design the synthesis filter bank can reduce to a large extent the complexity of the system. The design of the system as a whole is simplified by designing the synthesis filter bank separately from the design of the analysis filter bank. In this case each bank is optimized separately. This implies that for SDR applications we are proposing the use of the continuous-time HFB ADC (CT HFB ADC) structure utilizing FRM for digital filters.

6. 1 Future Research Direction

Our research work or investigation and results throw open several interesting issues for future research. We have shown that CT HFB ADC is one of the potential high performance A/D conversion techniques and is possible to use it for any industrial application that requires high resolution and at the same time achieving high sampling rate. We have shown that with sharp roll-off characteristics on filters better SFDR can be achieved in the presence of static gain and time-skew errors. However, we need further research on coming up with an efficient transformation to have more than two channels for CT HFB systems approximating either PR or PMR. This problem is still difficult to combat but with diligent work on devising equivalent transformation like cosine modulation which works perfectly for DT HFB systems but doesn't work for CT HFB system approximating PR or PMR. Since CT HFB system uses analog and digital filters, unlike DT HFB system which uses only discrete-time filters for both analysis and synthesis. Furthermore, efficient design procedures are still needed for CT HFB systems in cases where only IIR filters are used, i.e. IIR/IIRFRM class with IIR masking filters. Lastly, further work may include an analysis of the overall responses for the analysis and synthesis filter bank pairs with and without frequency masking (part of this was done by comparing the structures in chapter 4 and chapter 5, but it was somehow beyond the scope of our analysis.)

Reference:

[1] Harry Y-F. Lam, "Analog and Digital Filters: Design and Realization", Prentice Hall, Inc., Englewood Cliffs, New Jersey 07632, 1979

[2] S. K. Mitra, *"Digital Signal Processing, A Computer Based Approach,"* McGraw-Hill, 2001

[3] E. C. Ifeachor, and B. W. Jervis, "Digital Signal Processing, A Practical Approach," ", Prentice Hall, Pearson Education Limited, 2nd Ed, 2002

[4] A. V. Oppenheim, and R. W. Schafer, with J R. Buck, "Discrete-Time Signal Processing," Prentice Hall international, Inc., Upper Saddle River, New Jersey 07458, 2nd Ed, 1999

[5] N. J. Fliege, "Multirate Digital Signal Processing," John Wiley & Sons, Ltd, Chichester, New York, Brisbane, Singapore, Toronto, Reprinted 2000.

[6] P.P Vaidyanathan, *"Multirate Systems and Filter Banks"*, PTR Prentice Hall, Englewood Cliffs, New Jersey 07632, 1993

[9] S. R. Velázquez, "Hybrid filter banks for analog/digital conversion," Ph.D. dissertation, Dept. Elect. Eng. Comput. Sci., MIT Cambridge, MA, June 1997

[10] P. Löwenborg, *"Asymmetric filter banks for mitigation of mismatch errors in high-speed analog-to-digital converters,"* Ph.D. diss., Linköpings universitet, SE-581 83 Linköping, Sweden Linköping, 2002

[11] Linnéa Rosenbaum, "Contribution to low-complexity maximally decimated filter banks," MSc. thesis, Linköpings universitet, SE-581 83 Linköping, Sweden Linköping, Sept. 2003.

[12] Gordana Jovanovic-Dolecek, *"Multirate Systems: Design and Applications"*, Idea Group Publishing, 2002

[13] J. H. Reed, *Software Radio: A Modern Approach to Radio Engineering*, Prentice Hall PTR, Upper Saddle River, New Jersey 07458, pp.2, 1998

[14] SDR Forum, http://www.sdrforum.org

[15] Joseph Mitola, III, "The Software Radio Architecture," IEEE Communication Magazine, Vol. 33, no. 5, pp. 26-38, May 1995.

[16] http://itc.mit.edu/itel/docs/2002/Software_Radio_Lehr_Fuencis.pdf

[17] http://www.telfor.org.yu/telfor2001/radovi/11-15.pdf

[18] P. Löwenborg, H. Johansson, and L. Wanhammar, "A Survey of Filter Bank A/D Converters",

[19] Velazquez S. R., Nguyen T.R., and Broadstone S.R., "Design of hybrid filter banks for analog/digital conversion," IEEE Trans. Signal Processing, vol. 46, no. 44, pp 956-967, Apr. 1998.

[20] P. Löwenborg, H. Johansson, and L. Wanhammar, "On the frequency-response of M-channel mixed analog and digital maximally decimated filter bank," in Proc. European conf. Circuit Theory Design, Stresa, Italy, Aug. 29- Sept. 2, 1999, vol. 1, pp. 321-324.

[21] P. Löwenborg, H. Johansson, and L. Wanhammar, "Two-channel hybrid analog/digital filter bank with alias-free subbands," in Proc. IEEE Midwest Symp. Circuit Syst., Lansing, Michigan, Aug. 2000.

[22] P. Löwenborg, H. Johansson, and L. Wanhammar, "Two-channel Digital and Hybrid Analog/Digital Multirate Filter Banks with Very Low-Complexity Analysis or Synthesis Filters," provisionally accepted for publication in IEEE Trans. Circuits Syst. II.

[23] P. Löwenborg, H. Johansson, "Quantization noise in filter bank analog-to-digital converters," in Proc. IEEE Int. Symp. Circuits Syst., Sydney, Australia, May, 2001.

[24] Technical Description, "*Advanced Filter Bank (AFB) analog-to-digital converter Technical description,*" V-Corp Technologies, http://www.v-corp.com/analogfilterbank.htm

[25] Robert H. Walden, "Analog-to-Digital Converter survey and analysis", the 16th IEEE Instrumentation and measurement Technology Conference, pp.1558-1562, 1999.

[26] www.eecs.umich.edu/~mpflynn/Design%20Contest/Fall2002/Presentations/9_Ruba.pdf

[27] http://www.maxim-ic.com

[28] Sung Ho Cho, "*Software Defined Radio (SDR) Requirements*", the 5th Smart Antenna Workshop with Emphasis on SDR Application

[29] S. Albrecht, B. Li, X. Li, C. Pala, M. Ismail and H. Tenhunen, "*A sigma-delta based A/D architecture for DECT and GSM Radio Receivers*",

[30] B. W. Suter, K. S. Stevens, S. R. Velazquez, and T. Nguyen, "*Multirate as a Hardware Paradigm*",

[31] P. Löwenborg, H. Johansson, and L. Wanhammar, "*A two-channel hybrid analog and IIR digital filter bank approximating perfect magnitude reconstruction,*" in Proc. IEEE Nordic Signal Processing Symp, Kolmården, Norrköping, Sweden, June, 2000.

[32] Mark Looney, "*Advanced Digital Post-Processing Techniques Enhance Performance in Time-Interleaved ADC Systems*", http://www.analog.com/analogdialogue

[33] http://www.analog.com/UploadedFiles/Technical_Articles/119890034pg94.pdf

[34] W. Black and D. Hodges, "*Time-interleaved converter arrays,*" Journal of Solid State Circuits, Vol. SC-15, NO. 6, pp. 1022-1029, December 1980.

[35] Ramin Khoin-Poorfard, L .B. Lim, D. A. Johns, "*Time-interleaved Oversampling A/D Converters: Theory and Practice,*" IEEE Trans on Circuits and Systems-II: Analog and Digital Signal Processing, Vol. 44, NO. 8, August 1997

[36] J. Elbornsson, F. Gustafsson, Jan-Erik Eklund,"*Blind Adaptive Equalization of Mismatch Errors in Time Interleaved A/D Converter Systems," Submitted* to IEEE Trans on Circuits and Systems

[37] J. Elbornsson, F. Gustafsson, Jan-Erik Eklund, *"Analysis of Mismatch Noise in Randomly Interleaved ADC System,"*

[38] A. Petraglia and S. K. Mitra, *"Analysis of mismatch effects among A/D converters in a time-interleaved waveform digitizer,"* IEEE Trans. On instru. And meas., vol. 40, NO. 5, pp. 831-835, Oct 1991.

[39] Y. C. Jenq, *"Digital spectra of nonuniformly sampled signals: fundamentals and high-speed waveform digitizers,"* IEEE Trans. On instru. And meas., vol. 37, NO. 2, pp. 245-251, June 1988.

[40] S. Albrecht, B. Li, X. Li, C. Pala, M. Ismail and H. Tenhunen, *"A sigma-delta based A/D architecture for DECT and GSM Radio Receivers",*

[41] S. R. Velazquez, "Hybrid Quadrature Mirror Filter Bank Approach to Analog-to-Digital conversion, MSc thesis, May 1994.

[42] A. Petraglia and S. K. Mitra, "High-Speed A/D conversion incorporating a QMF bank," *IEEE Trans. Instrum. Meas.*, vol. 41, no.3, pp. 427-431, June 1992

[43] S. R. Velázquez, "A Hybrid Quadrature Mirror Filter Bank Approach to Analog-to-Digital Converter," Master dissertation, Dept. Elect. Eng. Comput. Sci., MIT Cambridge, MA, May 1994

[44] J. Franca, A. Petraglia and S. Mitra, "Multirate analog-to-digital systems for signal processing and conversion," *Proc. IEEE.*, vol. 85, pp. 242-262, Feb. 1997

[45] A. Petraglia, S.K. Mitra, "High speed A/D conversion incorporating a QMF bank," *IEEE Trans Instrum. Meas.*, vol. 41, pp. 427-431, June 1992

[46] L. Gaszi, "Explicit formulas for lattice wave digital filters," *IEEE Transactions on Circuits and Systems*, 32, 68-88. Jan 1985

[47] L. D. Mili` and M. D. Lutovac, ``Reducing the number of multipliers in the parallel realization of half-band elliptic IIR filters," *IEEE Trans. Signal Processing*, vol. 44, no. 10,pp. 2619--2623, Oct. 1996.

[48] H. W. Schussler and P. Steffen, "Halfband Filters and Hilbert Transformers,", *Circuits Systems Signal Processing,* vol. 17, no. 2, pp. 137 – 164, Feb. 1998.

[50] M. D. Lutovac and L. D. Mili`, "Design of computationally efficient elliptic IIR filters with a reduced number of shift-and-add operations in multipliers," *IEEE Trans. Signal Processing*, vol. 45, no. 10, pp. 2422--2430,Oct. 1997.

[51] Lj. Mili` and M. D. Lutovac, "Design of multiplierless IIR filters," *IEEE Int. Conf. Acoustics, Speech, Signal Processing, ICASSP97*, Munich, Germany, Apr. 1997, pp.2201--2204.

[52] M.D. Lutovac, D.V. Tosic, B.L. Evans, *Filter Design for Signal Processing Using MATLAB and Mathematica*,Prentice Hall, 2000.

[53] Y.C. LIM, *"Frequency-Response Masking Approach for the Synthesis of Sharp Linear Phase Digital Filters"*, IEEE Trans on circuit and systems, Vol. CAS-33, NO. 4, APRIL 1986

[54] M.D.Lutovac, Lj.D.Milic, "IIR Filters Based on Frequency-Response Masking Approach, *"5th Int. Conf. TELSIKS 2001*, Nis, Yugoslavia, 2001, pp.163-170

[55] M.D.Lutovac, Lj.D.Milic, "Design of High-Speed IIR Filters Based on Elliptic Minimal Q-Factors Prototype, "*Conf. ETRAN 2002*, Banja Vrucica, 2002, pp. 103-106

[56] Lj. D. Milic, M. D. Lutovac, "Efficient Algorithm for the Design of High-Speed Elliptic IIR Filters," *Int. Journal of Electronics and Communications, AEU*, Vol. 57, No. 4, 2003, pp. 255-262

[57] Lj.D.Milic, M.D.Lutovac, "Efficient Multirate Filtering Using EMQF Subfilters," *Conf. TELSIKS 2003,* Nis, Serbia, 2003, pp.301-304

[58] M. D. Lutovac, Lj. D. Milic, "Approximate linear phase multiplierless IIR halfband filter," *IEEE Signal Processing Letters*, Vol. 7, no. 3, Mar. 2000, pp. 52-53

[59] Lj. D. Milic, M. D. Lutovac, "Reducing the number of multipliers in the parallel realization of half-band elliptic IIR filters," *IEEE Trans. Signal Processing*, Vol. 44 no. 10, Oct. 1996, pp. 2619-2623

[60] M. D. Lutovac, Lj. D. Milic, "Elliptic half-band IIR filters," *Facta Universitatis (Nis), Series: Electronics and Energetics*, Vol. 9, no. 1, Jun. 1996, pp. 43-59,

[61] M. D. Lutovac, Lj. Milic, "Lattice wave digital filters with a reduced number of multipliers, "*Yugoslav IEEE MTT Chapt. Inf.*, Vol. 2, no. 3, Jun. 1996, pp. 29-39

[62] D. Rabrenovic, M. D. Lutovac, "Elliptic filters with minimal Q-factors," *Electronics Letters*, Vol. 30, no. 3, Feb. 1994, pp. 206-207

[63] Lj.D.Milic, M.D.Lutovac, D. Ilisevic, "Characteristics of two-channel IIR QMF banks" *Conf. TELFOR 2000*, Beograd, Yugoslavia, 2000, pp.333-336